INORGANIC AND ORGANIC HYBRID MATERIALS FOR ENVIRONMENTAL REMEDIATION

A Dissertation

Presented to the Faculty of the Graduate School

of Cornell University

In Partial Fulfillment of the Requirements for the Degree of

Doctor of Philosophy

by

Xiaonan Duan

August 2013

INORGANIC AND ORGANIC HYBRID MATERIALS FOR ENVIRONMENTAL REMEDIATION

Xiaonan Duan, Ph. D.

Cornell University 2013

Wastewater is the main source of environmental pollution and it contains numerous pollutants, and many of them, including phenolic compounds and heavy metal ions, are very toxic and potentially hazardous to public health. The first part of the thesis focuses on phenol remediation. We study new hierarchical hybrid biocatalysts comprised of horseradish peroxidase (HRP), magnetic nanoparticles and microparticles for advanced oxidation processes. The hybrid peroxidase catalysts exhibit activity three times higher than free HRP and are able to remove three times more phenol compared to free HRP under similar conditions. In addition, the hybrid catalysts reduce substrate inhibition, which is common with free or conventionally immobilized enzymes. We improve the reusability of the system when the HRP/magnetic nanoparticle hybrids are supported on micron scale magnetic particles.

The second part of the thesis focuses on a mesoporous bis-amine bridged polysilsesquioxane sorbent for heavy metal ion removal. We synthesize a mesoporous sorbent by hydrolysis and condensation of amine-bridged precursor in the presence of a nonionic surfactant. The sorbent exhibits a high adsorption capacity of 77 mg/g (1.2 mmol/g) and 276 mg/g (1.3 mmol/g) for Cu (II) and Pb(II), respectively. After metal adsorption we can easily regenerate the system to full capacity. The sorbent shows high selectivity for Cu (II) over Ni (II) and Co (II) but it becomes deactivated in the

presence of a small amount of adsorbed Cr (III) ions. We also apply this sorbent to adsorb CO_2. It exhibits fast CO_2 capture kinetics and has a CO_2 capacity of 2.4 mmol/g. We can fully regenerate the sorbent and it shows good stability over repetitive adsorption-desorption process over 10 cycles.

BIOGRAPHICAL SKETCH

Xiaonan Duan was born to parents Wenguang Duan and Qiuyun Wang in Xian, China on October 18, 1986. She has a little sister, Xiaoyue Duan. She spent her childhood and high school time in Xian, her hometown. At the age of 18, she went to Shanghai, China for college at Fudan University and received her B.S. in Materials Science in 2008. After graduation, she continued her graduate studies in Materials Science and Engineering at Cornell University.

To my parents, my sister, and my husband.

ACKNOWLEDGMENTS

Firstly, I want to express my heartfelt gratitude to my advisor Professor Emmanuel P. Giannelis for his guidance and for giving me the freedom in research. I would also love to acknowledge the other two committee members, Professor Paulette Clancy, and Professor Lara Estroff for their support in the completion of this dissertation. In addition, I would love to thank people who I worked and collaborated during my graduate research. Special thanks go to Dr. Stephane Corgie, Dr. Genggeng Qi, Prof. Peng Wang, Dr. Liling Fu, Prof. Meitang Liu and Prof. Paulo Monteiro. My gratitude also extends to all lab members for their help and support, in particular to Lou, Qi, Nikhil, Panos, Yan, Vivian, Weiran, Liling, Apostolos, Tiffany, Ritu, Yue, Ani, Anuja, Natalie, Pat, Marta, Antonios, Kausik, Pai, Emma, Turki, Suren, and the rest of the Giannelis group. I also want to thank the KAUST-CU for funding and the staff: Dr. David Jung, Celia Szczepura, Lorie Walker and Angela Yontz.

The life at Cornell is an extraordinarily amazing experience in my life. I will cherish forever the fun time I spent with my friends, the breathtaking scenery of Ithaca in the summer and fall, and the extremely cold winter time. This work would not be possible without the love and support of my parents and my sibling, Yueyue. They are the rock of my life. Finally, I want to especially thank my husband, Guozhang. We started the Ph.D. programs together in different departments at Cornell and supported each other during this journey. His love, care and encouragement give me the incentive to finish this work.

TABLE OF CONTENTS

LIST OF FIGURES

LIST OF TABLES

LIST OF ABBREVIATIONS

CHAPTER 1

INTRODUCTION

1.1 Wastewater: Environmental and health risks

Wastewater is the main source of environmental pollution. It is a combination of water and wastes originating from homes, businesses, institutions, agricultural and industrial facilities. Wastewater generally contains numerous pollutants, and many of them are very toxic and potentially hazardous to public health.

1.1.1 Well-known toxic pollutants in wastewater

Heavy metal ions are one of the major pollutants in wastewater. Common sources of metal pollution come from electroplating, mining, plastic manufacturing, and alloy industries.[1-4] These metals ions are environmentally persistent and non-biodegradable; therefore, waters containing heavy metal ions, if not properly managed, will result in long-term adverse effect on wild life and human health.[5,6] For example, exposure to higher levels of copper ions can lead to gastrointestinal illness, muscle pain, liver and kidney damage.[7,8] Uptake of lead ions causes neurological problems, infertility and spontaneous abortion. Children are more susceptible to lead poisoning than adults, since they can absorb a higher dose of lead per body weight than adults. Symptoms include lower intelligence quotient (IQ) and behavior disorder.[9]

Organic chemicals especially phenolic compounds are another category of well-known toxic contaminants in water.[10-12] Phenolic derivatives are widely used in oil refineries,

coal-conversion, paper manufacturing, metal casting and chemical industries.[13] They generate an unpleasant taste and can cause severe damages on different biological processes.[14,15] Most phenolic compounds are recognized as hazardous and even carcinogenic on human digestive, nervous and respiratory systems.[16-20] Some common compounds are listed in Figure 1.

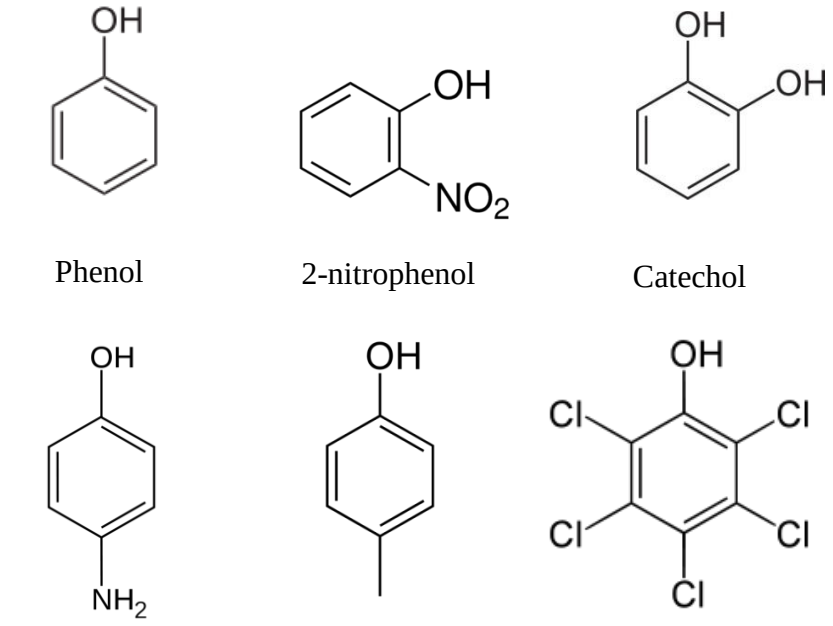

Figure 1.1 Chemical structures of common phenolic compounds in wastewater

1.1.2 "Emerging contaminants" in wastewater

Besides these well-studied pollutants, new chemical and pharmaceutical developments in the last two decades have also led to the presence of new compounds in wastewater, named as "emerging contaminants".[21] They are mainly aromatic compounds and

come from daily products such as personal care products, plastics and pharmaceuticals.[22,23] In contrast to traditional pollutants, these "emerging contaminants" are either relatively new organic chemicals or are only now detectable because of technological advances.[24] They are without clear regulatory status and so little is known of the health risks that they pose. The lack of understanding of their impact on human health and environment creates a serious problem in the long term. Some of these pollutants are shown in Figure 2.

Polychlorinated biphenyls (PCBs) are a group of chlorinated aromatic hydrocarbons and are often discharged in the environment.[25] PCBs have shown adverse effects on the immune system, nervous system and endocrine system.[18,19] Phthalates and bisphenol A (BPA) are extensively used as plasticizers in plastics ranging from food storage containers and blood bags to metal-based cans and hard plastic bottles, and they are also incorporated into cosmetics and perfumes.[26,27] They have been found to be endocrine-disrupting and can influence the sexual development of children.[28] The most used phthalate is bis(2-ethylhexyl) phthalate (DEHP). In May 2011, the illegal use of DEHP in clouding agents for food and drinks was reported in Taiwan and this serious food scandal led to a growing concern to these emerging contaminant usages in personal products.[29]

Pharmaceutical compounds such as hormones, antibiotics, anti-cancer and anti-depression drugs have been detected in drinking water, surface water and sewage effluent.[21,30,31] Many are resistant so as to retain their activity through manufacture, storage and retail processes. Pharmaceuticals are excreted unchanged or metabolized from human body and enter wastewater.[32,33] Studies demonstrate that pharmaceuticals in water can act as endocrine-disruptors that mimic hormones and adversely impact

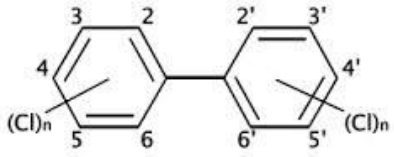

PCB

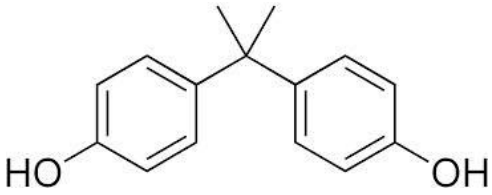

BPA

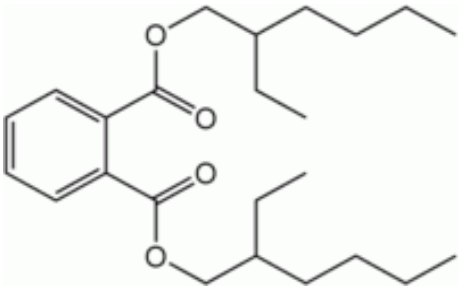

DEHP

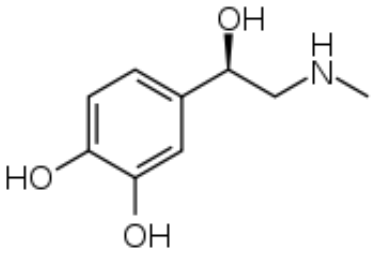

Epinephrine (a type of hormone)

Figure 1.2 Chemical structures of some emerging contaminants in wastewater

the reproduction of fish and other aquatic animals.[34] Even though the concentrations of drugs monitored at present are too low to affect human health, much more public attention should be paid on this issue.

1.2 Wastewater Treatment Process

There are generally several levels of treatment for wastewater. A modern wastewater treatment plant typically includes these stages: preliminary, primary, secondary, advanced treatment and disinfection.[35]

1.2.1 Preliminary treatment

This first treatment is the removal of coarse solids and large debris often found in raw wastewater such as plastics, sticks and cans, which is necessary to enhance the operation of the following treatment units. It usually includes coarse screening, and comminution of large objects.

1.2.2 Primary treatment

Primary treatment is intended to mainly remove suspended solids, grease and heavy organic matter by means of sedimentation. Some common chemical additions may be used for flocculation to enhance this step. The effluent from primary sedimentation is called the primary effluent. This treatment is designed to make a liquid effluent for downstream treatments.

1.2.3 Secondary treatment

The objective of secondary treatment is to remove common dissolved and colloidal organics. This is accomplished through a biological process. The most commonly used

process is called ‘activated sludge’, which is an aerobic biological conversion process that uses microorganisms, including bacteria, fungi, and protozoa, to speed up the decomposition of organic matter. They consume the soluble and suspended organic materials and subsequently produce more microorganisms and inorganic end-products (CO_2, NH_3, and H_2O).[36,37] After the aeration step, the activated sludge is separated from the liquid and the clarified liquid is called secondary effluent.

1.2.4 Advanced treatment

The advanced treatment is specifically designed to further remove wastewater constituents, which are generated from specific sources/industries. It is also referred to as ‘tertiary treatment’ and this additional treatment can be as simple as the addition of a filter or as complex as many unit processes for contaminants.[38] A variety of methods including activated carbon, filtration, ion exchange, reverse osmosis, advanced oxidation and adsorption can be used.[39-46] The treatment processes are selected depending on the targets. The pollutants needed to be treated are usually in high level of concentrations and recalcitrant such as heavy metals, phosphorus, phenolic compounds and the new emerging compounds mentioned above.[36,47] Since the objective of advanced treatment is either to remove specific contaminants or to produce an effluent of higher quality than normally made by secondary treatment, this step is the current focus of research in wastewater treatment.

1.2.5 Disinfection

Before the final effluent is discharged into the environment for the use of drinking and irrigation, the last step is disinfection. The goal is to substantially reduce the amount of remaining microorganisms. The most common and convenient method is chlorination. Other processes include ozone and ultraviolet light.

1.3 Outline of the dissertation

In chapter two, we study new hierarchical hybrid catalysts comprised of horseradish peroxidase (HRP), magnetic nanoparticles and microparticles for advanced oxidation processes. We demonstrate their utility in the removal of phenol in synthetic wastewater. Phenol is used as a model compound, but peroxidases, HRP in particular, are well known to have a broad substrate range and have been shown to polymerize numerous aromatics including nonylphenols, Bisphenol A (BPA), dyes, PAH, hormones, and pesticides.

In chapter three, we present a mesoporous bis-amine bridged polysilsesquioxane sorbent for heavy metal ion removal. The mesoporous sorbent was synthesized by hydrolysis and condensation of amine-bridged precursor in the presence of a nonionic surfactant. We test the non-competitive adsorption of Cu (II) and Pb (II) ions, competitive tests and reuse stability. Amine can also react with CO_2 besides metal ions. In chapter four, we apply the sorbent to absorb CO_2 and discuss its CO_2 capture capacity, kinetics and reusability.

REFERENCES

1. Benhamou, A.; Baudu, M.; Derriche, Z.; Basly, J. P. Aqueous Heavy Metals Removal on Amine-functionalized Si-MCM-41 and Si-MCM-48. *J. Hazard. Mater.* **2009**, *171*, 1001–1008.

2. Cavus, S.; Gurdag, G. Noncompetitive Removal of Heavy Metal Ions from Aqueous Solutions by Poly[2-(acrylamido)-2-methyl-1-propanesulfonic Acid-Co -Itaconic Acid] Hydrogel. *Ind. Eng. Chem. Res.* **2009**, *48*, 2652–2658.

3. Mureseanu, M.; Reiss, A.; Stefanescu, I.; David, E.; Parvulescu, V.; Renard, G.; Hulea, V. Modified SBA-15 Mesoporous Silica for Heavy Metal Ions Remediation. *Chemosphere* **2008**, *73*, 1499–1504.

4. Lam, K. F.; Chen, X.; Fong, C. M.; Yeung, K. L. Selective Mesoporous Adsorbents for Ag+/Cu2+ Separation. *Chem. Commun.* **2008**, 2034–2036.

5. Duan, X.; Qi, G.; Wang, P.; Giannelis, E. P. A Highly Efficient and Selective Polysilsesquioxane Sorbent for Heavy Metal Removal. *ChemPhysChem* **2012**, *13*, 2536–2539.

6. Denizli, A.; Sanli, N.; Garipcan, Bora;Patir, Suleyman; Alsancak, G. Methacryloylamidoglutamic Acid Incorporated Porous Poly (methyl Methacrylate) Beads for Heavy-metal Removal. *Ind. Eng. Chem. Res.* **2004**, *43*, 6095–6101.

7. Liu, C.; Bai, R. Adsorptive Removal of Copper Ions with Highly Porous Chitosan/cellulose Acetate Blend Hollow Fiber Membranes. *J. Membr. Sci.* **2006**, *284*, 313–322.

8. Xue, X.; Li, F. Removal of Cu(II) from Aqueous Solution by Adsorption onto Functionalized SBA-16 Mesoporous Silica. *Microporous Mesoporous Mater.* **2008**, *116*, 116–122.

9. Flora, G.; Gupta, D.; Tiwari, A. Toxicity of Lead: A Review with Recent Updates. *Interdiscip. Toxicol.* **2012**, *5*, 47–58.

10. Adelman, D. A Cautiously Pessimistic Appraisal of Trends in Toxic Regulation. *Wash. U. J. Law & Pol.* **2010**, *32*, 377–442.

11. Cooper, V. A.; Nicell, J. A. Removal of Phenols From A Foundry Wastewater Using Horseradish Peroxidase. *Wat. Res.* **1996**, *30*, 954–964.

12. Qayyum, H.; Maroof, H.; Yasha, K. Remediation and Treatment of Organopollutants Mediated by Peroxidases: a Review. *Crit. Rev. Biotechnol.* **2009**, *29*, 94–119.

13. Wu, J.; Taylor, K. E.; Bewtra, J. K.; Biswas, N. Optimization of the Reaction Conditions for Enzymatic Removal of Phenol from Wastewater in the Presence of Polyethylene Glycol. *Wat. Res.* **1993**, *27*, 1701–1706.

14. Keith, Larry H;Telliard, W. A. Priority Pollutants: I-a Perspective View. *Environ. Sci. Technol.* **1979**, *13*, 416–423.

15. Dabrowski, A.; Podkościelny, P.; Hubicki, Z.; Barczak, M. Adsorption of Phenolic Compounds by Activated Carbon--a Critical Review. *Chemosphere* **2005**, *58*, 1049–1070.

16. Bayramoğlu, G.; Arica, M. Y. Enzymatic Removal of Phenol and P-chlorophenol in Enzyme Reactor: Horseradish Peroxidase Immobilized on Magnetic Beads. *J. Hazard. Mater.* **2008**, *156*, 148–155.

17. Aitken, M. D. Waste Treatment Applications of Enzymes: Opportunities and Obstacles. *Chem. Eng. J.* **1993**, *52*, B49–B58.

18. Babich, H.; Davis, D. L. Phenol: a Review of Environmental and Health Risks. *Regul. Toxicol. Pharmacol.* **1981**, *1*, 90–109.

19. Michalowicz, J.; Duda, W. Phenols–Sources and Toxicity. *Pol. J. Environ. Stud.* **2007**, *16*, 347–362.

20. Zhang, G.; Nicell, J. A. Treatment of Aqueous Pentachlorophenol by Horseradish Peroxidase and Hydrogen Peroxide. *Wat. Res.* **2000**, *34*, 1629–1637.

21. Deblonde, T.; Cossu-Leguille, C.; Hartemann, P. Emerging Pollutants in Wastewater: a Review of the Literature. *Int. J. Hyg. Environ. Health* **2011**, *214*, 442–448.

22. Tambosi, J. L.; Sena, R. F. de; Favier, M.; Gebhardt, W.; José, H. J.; Schröder, H. F.; Moreira, R. D. F. P. M. Removal of Pharmaceutical Compounds in Membrane Bioreactors (MBR) Applying Submerged Membranes. *Desalination* **2010**, *261*, 148–156.

23. Grassi, M.; Rizzo, L.; Farina, A. Endocrine Disruptors Compounds, Pharmaceuticals and Personal Care Products in Urban Wastewater: Implications for Agricultural Reuse and Their Removal by Adsorption Process. *Environ. Sci. Pollut. Res.* **2013**, *20*, 3616–3628.

24. Petrovic, M.; Gonzalez, S.; Barcelo, D. Analysis and Removal of Emerging Contaminants in Wastewater and Drinking Water. *Trends Anal. Chem.* **2003**, *22*, 685–696.

25. Benabdallah El-Hadj, T.; Dosta, J.; Torres, R.; Mata-Álvarez, J. PCB and AOX Removal in Mesophilic and Thermophilic Sewage Sludge Digestion. *Biochem. Eng. J.* **2007**, *36*, 281–287.

26. Barnabé, S.; Beauchesne, I.; Cooper, D. G.; Nicell, J. A. Plasticizers and Their Degradation Products in the Process Streams of a Large Urban Physicochemical Sewage Treatment Plant. *Wat. Res.* **2008**, *42*, 153–162.

27. Shea, K. M. Pediatric Exposure and Potential Toxicity of Phthalate Plasticizers. *Pediatrics* **2003**, *111*, 1467–1474.

28. Tsutsumi, Y.; Haneda, T.; Nishida, T. Removal of Estrogenic Activities of Bisphenol A and Nonylphenol by Oxidative Enzymes from lignin-Degrading Basidiomycetes. *Chemosphere* **2001**, *42*, 271–276.

29. Yen, T.-H.; Lin-Tan, D.-T.; Lin, J.-L. Food Safety Involving Ingestion of Foods and Beverages Prepared with Phthalate-plasticizer-containing Clouding Agents. *J. Formosan Med. Assoc.* **2011**, *110*, 671–684.

30. Maruya, K. a; Vidal-Dorsch, D. E.; Bay, S. M.; Kwon, J. W.; Xia, K.; Armbrust, K. L. Organic Contaminants of Emerging Concern in Sediments and Flatfish Collected Near Outfalls Discharging Treated Wastewater Effluent to the Southern California Bight. *Environ. Toxicol. Chem.* **2012**, *31*, 2683–2688.

31. Barnes, K. K.; Kolpin, D. W.; Furlong, E. T.; Zaugg, S. D.; Meyer, M. T.; Barber, L. B. A National Reconnaissance of Pharmaceuticals and Other Organic Wastewater Contaminants in the United States--I) Groundwater. *Sci. Total Environ.* **2008**, *402*, 192–200.

32. Westerhoff, P.; Yoon, Y.; Snyder, S.; Wert, E. Fate of Endocrine-disruptor, Pharmaceutical, and Personal Care Product Chemicals During Simulated Drinking Water Treatment Processes. *Environ. Sci. Technol.* **2005**, *39*, 6649–6663.

33. Benotti, M. J.; Trenholm, R. a; Vanderford, B. J.; Holady, J. C.; Stanford, B. D.; Snyder, S. A. Pharmaceuticals and Endocrine Disrupting Compounds in U.S. Drinking Water. *Environ. Sci. Technol.* **2009**, *43*, 597–603.

34. Snyder, S. a; Benotti, M. J. Endocrine Disruptors and Pharmaceuticals: Implications for Water Sustainability. *Water Sci. Technol.* **2010**, *61*, 145–154.

35. Sonune, A.; Ghate, R. Developments in Wastewater Treatment Methods. *Desalination* **2004**, *167*, 55–63.

36. Johnson, A.; Sumpter, J. Removal of Endocrine-Disrupting Chemicals in Activated Sludge Treatment Works. *Environ. Sci. Technol.* **2001**, *35*, 4697–4703.

37. Hesselmann, R. P.; Werlen, C.; Hahn, D.; Meer, J. R. van der; Zehnder, A. J. Enrichment, Phylogenetic Analysis and Detection of a Bacterium That Performs Enhanced Biological Phosphate Removal in Activated Sludge. *System. Appl. Microbiol.* **1999**, *22*, 454–465.

38. Nemade, P. D.; Kadam, A. M.; Shankar, H. S. Wastewater Renovation Using Constructed Soil Filter (CSF): a Novel Approach. *J. Hazard. Mater.* **2009**, *170*, 657–665.

39. Nicell, J. A. Kinetics of Horseradish Peroxidase-Catalysed Polymerization and Precipitation of Aqueous 4-Chlorophenol. *J. Chem. Technol. Biotechnol.* **1994**, *60*, 203–215.

40. Gianfreda, L.; Iamarino, G.; Scelza, R.; Rao, M. A. Oxidative Catalysts for the Transformation of Phenolic Pollutants: A Brief Review. *Biocatal. Biotransform.* **2006**, *24*, 177–187.

41. Oller, I.; Malato, S.; Sánchez-Pérez, J. A. Combination of Advanced Oxidation Processes and Biological Treatments for Wastewater Decontamination--a Review. *Sci. Total Environ.* **2011**, *409*, 4141–4166.

42. Beker, U. G.; Guner, F. S.; Dizman, M.; Erciyes, A. T. Heavy Metal Removal by Ion Exchanger Based on Hydroxyethyl Cellulose. *J. Appl. Polym. Sci.* **1999**, *74*, 3501–3506.

43. Jorgensen, T. C.; Weatherley, L. R. Ammonia Removal from Wastewater by Ion Exchange in the Presence of Organic Contaminants. *Wat. Res.* **2003**, *37*, 1723–1728.

44. Dabrowski, A.; Hubicki, Z.; Podkościelny, P.; Robens, E. Selective Removal of the Heavy Metal Ions from Waters and Industrial Wastewaters by Ion-exchange Method. *Chemosphere* **2004**, *56*, 91–106.

45. Chan, B. K. C.; Dudeney, A. W. L. Reverse Osmosis Removal of Arsenic Residues from Bioleaching of Refractory Gold Concentrates. *Miner. Eng.* **2008**, *21*, 272–278.

46. Sun, L.; Perdue, E. M.; McCarthy, J. Using Reverse Osmosis to Obtain Organic Matter From Surface And Ground Waters. *Wat. Res.* **2008**, *29*, 1471–1477.

47. Nakada, N.; Tanishima, T.; Shinohara, H.; Kiri, K.; Takada, H. Pharmaceutical Chemicals and Endocrine Disrupters in Municipal Wastewater in Tokyo and Their Removal During Activated Sludge Treatment. *Wat. Res.* **2006**, *40*, 3297–3303.

CHATPER 2

HIERARCHICAL HYBRID PEROXIDASE CATALYSTS FOR REMEDIATION OF SYNTHETIC PHENOL WASTEWATER

2.1 Introduction

The diversity of anthropogenic sources of phenol and its-derivatives, their occurrence in our daily life, and concentration in our environment have all drastically increased in the past century. Acute exposure to phenols is accidental, yet often lethal; diffuse exposure is known or suspected to induce mutagenicity, teratogenicity, carcinogenicity, immunosuppression, endocrine disruption, and infertility.[1] In the European Union, phenol-containing molecules account for a significant portion of regulated or banned substances in products and the environment according to the Registration, Evaluation, and Authorization of Chemicals (REACH) restricted substance list (RLS).[2] In the United States, phenol is one of the first molecules to be regulated by the Environmental Protection Agency (EPA) and, as of 2012, 73 out of the 126 priority pollutants in water as defined in the Clean Water Act (CWA) are phenol derivatives.[3]

One approach to minimize the effect of pollutants is to use various sorbents and membranes. However, sorbents and membranes usually come at high cost, may lack specificity, and, more importantly, they do not convert the pollutants to less reactive forms.[4] Biological routes have been suggested and phenol-degrading species identified, but the biocide potency of many phenolic derivatives drastically decreases the efficiency of whole microbial communities in active sludge.[5] More robust treatments, referred to as Advanced Oxidation Processes (AOP), can inactivate phenolics and are

based on oxidative mechanisms using either radiation (e.g., UV treatment) or high redox potential reactants (ozone, peroxides, Fenton reagents and catalysts) or combination thereof.[6,7] The detailed mechanism involves the oxidation of the aromatic ring to form free-radical species; in this state, the ring is destabilized and can break or the radicals can react with each other and polymerize into insoluble polyphenols. Polyphenols form an aromatic, nonreactive sludge, which can be easily recovered. However, the conventional (uncatalytic) AOP processes for phenolic removal require large amounts of energy, chemicals and materials.[5-7] A lot of research efforts have been invested in finding suitable catalytic AOP-based treatments and suitable nano- and bio- catalysts have been at the center of the attention.

The main advantage of nanosized catalysts is their high surface-to-volume ratio, which leads to increased availability of active sites. A broad range of metal oxide nanoparticles have been shown to possess intrinsic peroxidase-like catalytic properties in the sense that they can mediate the oxidation of peroxidase substrates in the presence of hydrogen peroxide.[8-13] However, the specificity and yield of these reactions are low, and the concentration of substrate and catalysts needs to be high. In sharp contrast, enzymatic reactions based on peroxidase enzymes are fast, efficient, and require mild conditions.[14-17] Unfortunately, peroxidases, such as Horseradish Peroxidase (HRP), are biochemically self-regulated enzymes and are highly prone to substrate and product inhibition that results in poor performance under real process conditions.[18-20] Enzyme immobilization on various support materials has been proposed and examined in order to overcome these drawbacks as immobilization can assist with separation, reusability and continuous flow processes. Even though improved stability has been reported, the loss of enzymatic activity from changes in

conformation and steric hindrance offsets any gains.[21-25] Therefore, new approaches for higher performance catalysts for AOP are still needed.

What fundamental traits should be engineered into industrial catalysts? The catalysts should have high activity and low inhibition, be reusable, maximize the use of the enzyme component and be flexible enough in their design to accommodate different concentrations and diversity of substrates; the materials, reagents and the energetics have to be cost-effective.

We have previously reported that magnetic nanoparticles (MNPs) can be used as immobilization supports for HRP and the resulting assemblies of the MNPs and HRP, termed as BioNanoCatalysts (BNCs), dramatically improve the activity of HRP in bio-chemical assays that are typically used to measure enzymatic activities.[26,27] The observed increase in HRP activity is accompanied by an unexpectedly surprising drop in enzyme inhibition, which is very desirable. To our knowledge, the magnitude and combination of these two effects on native enzymes are unique.

In this chapter, it is, for the first time, the use of BNCs and their binding on micro magnetic particles for the phenol remediation application. We present that the simple, cost-effective hierarchical catalysts exhibit higher activity than the free HRP and are able to remove larger amounts of phenol compared to the free HRP under similar conditions. In addition, they show reduced substrate inhibition and limited inactivation from reaction products. The new hybrid catalyst allows for reusability and can be confined with a specially designed magnetically-driven reactor.

2.2 Experimental Sections

2.2.1 Materials

All chemicals were obtained from commercial sources and were used without further purification. Horseradish Peroxidase (HRP, E.C. 1.11.1.7, type VI-A) was obtained from Sigma Aldrich as lyophilized powder, and its Reinheitszahl Index-Rz (A_{403}/A_{280}) was measured to be 2.9. 1-Step Turbo TMB - ELISA Substrate and Amplex® Red Hydrogen Peroxide/Peroxidase Assay Kit were purchased from Thermo Scientific and Life technologies respectively. HCl (12 M) was obtained from Fisher Scientific. Hydrogen peroxide, $FeCl_3 \cdot 6H_2O$, $FeCl_2 \cdot 4H_2O$, phosphate buffer solution (1.0 M, pH 7.4), sodium hydroxide, phenol and sodium chloride were purchased from Sigma Aldrich. Deionized water (DI water) was generated with a Milli-Q integral ultrapure water purification system.

2.2.2 Characterization

Scanning electron microscope (SEM) images were obtained on a Keck Field Emission SEM, LEO 1550 model. Bright-field transmission electron microscopy (TEM) images were obtained on a FEI Tecnai T12 Spirit Twin TEM/STEM operated at 120kV. X-Ray diffraction patterns were obtained on a Scintag diffractometor using CuKα (λ=1.54 Å) radiation. Nitrogen adsorption-desorption isotherms were obtained on a Micrometrics ASAP 2020 physi-sorption instrument. The specific surface area of the samples was calculated by the Brunauer-Emmett-Teller (BET) method. Pore size distributions were calculated from the N_2 adsorption isotherm using the Barrett–Joyner–Halenda (BJH) method. Magnetic measurements were conducted on a Quantum Design magnetometer. The magnetization hysteresis curves were obtained at 300 K and the applied magnetic field was varied between 20 Oe and 40 kOe.

Dynamic light scattering (DLS) was tested at 25^{o}C using a Malvern Zetasizer Nano-ZS. Fourier-transform infrared (FTIR) spectra were obtained from a high-throughput FTIR spectrometer (HTS-XT-Vertex70, Bruker, Germany) in transmittance analysis, where the samples were dried on a silicon wafer.

2.2.3 Iron oxide synthesis

The synthesis of magnetic nanoparticle by co-precipitation has been described previously.[26,27] Briefly, an acidic solution (25 ml) of $FeCl_2 \cdot 4H_2O$ (2g) and $FeCl_3 \cdot 6H_2O$ (5.2g) were added dropwise to NaOH (250 ml, 1.5 M) under nitrogen protection with vigorous stirring. Nitrogen was bubbled into all solutions for 15 minprior to reaction. The black precipitate was captured by neodymium magnet, washed and neutralized. Aliquots were kept under N_2 atmosphere at 4 ℃, in DI water until further use.

2.2.4 Hybrid catalyst synthesis

The BNCs were formed by mixing appropriate amounts of a suspension of MNP (1200 μg/ml) with a solution of HRP (1500 nM). After mixing, the suspension was incubated at 4 ℃ for over 3 hr. BMC were synthesized similarly except micron size magnetic particles (MMP) were used. Hierarchical assemblies were made by adding MMP to pre-formed BNC and, incubated at 4 ℃ for over 3 hr.

2.2.5 Phenol removal assay reaction, kinetic study and reuse of catalyst

Phenol assays were prepared by first mixing the phenol, bio-catalysts and phosphate solution. The reaction was then initiated by adding hydrogen peroxide. After reaction, the assay was centrifuged (12000g, 10 min) and the sample drawn from the mixtures

was added with 500 mM sodium chloride solution. The precipated sample was centrifuged again (12000g, 10 min) and the residual phenol was measured from the supernatant. For each reaction, three replicas were tested each time. For the kinetic experiments, the reaction was arrested at different time intervals by immersing the tube in boiling water for 5 minutes. For the reusability experiments, the assay was carried out for 2 hours, and the catalyst was captured by a small magnet and reused in subsequent assays. The concentration of residual phenol was measured for each reaction cycle. Phenol concentration was determined spectrophotometrically using an automated plate-reader (Synergy 4, Biotek) at 280 nm in UV-transparent microplates. The concentration of phenol was calculated from the background corrected absorbance at 280 nm, using an internal standard calibration curve for each assay. The enzyme concentration used for the assay did not significantly contribute to the background.

2.3 Results and Discussions

2.3.1 Materials properties

The X-ray Diffraction pattern of the magnetic nanoparticles is shown in Figure 2.1, which confirms the magnetite or maghemite structure.[28,29] The corresponding peaks are listed in Figure 1.

The Scherrer equation is a formula that calculates the crystallite size in a solid to the broadening of a peak in X-ray diffraction pattern. As can be seen below, B is the peak full width at Half Maximum (FWHM), d is the crystallite size, λ is the X-ray wavelength, and θ is the Bragg angle. The crystallite size is 9 ± 1 nm, using the Scherrer equation.

$$B(2\theta) = \frac{0.94\lambda}{d\cos\theta}$$ ...Equation (1)

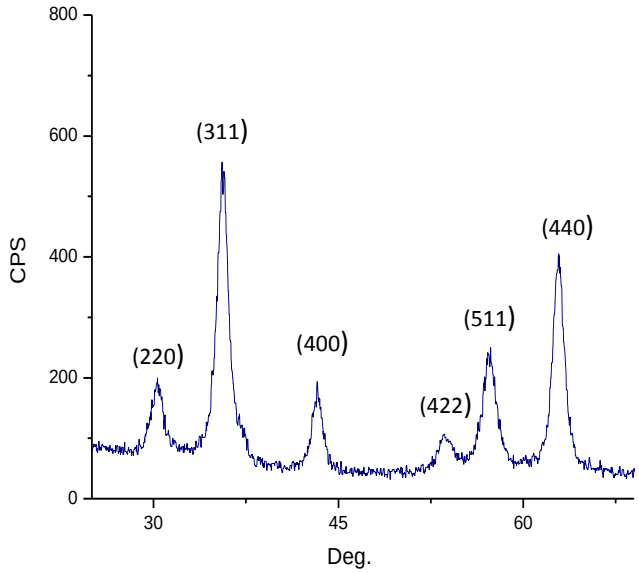

Figure 2.1 XRD pattern of Magnetic Nanoparticles (MNP).

Figure 2.2 shows the magnetization hysteresis of MNP, which is normalized to the mass and tested at 300 K. The applied magnetic field is varied between -40,000 Oe and +40,000 Oe. The saturation magnetization (Ms) is 58.3 emu/g. From Figure 2.2b, the remanence (Mr) is 1.0 emu/g. The remanence ratio (s=Mr/Ms) is 0.02. TEM images of the MNPs and the histogram of size distribution are shown in Figure 2.3. The average particle size is 8 ± 2 nm as processed by JMicroVision (V 1.27) and is in good agreement with the diameter 9 ± 1 nm calculated from XRD.

There is no ligand/polymer functionality added to the nanoparticles during the synthesis. Due to the high surface tension, the nanoparticles tend to aggregate into clusters, which are observed in Figure 2.3. The DLS data, shown later, also confirm the aggregation.

2.3.2 Preparation of HRP

The original lyophilized powder HRP was made to 0.1 mg/ml. The aqueous solution was tested in a quartz cuvette for absorbance. Readings at 403 nm and 280 nm were recorded and the ratio referred as the Reinheitszahl Index-Rz (A_{403}/A_{280}) was measured to be 2.9.

The HRP molar concentration is determined based on Beer's Law.

$A = \varepsilon l c$ …Equation (2)

A: absorbance

ε: extinction coefficient

l: path length

c: concentration

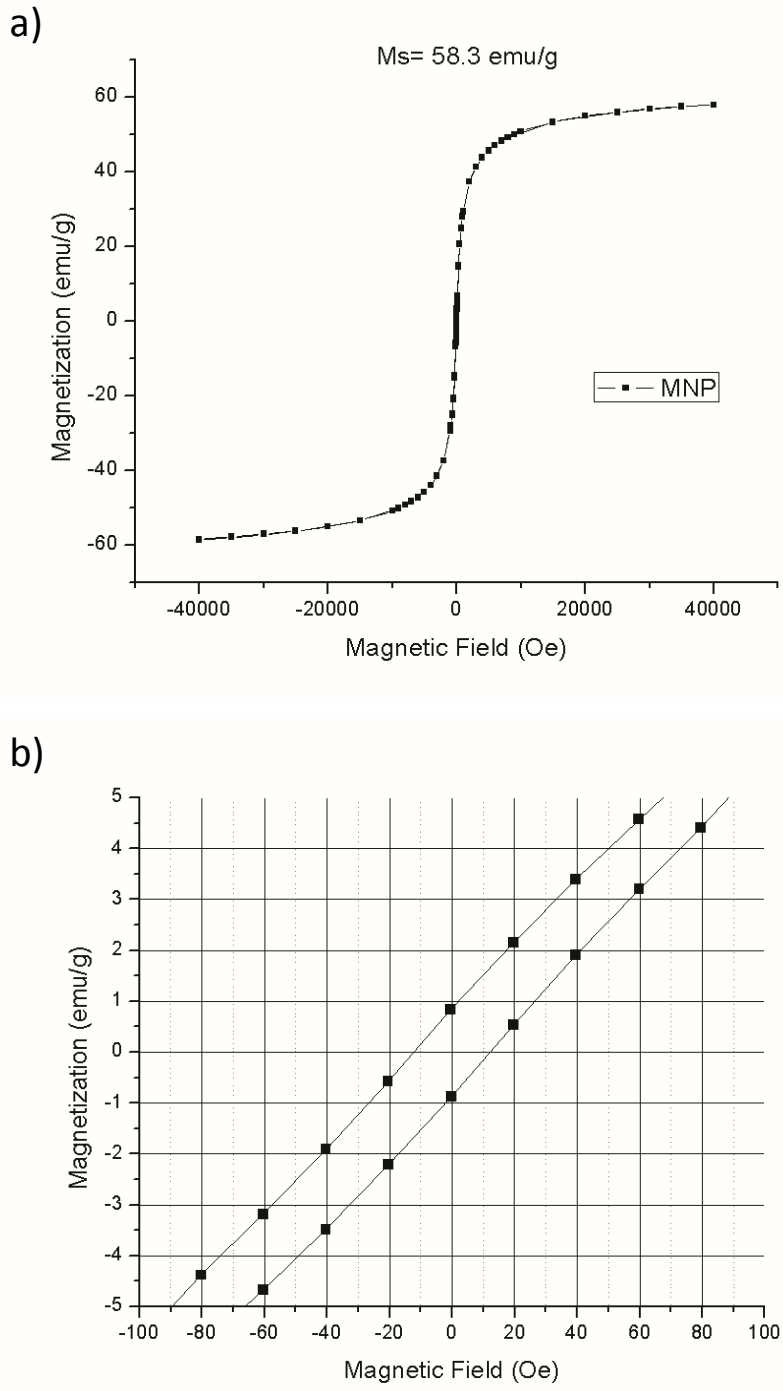

Figure 2.2 a) Magnetization hysteresis curves of the iron oxide particles b) magnetization to show the remanence between -100 Oe and 100 Oe.

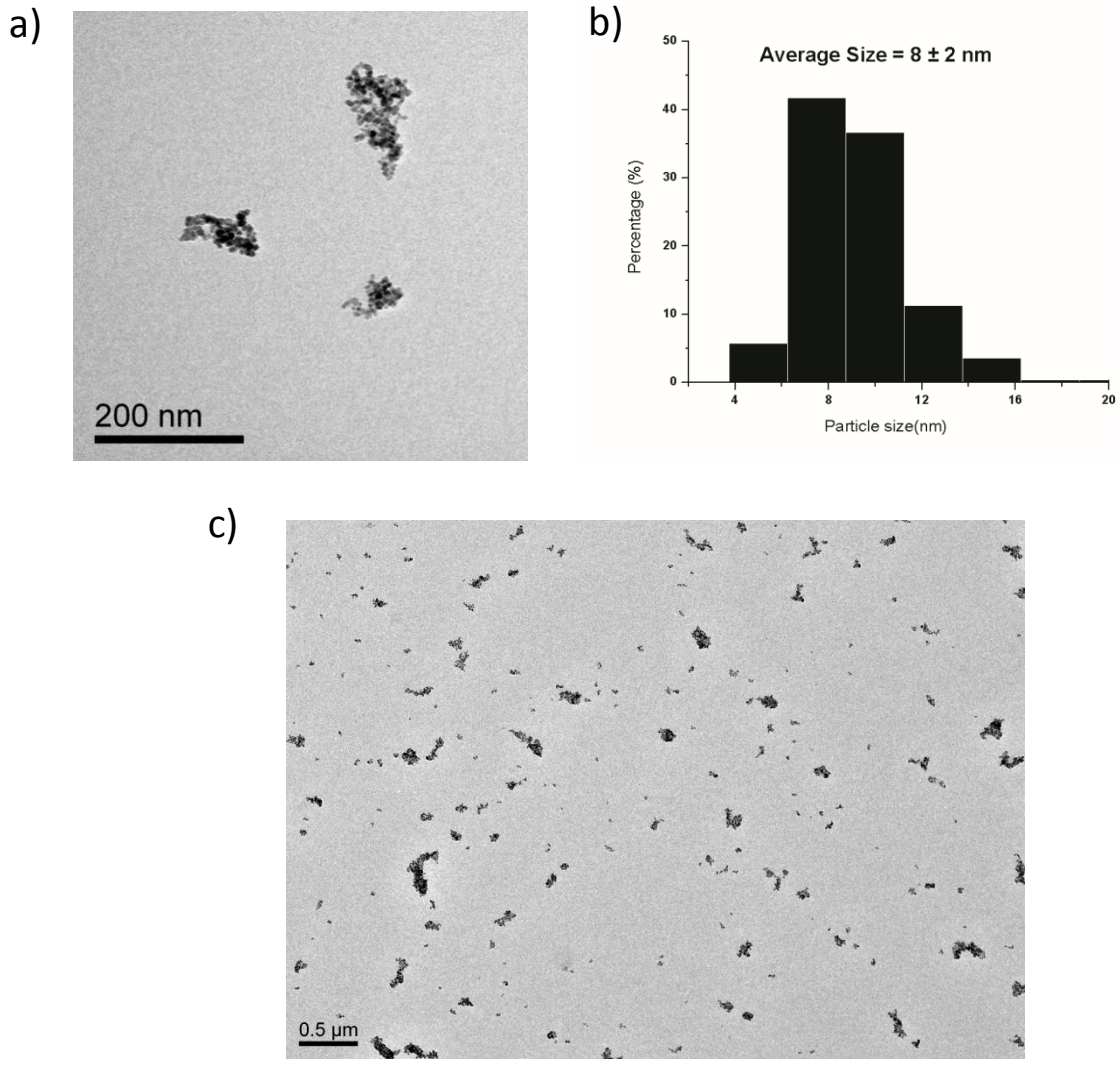

Figure 2.3 a) TEM images of MNPs, b) the size distribution of particles using processed using JMicroVision (V 1.27), c) an overview TEM image of MNP.

The absorbance is tested at 403 nm and the corresponding extinction coefficient is 100 1/mM·cm. The path length is 1 cm as the cuvette length. Solutions of HRPs with concentration of 100 μM are stored in freezer for further use.

2.3.3 Formation of BNC

The BNCs were formed by adding appropriate amounts of a suspension of MNP (1200 μg/ml) to a solution of HRP (1500 nM). The MNP solution was firstsonicated for 10 min before mixing with HRP. The mixed suspension was then incubated at 4℃ for over 3 hr. The resulting assemblies are called BioNanoCatalysts (BNCs). We refer to these as BNC-x, where x represents the ratio of concentration of MNP (μg/ml) to the concentration of HRP (nM). For example, if the BNC is composed of MNP in 60 μg/ml and HRP in 30 nM, this BNC is called BNC-2.

DLS measures the size of particles and colloids inside a liquid medium. It measures time-dependent fluctuations of scattered coherent light which is caused by diffusive Brownian motion of particles.[30] In this test, the light source is a He-Ne laser at 633 nm. The experimentally measured diffusion coefficient can be converted to a hydrodynamic diameter via the Stokes-Einstein relation.

$$D_H = \frac{kT}{3\pi\eta D} \quad \text{…Equation (3)}$$

D_H: hydrodynamic diameter

K: Boltzmann constant

η: solvent viscosity

T: absolute temperature

D: diffusion coefficient

The sizes of pure MNP, and BNCs with different concentrations of HRPs are compared in DLS, with the fixed concentration of nanoparticles (60 μg/ml). As shown in Figure 2.4a, the average cluster size is around 60 nm, indicating slight nanoparticle aggregation. There is no significant size change between MNP and BNCs. The zeta potential of free HRP is shown in Figure 4b. There are two peaks, one at -40 mV and the other at 100 mV. The zeta potentials of pure MNP and BNCs are essentially unchanged, also listed in Table 2.1. The mechanism of BNC formation is hypothesized to be a combined interaction of physical adsorption and electrostatic forces. The enzymes are adsorbed onto the nanoparticle clusters.

The extent of enzyme binding onto MNP was measured. BNCs are centrifuged at 12000 g for 10 min. The supernatants are drawn and diluted to the testing range. The supernatant enzyme concentrations were determined by tetramethylbenzidine (TMB)-ELISA assays. The TMB-ELISA Substrate (130 μl) were mixed with the supernatant (20 μl) and incubated for 15 minutes after which H_2SO_4 (100 μl, 0.5 M) was added to stop the reaction. The concentration was calculated from the yellow samples' reading at 450 nm, based on the standard calibration curve tested at the same time.

The effective binding was calculated using the equation: 1-([S]/ [total enzyme]), where [S] is the concentration of the enzyme in the supernatant. The results are listed in Table 2.2. For BNC-0.25, the binding is incomplete; in contrast, almost all the HRPs can bind onto MNPs in BNC-1 and BNC-2. The increase of MNP addition from BNC-0.25 to BNC-2 is shown in Figure 2.5, which is consistent with the gradual increase in the percentage of binding.

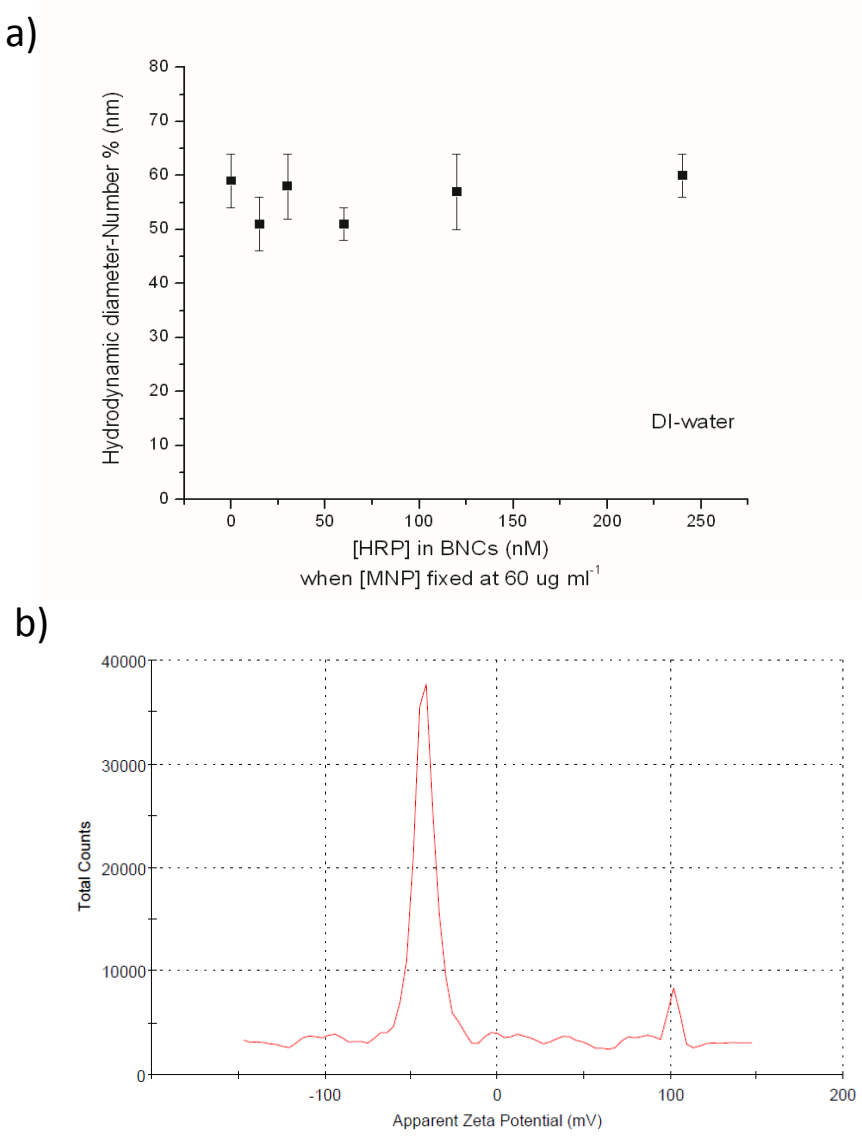

Figure 2.4 a) DLS data of hydrodynamic diameter of MNP and BNCs at the fixed concentration MNP 60 µg/ml b) Zeta potential of free HRP.

Table 2.1 Zeta potential of pure MNP and BNC-2 at pH=6.0.

	Average zeta potential (mV)	Standard deviation (mV)
Pure MNP	-23.70	0.95
BNC-2	-24.33	0.31

Table 2.2 Effective bindings of HRP onto MNP in BNCs. Standard deviations are based on triplicate results.

name of the BNCs	effective binding %
BNC-0.25	75.1% ± 0.7%
BNC-0.5	87.4% ± 0.2%
BNC-1	94.3% ± 1.3%
BNC-2	96.4% ± 2.9%

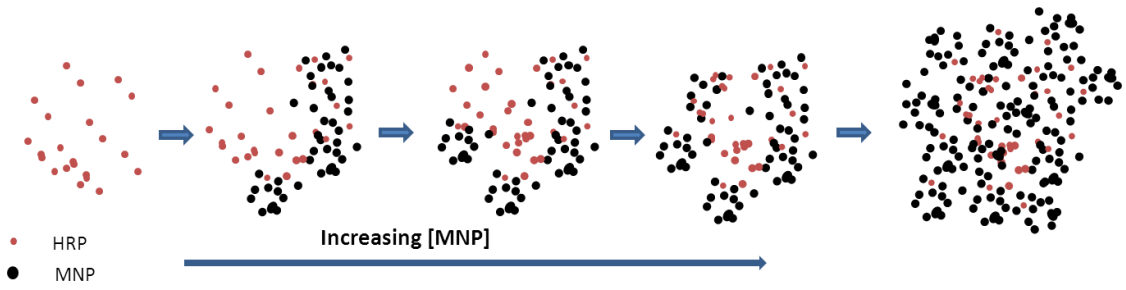

Figure 2.5 Formation process of BNCs by increasing the concentration of MNP with a fixed concentration of HRP.

2.3.4 HRP cycle mechanism

The mechanism of catalysis of HRP has been investigated extensively.[20] HRP catalyzes the oxidation of phenolic compounds in the presence of H_2O_2, producing free radicals. The cycle is illustrated in Figure 2.6a, where the AH_2 and $AH^{\cdot}$ represent the phenolic compound and its radical species.

In a typical HRP cycle—firstly H_2O_2 converts HRP into an active compound I, a high oxidation state intermediate. Next, Compound I oxidizes a phenolic compound. A free radical is generated and released to solution leading to Compound II. Similarly, compound II oxidizes another phenolic compound to a radical and compound II is reduced to the native HRP, thereby completing the cycle (Figure 2.6a). The phenoxy radicals react with each other in a non-enzymatic process to form polymers, which can be removed by further precipitation with salts or condensation. Figure 2.6b shows images of the phenol solution before treatment and the polymerized phenol after enzymatic reaction.

The main hurtle of using enzymes as biocatalyst is the number of reactions they can carry before being inactivated; this is known as the total turnover number (TTN). In the case of peroxidases, inactivation is the result of two distinct mechanisms: substrate inhibition that is H_2O_2-dependent and product inhibition that is correlated with free radical concentration.

In excess of hydrogen peroxide, the enzyme is susceptible to an oxidative inactivation.[18] The compound II can turn into catalytically-inactive Compound III, as shown in Figure 2.6. A decrease of peroxidase activity has been observed. Even though it is not a permanent inactivation, the return to native enzyme form is very slow, hence resulting in a direct loss of catalytic ability.

Product inhibition is another inactivation mechanism, which results from the adsorption or entrapment of HRP on the produced polymer, which hinders access of the substrate to active sites on the HRP. Both mechanisms lead to an increase in the amount of enzyme required for full removal and are responsible for the poor efficiency of peroxidase enzyme in remediation processes.

a)

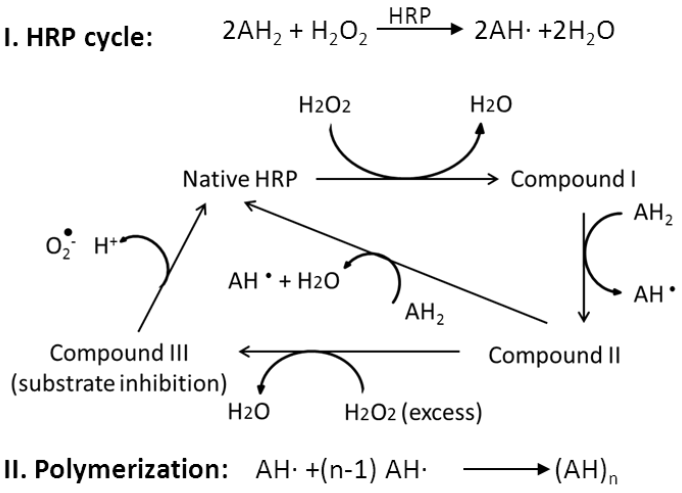

b)

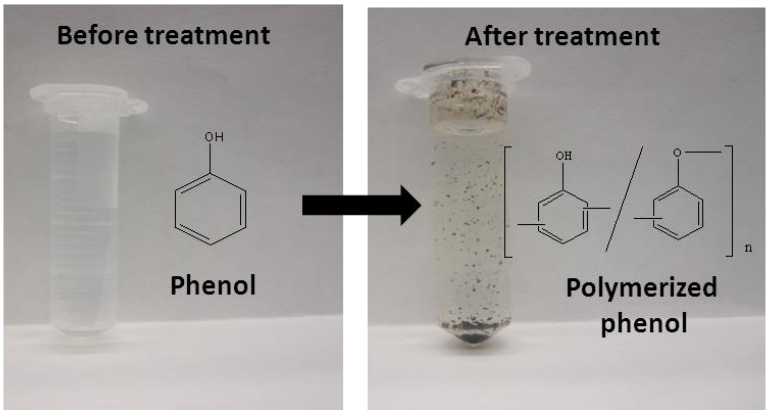

Figure 2.6 a) Schematic of HRP reaction cycle diagram and polymerization reaction; b) images of phenol solution before treatment and polymerized phenol after enzymatic treatment.

2.3.5 Phenol spectrum and its linear standard calibration curve

Figure 2.7a shows the spectrum of pure phenol from 200 nm to 700 nm. Due to the aromatic ring in phenol, it absorbs UV light. Phenol has a characteristic peak at 280 nm and there is a linear relationship between its absorbance and the concentration of phenol in a certain range, shown in Figure 2.7b. Therefore, in this chapter, the phenol concentration is determined by this spectral analysis using internal standard calibration.

2.3.6 Reaction ingredients

Reactions of phenol conversion are carried out at room temperature. The initial ingredients are phenol, HRP/BNC, hydrogen peroxide and dilute phosphate solution. Since the measurement of phenol concentration is directly based on spectral absorbance at 280 nm, the spectrum of other species used in the reactions should be evaluated first and a method needs to be developed to rule out potential interference at 280 nm. Figure 2.8 shows the spectra of free HRP, BNC-2, phenol and polymerized phenol. In these spectra, the concentrations of each species are the ones used in real reactions. In the reading at 280 nm, there is no absorbance for HRP and phosphate. However, for BNC biocatalyst, there is background contribution. Comparing the phenol and poly-phenol spectrum in Figure 2.8b, it shows a new peak around 430 nm in poly-phenol and there is a blue shift and slight shape change for the peak at the ultraviolet range.

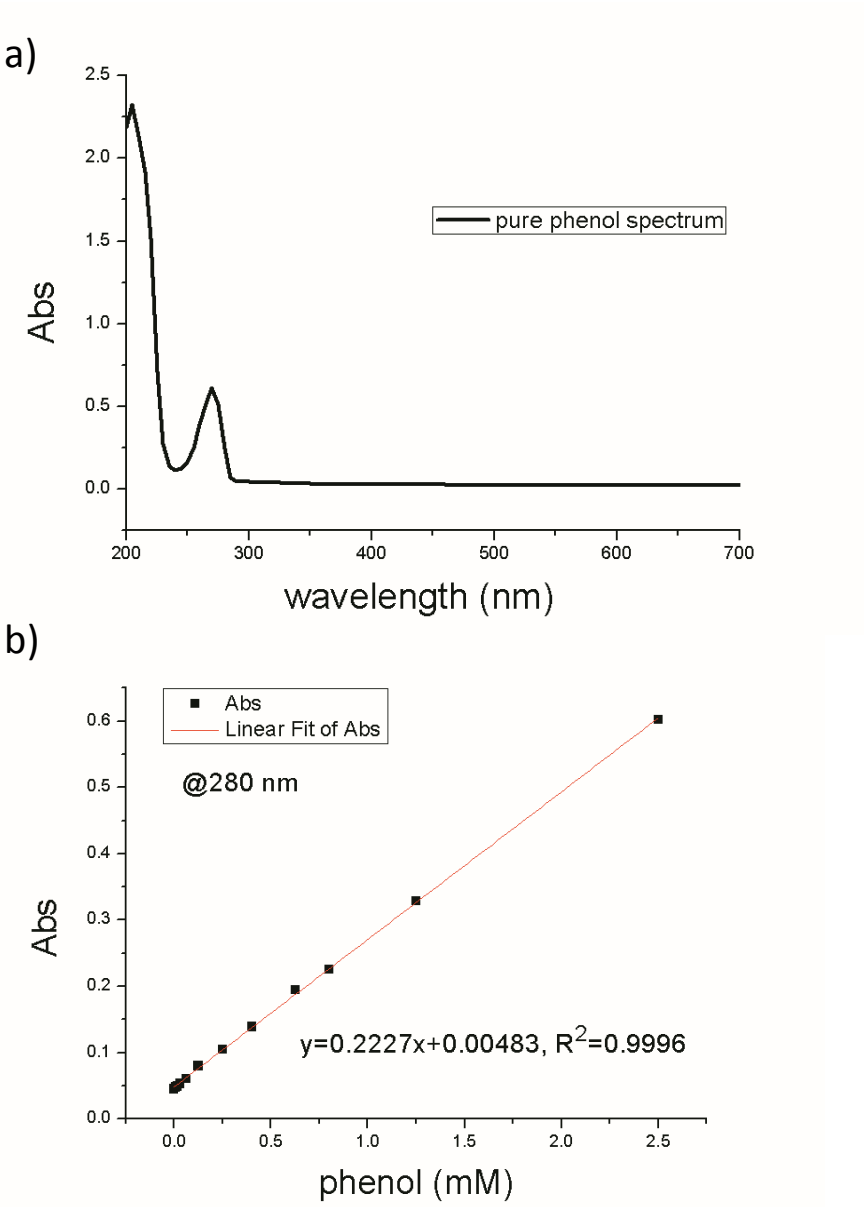

Figure 2.7 a) Pure phenol spectrum in UV-Vis spectrometer with a characteristic peak at 280 nm b) standard calibration curve of phenol concentration at 280 nm.

Salt solutions are effective for neutralizing charges of particles and colloids. Therefore, sodium chloride is used as a coagulation agent to precipitate polymerized phenol and biocatalyst in this system. The reaction procedure using salt is as follows: the phenol conversion is firstly carried out in the absence of NaCl. The samples are then centrifuged to separate MNP and salt is added to the supernatant at different concentrations. The final spectra are tested and shown in Figure 2.9. We can see that in the final spectra, the signal resulting from polymerized phenol decreases as the salt concentration increases. When the NaCl concentration is above 20 mM, all the polymerized phenol can be precipitated. Therefore, for all the tests, the procedure above was followed and the salt concentration was over 20 mM to ensure complete polymerization and phenol precipitation.

a)

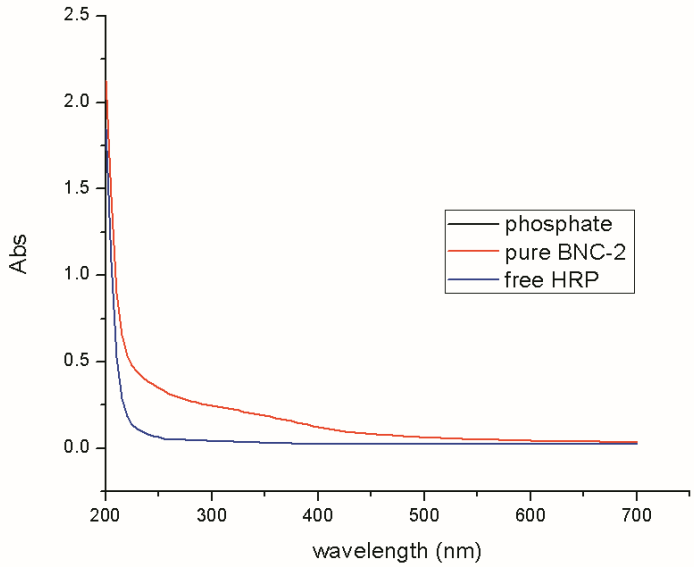

b)

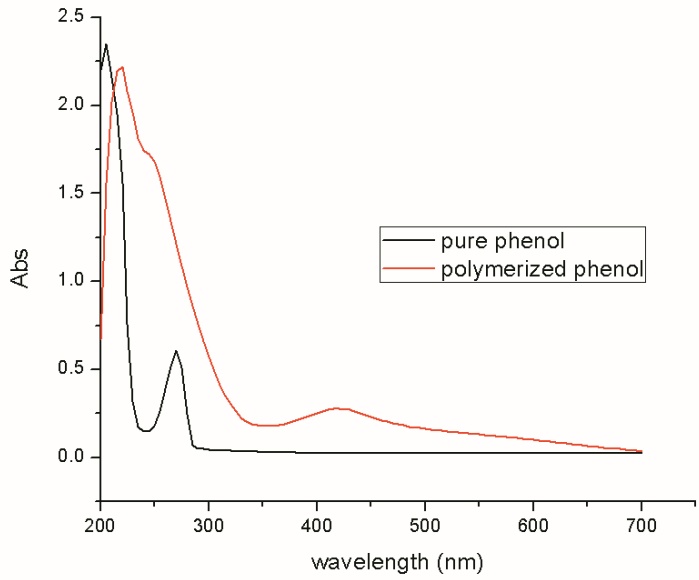

Figure 2.8 a) UV-Vis spectra of free HRP and BNC-2 b) pure phenol and polymerized phenol.

a)

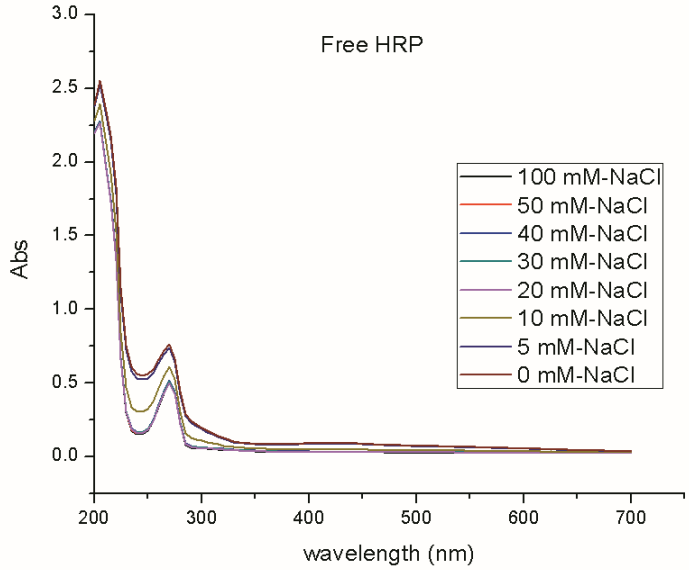

b)

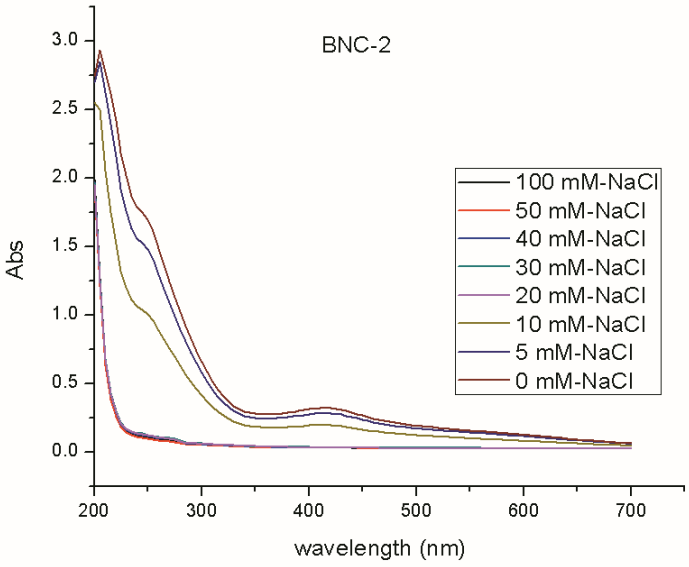

Figure 2.9 Spectra analysis of final products after reaction and treatment in different NaCl solutions a) using free HRP as the catalyst b) using BNC-2 during reaction.

2.3.7 Phenol removal and cost comparison

Phenol conversation reactions are tested following the procedures described above. Figure 2.10 shows the results of phenol removal using different BNCs and also compares them to the free HRP. The results show that all systems actively remove phenol but the BNCs are more effective than the free enzyme for the same concentration of HRP. The slope of the initial linear part for BNC-2 is more than 4 times that for the free enzyme, implying that the enzyme performs more efficiently in the BNCs. Moreover, to reach more than 90 % phenol removal, the amount of HRP required in the BNCs is 3 to 4 times less than that required for free HRP.

For practical applications, for the same level of pollutant removal, minimizing the amount of enzyme required is critical, since it accounts for most of the cost. From Figure 2.10, 3-4 times less enzyme is necessary to reach the same level of phenol removal, when the BNC is used.

We analyzed the cost comparison of MNP and HRP in the BNC-. For this calculation, we start with the concentrations of MNP and HRP, whose units are μg/ml and nM respectively.

$$\frac{[MNP]}{[HRP]} = \frac{ug/ml}{nM} = \frac{ug/ml}{nmol/L} = \frac{mg/L}{nmol/L} = \frac{mg}{nmol}$$

So in BNC-2, $\frac{[MNP]}{[HRP]} = \frac{ug/ml}{nM} = \frac{mg}{nmol} = 2$, which means 2 mg MNP will associate with 1 nmol HRP. The cost to synthesize MNP is 1.79×10^{-3} \$/mg and the price of HRP is 0.185 \$/nmol (prices were all obtained from Sigma-Aldrich on 11-01-2012).

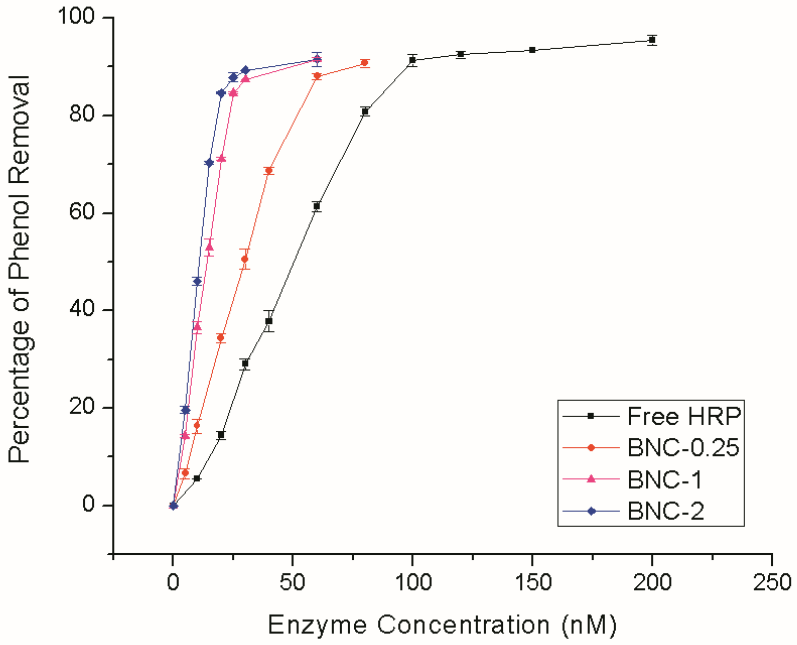

Figure 2.10 Phenol removal as a function of enzyme concentration for several systems after 12 hr at room temperature and [phenol]=[H_2O_2]=1mM. The error bars are the standard deviation of triplicates.

Therefore, the price ratio of HRP over MNP in BNC-2 is:

$$\text{price ratio} = \frac{1\ nmol\ \text{of HRP}}{2mg\ \text{of MNP}} = \frac{0.185\ \$/\text{nmol} \times 1\ \text{nmol}}{1.79 \times 10^{-3} \$/\text{mg} \times 2\ mg} = 52$$

Since the cost of the HRP is about 50 times that of the magnetic nanoparticles in BNC-2, the BNCs provide a real economic advantage compared to the neat HRP enzyme.

2.3.8 Kinetics

The kinetics of phenol removal using different catalyst systems are presented in Figure 2.11. The following conclusions can be drawn: (1) MNPs in the absence of HRP show no activity for phenol removal; (2) all BNCs are more active than the free HRP; (3) only assays containing the BNCs are capable of fully removing phenol.

All systems reach a final plateau after 2 hours. Thus, subsequent tests were run for at least 2 hours. The initial reaction velocities are summarized in Table 2.3. Similar to the extent of removal, the velocity generally increases as the ratio of MNP to HRP increases and reaches a plateau. For a fixed enzyme concentration, the relative increase in velocity equals the relative increase in activity (velocity/enzyme concentration). BNC-2 (and BNC-4) shows the highest activity, more than three times higher than that of free HRP. Note that the increased activity of the BNCs is unusual, since conventional enzyme-immobilization methods typically lead to an enzymatic activity loss. The results are consistent with the increased activity of HRP/nanoparticle assemblies reported earlier and are due to the presence of localized magnetic field effects (*vide infra*).[26,27] The plateau in velocity starting with BNC-2 is attributed to a saturation point where all the enzyme molecules interact with MNP. Adding more

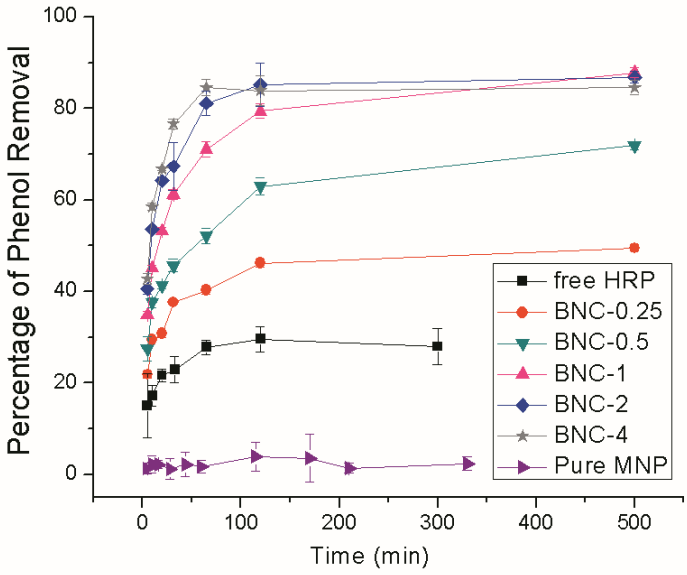

Figure 2.11 Kinetics of phenol removal for free HRP and hybrid catalyst systems at room temperature and [phenol]=[H_2O_2]=1 mM. The error bars are the standard deviation of triplicates.

magnetic nanoparticles after that point does not affect the HRP molecules and does not increase the activity. We conclude that the HRP bound to the MNPs have a higher activity.

Table 2.3 Velocities of phenol removal and relative increase in velocity at fixed concentration of HRP (30 nM)

	velocities (mM/s)	Relative increase in velocity
Free HRP	7.33×10^{-5}	1.00
BNC-0.25	8.67×10^{-5}	1.18
BNC-0.5	1.40×10^{-4}	1.91
BNC-1	1.94×10^{-4}	2.64
BNC-2	2.51×10^{-4}	3.42
BNC-4	2.49×10^{-4}	3.39

2.3.9 Substrate inhibition

All peroxidases are prone to substrate inhibition; excessive H_2O_2 concentrations lead to the formation of an inactivated form of the enzyme, as discussed earlier. From a stoichiometric standpoint, one molecule of H_2O_2 is required for the formation of two free phenoxy radicals that can subsequently polymerize (Figure 2.6). However, peroxidase based processes are not very resilient and need to be operated at sub-optimal concentrations of H_2O_2 to avoid local hot spots.[19] Therefore, the effect of H_2O_2 on the phenol removal was investigated. The extent of removal is dramatically enhanced compared to the free enzyme and a shift towards higher H_2O_2 concentration for reaching the maximum removal is observed (Figure 2.12). Interestingly, the H_2O_2 concentration range is effectively broadened as well. Substrate inhibition is limiting the use of peroxidases in many bioprocesses and, since BNCs increase the enzyme's tolerance to H_2O_2 as well as the extent of phenol removal, they offer practical advantages for the use of peroxidases.

2.3.10 Fundamentals and potential mechanism at play

The key role of magnetic field effects in the BNC assemblies has been demonstrated, contrasting the results with BNC-2 non-magnetic SiO_2 nanoparticles of similar particle size. These were mixed with HRP and then tested similarly in a phenol assay, resulting in final removal of $41.1\% \pm 0.7\%$ (the free enzyme removal is $32.2\% \pm 1.1\%$ under the same conditions). For comparison, the removal using the BNC in the same particle/enzyme mixed ratio is $91.0\% \pm 1.2\%$. The increased extent and velocity of the reactions with BNCs have been attributed to the localized magnetic field effects and surface morphology.

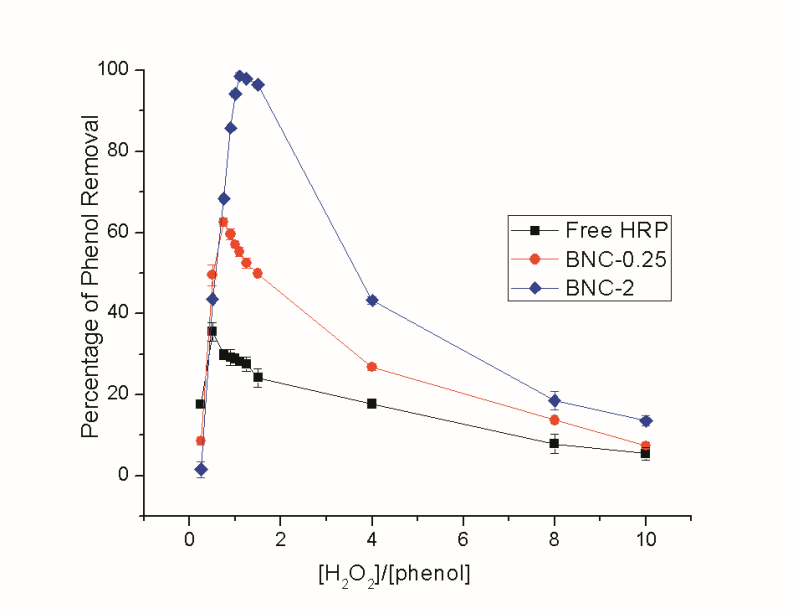

Figure 2.12 Extent of phenol removal for different ratios of $[H_2O_2]$ to [phenol] after 12 hr at room temperature: [phenol]=1mM and [HRP]=30nM. The error bars are the standard deviation of triplicates.

The magnetic field affects the spin dynamics and alters the Intersystem Crossing (ISC), thereby influencing biochemical processes.[31,32] Accordingly, a new mechanism focusing on the effect of magnetic nanostructures on chemical reactions has been proposed by Cohen,[33,34] consistent with our experimental results.[26,27] According to Cohen, catalytic reactions can be mediated by short-range magnetic interactions. Magnetic field gradients produced in nanostructures can be strong enough to affect radical pairs and each electron experiences a different local field enhancing the ISC rate. In our system, we believe that nanoparticles can generate local magnetic fields that play a role in mediating radical chemistry in the HRP cycle. From nitrogen sorption measurements, the average Barrett-Joyner-Halenda (BJH) pore diameter of the aggregates of the MNPs is 8 nm and, since the dimensions of an HRP molecule are 6.4 x 4.3 x 3.7 nm, [25] several HRP molecules can be accommodated within the pores of the MNP aggregates. This close proximity with the nanoparticles allows the enzyme molecules to "feel" the magnetic field generated by the MNPs. Since the magnetic field intensity scales inversely with the distance from the nanoparticle surface,[27] the effect can be considerable near the nanoparticles (especially for molecules confined within the pores). It is believed that this nanomagnetic flux influences the ISC in the HRP cycle, leading to the increase of reaction velocity. In a similar fashion, changes in spin chemistry might also influence the substrate inhibition. The return of compound III to the resting state via superoxide ions (Figure 2.6) also involves spin-correlated radical pairs.[35] In the vicinity of nanoparticles, magnetic field gradients might positively affect the HRP recovery and reduce inhibition, thus leading to a shift to higher and broader concentration of H_2O_2 (Figure 2.12).

Another reason for the dramatic improvement may be due to surface and structural effects. The end-product, polyphenols, can polymerize onto the enzymes hence

physically inactivating the catalysts. The Brunauer-Emmett-Teller (BET) surface area of MNP is 110 m²/g. The large surface provided by the MNP structure may lessen the polyphenol deposition on the HRP to some extent. This protection of HRP would increase the stability of HRP and provide an increased amount of HRP active sites for reaction. Another possibility might be that some of the produced radicals migrate and form polyphenol outside the pores of the biocatalyst. The so-formed polyphenol polymer chains are prevented from entering the restricted pore space and thus enzyme inactivation is prevented.

2.3.11 Reusability

Reusability is an important feature for any catalytic material and is the key to process efficiency. We investigated the reusability of BNC-2 using a rare earth magnet to capture and reuse the catalyst. A dramatic loss to the extent of removal from 91.0 % ± 1.2 % to 3.0 % ± 0.8% is observed in the second cycle. During the second cycle, the BNC became cloudy, suggesting that particle aggregation took place. Figure 2.13 illustrates the packing process during capture and the increased size from DLS data confirms the aggregation.

In view of the loss of BNC performance, a novel approach to stabilize BNCs was designed and tested. A new material, micron size magnetic particles (MMP), is introduced to the system. The physical properties of MMP are shown in Figure 2.14. The XRD confirms the magnetite or maghemite struture and the magnetization curves show the ferromagnetic nature of the material.

a)

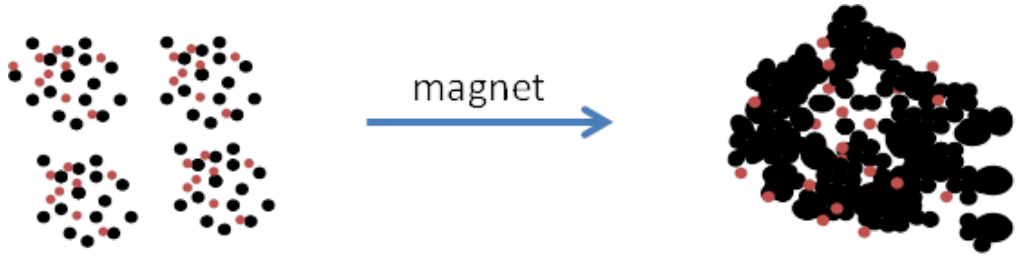

b)

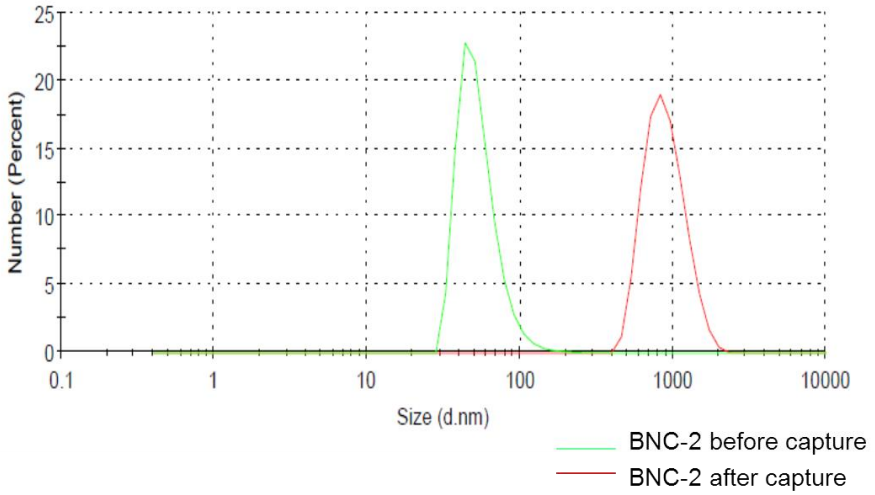

Figure 2.13 a) Aggregation scheme of BNC during magnet capture b) DLS data for the BNC before capture and after magnet capture.

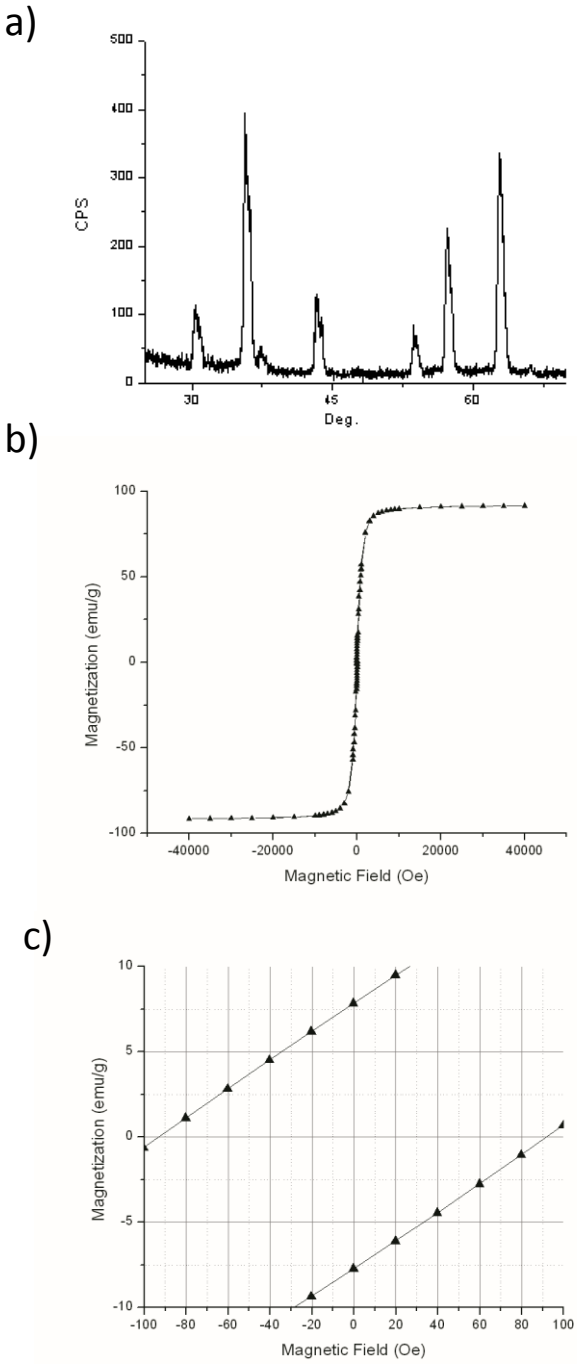

Figure 2.14 Properties of MMP a) XRD spectrum b) Magnetization hysteresis curves of c) a zoom-in of magnetization to show the remanence of MMP.

The MMP is used as a scaffold to support the BNC assembly. This new hierarchical catalyst is called Magnetic Hierarchical BNCs (MH-BNCs). The BNC-2 is magnetically attached onto the MMPs in MH-BNCs. The amount of BNC on the MMP was calculated by measuring the absorbance at 500 nm of the supernatant using a magnet to capture and separate the MH-BNC, since the intensity at 500 nm is proportional to the concentration of BNC. The BNC concentration in the supernatant was calculated based on the standard BNC calibration curve measured at the same time. After obtaining the concentration of supernatant ([S]), the effective binding is calculated based on the equation: 1-([S]/ [total BNC]). The results are shown in Figure 2.15.

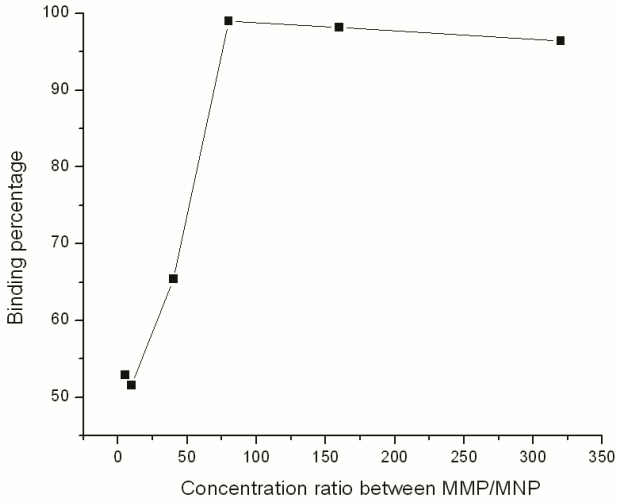

Figure 2.15 The extent of binding of BNC onto MMP for different ratios of MMP/MNP in the MH-BNC system.

MH-BNCs were synthesized as shown schematically in Figure 2.16. The BNCs are attached onto the larger magnetic particles MMPs, an attachment facilitated by magnetic interactions, which was also confirmed in the SEM images (Figure 2.17). Two systems were examined, with MMP to MNP mass ratios of 10 and 80, respectively, and their phenol removal after 5 cycles was evaluated (Figure 2.17). Both systems with the MMPs were significantly better than the BNCs alone in terms of reuse, with the system containing more MMP performing better.

We attribute the improved phenol removal performance to the formation of the hierarchical assemblies. In that regard, the system with the higher amount of MMP ensures that all of the BNCs are attached to the larger magnetic particles (Figure 2.15), which exhibited 90% phenol removal in the second cycle, almost the same as the first cycle. When an MMP/MNP ratio of 10 was used, only about 50% of the BNC was bound (Figure 2.15) and phenol removal for the second use is only 30% (Figure 2.17). The use of both nanometer and micron size magnetic particles provides two levels of assembly and clearly provides an advantage for the reusability of the catalysts.

We confirmed that the gradual decrease of phenol removal after each cycle (see above) is due to the accumulation of polyphenol on the catalysts using FTIR spectroscopy. Figure 2.18 shows the spectra after 1, 3, and 5 cycles. The build-up of polyphenols with each cycle can be clearly observed in FTIR (fingerprint region: 1700-800 cm^{-1}).

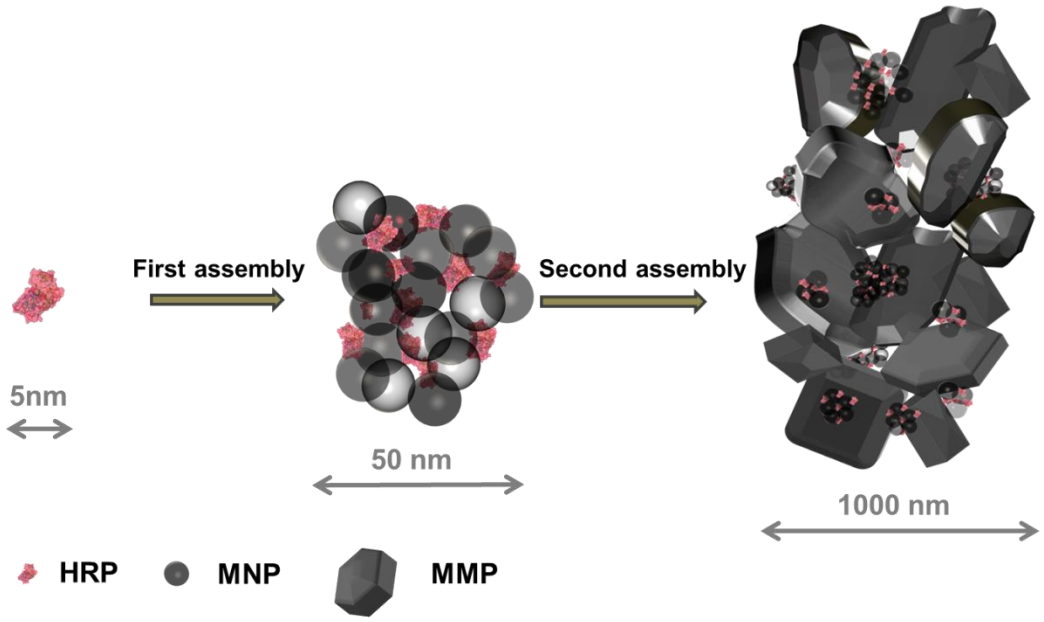

Figure 2.16 Schematic of proposed catalyst assembly of Magnetic Hierarchical BNCs (MH-BNCs).

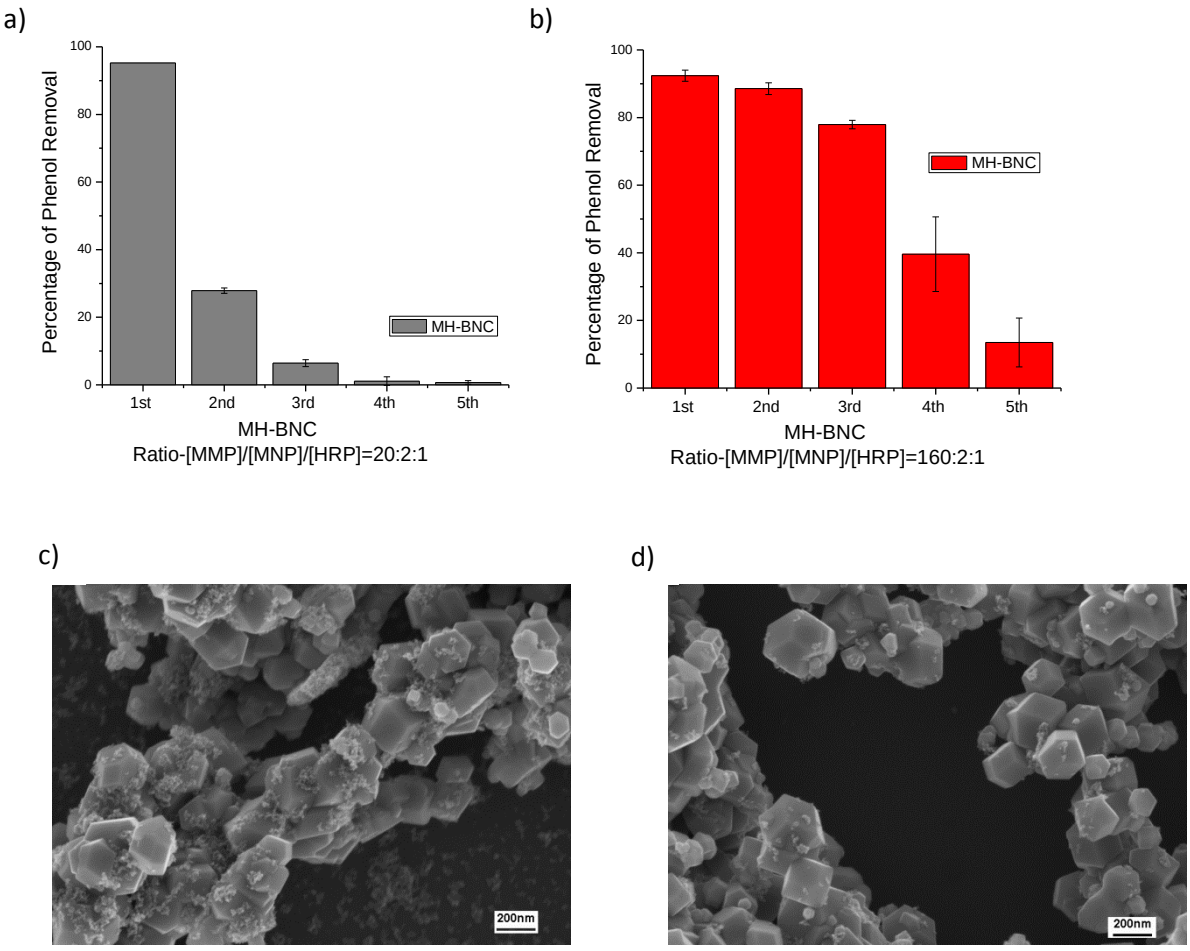

Figure 2.17 Reuse performance of catalysts after each cycle for five cycles: [phenol]=[H_2O_2]=1 mM; reaction time 2 hr at room temperature; [HRP]=30nM, [MNP]=60 ug/ml. a) [MMP]/[MNP]/[HRP]=20:2:1 b) [MMP]/[MNP]/[HRP]=160:2:1. The error bars are the standard deviation of triplicates. c) representative SEM of the [MMP]/[MNP]/[HRP]=20:2:1 and d) [MMP]/[MNP]/[HRP]=160:2:1 catalysts. The concentration of MMP was fixed at 600 ug/ml for both SEM images.

a): MH-BNC: Ratio-[MMP]/[MNP]/[HRP]=20:2:1

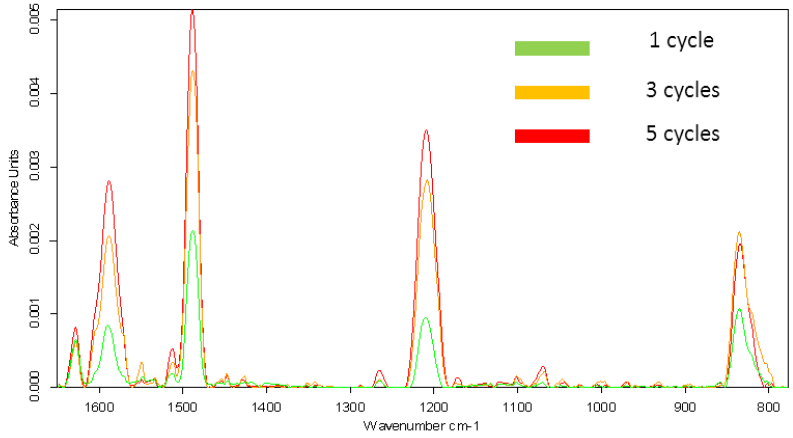

b): MH-BNC: Ratio-[MMP]/[MNP]/[HRP]=160:2:1

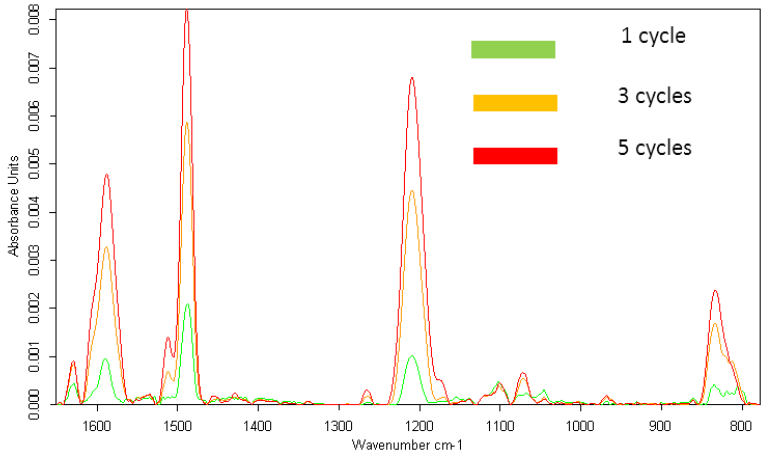

Figure 2.18 FTIR spectra of two MH-BNC system after reuse. Each cycle was run for 2 hr at room temperature with an [phenol]=[H_2O_2]=1 mM. [HRP]=30nM, [MNP]=60 ug/ml. a) less MMP, 600 ug/ml, of MH-BNC, where the ratio [MMP] /[MNP]/ [HRP]=20:2:1 b) more MMP, 4800ug/ml, in MH-BNC, where the ratio [MMP]/[MNP]/[HRP]=160:2:1. The smoothed spectra (25 point) were standardized for a magnetite signal and background-corrected.

2.3.12 Enzyme loss of MH-BNC during recycles

We also measured the amount of enzyme loss during each reuse cycle. The release of enzyme from the catalysts during each cycle was studied by placing the hybrid catalysts in low-binding tubes. There are three cycles in total. The supernatant solution was diluted to the testing range. The Amplex® Red kit was used to test the enzyme concentration following the product instructions. In brief, we prepared Amplex® Red reagents (100 μM) containing H_2O_2 (2 mM) in sodium phosphate (0.05 M, pH 7.4). Samples, standards and controls (50 μl) were pipetted into individual wells of a microplate. The Amplex® Red reagent/H_2O_2 (50 μl) working solution was added to each microplate well containing standards, controls and samples, followed by a 1 minute shaking protected from light. We used a microplate reader equipped for excitation at 550 nm and fluorescence emission detection at 590 nm. The enzyme concentrations of supernatant were calculated from the background-corrected fluorescence, using an internal standard calibration curve for each assay.

For the HRP catalyst with MMP/MNP/HRP ratios of 160:2:1 the average loss of HRP per cycle after three cycles is 0.32 ‰± 0.05‰, which was deemed to be an very insignificant loss of the catalyst implying a strong bonding of HRP on the support. The corresponding loss for MMP/MNP/HRP ratios of 160:0:1 is 1.12‰± 0.04‰ (Table 2.4).

Table 2.4 Enzyme release from MH-BNC during reuse cycles.

a) MH-BNC, where MMP/MNP/HRP=160:2:1

	leakage of enzyme in ‰	Standard deviation in ‰
S1/total enzyme	0.25	0.02
S2/total enzyme	0.38	0.07
S3/total enzyme	0.34	0.05

b) Biocatalyst, where MMP/MNP/HRP=160:0:1

	leakage of enzyme in ‰	Standard deviation in ‰
S1/total enzyme	1.30	0.03
S2/total enzyme	1.14	0.07
S3/total enzyme	0.93	0.03

2.3.13 Comparison of BMC and BNC

HRP also binds to micron-sized magnetic particles (MMP), albeit to a lesser extent, and the resulting hybrid catalysts are referred to as BioMicroCatalysts (BMC). BMC with different compositions are denoted as BMC-x, where x represents the ratio of the concentration of MMP (μg/ml) to the concentration of HRP (nM).

Figure 2.19 shows the performance comparison of BMCs and BNCs. Clearly, the performance of BMC-2 is significantly worse than that of BNC-2 (Figure 2.19a). In fact, BMC-2 shows a virtually identical performance to the free HRP. The surface area of MMP is 6 m^2/g, which is almost 20 times less than that of MNP. Interestingly in order to achieve the same level of phenol removal, twenty times more MMP than MNP is needed (Figure 2.19b). These results reinforce the importance of high surface to volume ratio of the nanoparticles.

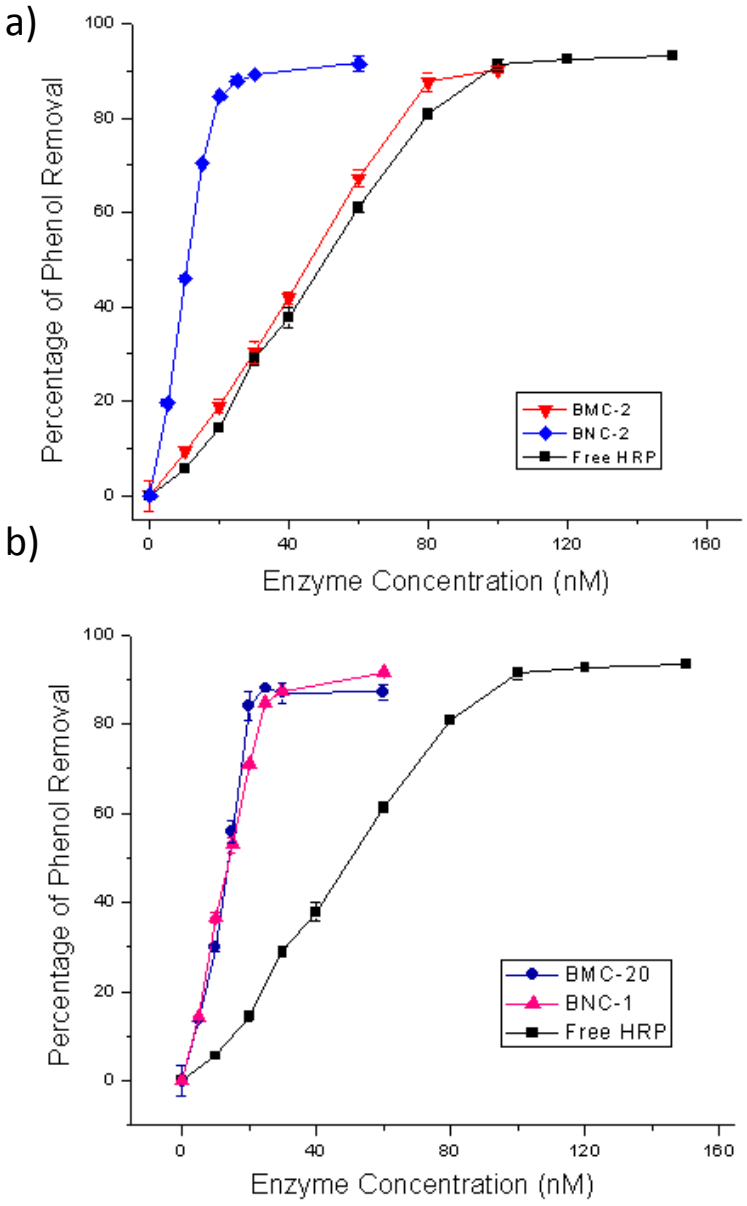

Figure 2.19 Phenol removal extent using BNC and BMC. Initial [phenol]=[H_2O_2]=1 mM and reaction after 12 hours at room temperature. a) the BNC and BMC are in the same mass concentration (μg/ml) of reaction assays. b) the BNC and BMC obtain the same surface area (m^2/g) in the reaction. The error bars are the standard deviation of triplicates.

2.3.14 Broader Discussion

The hierarchical material confining peroxidase enzymes can be used as enhanced performance catalyst for Advanced Oxidation Process (AOP) of phenol. The rational and cost-effective design that is implemented for the catalysts increases the peroxidase activity, reduces substrate inhibition, limits inhibition due to products, and allows for reusability. These net advantages now make HRP relevant to larger scale processes by lifting most of the limitations that have, so far, prevented the use of the free or conventionally immobilized enzymes. Peroxidases are catalysts optimized by nature and designed to provide specificity, control and efficiency to chemical reactions involving radicals. The fact that all peroxidases are so potent explains why they come with a safeguard that triggers inactivation in excess substrate. This safeguard disappears when the enzymes are confined in magnetic structures. Improvement of peroxidase enzymes has been receiving considerable attention for decades, and materials that mimic catalysis and are more resilient are actively sought after to alleviate this limitation. The "humble" nanomaterials and "simple" hierarchical confinement structures provides the *sine qua non* condition for the success of robust, economically sound, yet cutting-edge bioprocesses for industrial and environmental application. The sheer number of known peroxidases, number of substrates they can act on, theoretical reaction yields, and the diversity of reactions that can perform justifies the development of enzyme-based bioprocesses provided that their catalytic performances can be significantly magnified.

For this phenol AOP, we have exploited the oxidative dehydrogenation and H_2O_2 dismutation (catalase-like) reactions of HRP. However peroxidases can also perform highly selective and stereoscopic oxidative halogenation [42] and oxygen-transfer reactions [43] that are both key and complex reactions for the production of fine

chemicals. Although evidence of increased activity of those remain to be proven, the lift of substrate inhibition and reusability without a drop in activity constitute a strong argument for the hierarchical materials approach using enzyme catalysts at their core.

Finally, hierarchical materials address another fundamental concern, namely safety and sustainability. As nanotechnologies are increasingly introduced to bioprocesses and environment, the question arises about the fate of these highly reactive particles and the risk to health and safety. Taking advantage of nanoscale effects while confining low concentration nanoparticles on highly recoverable structures eliminates the inherent risks associated with nanoparticles. In addition, it has the potential to provide a truly facile and eco-friendly technology where "end-of-life" catalysts can be recovered quickly, concentrated and easily disposed.

The resulting catalysts are simple, cost-effective, innocuous inorganic and bio-materials. This blueprint can be used for similar functional architectures of catalysts for enzyme benefiting from magnetic field effects. For example, some peroxidases can be used for have large spectrum biocide activities and could be used for the decontamination of pathogens or for halogenation of phenolics. The catalytic reactions performed by fully functional peroxidase biocatalysts hence offer considerable potential for the development of a number of important renewable resources and find applications in a wide array of processes. Process efficiency, safety and economic viability have to be at the core of the design of such enhanced biocatalysts.

2.4 Conclusions

In conclusion, we have demonstrated a practical and cost-effective catalyst for phenol removal based on an enzymatic advanced oxidation process. Although phenol was used as a model compound in this study, peroxidases, HRP in particular, are well known to have a broad substrate range and have been shown to polymerize numerous aromatics including nonylphenols, Bisphenol A (BPA), dyes, PAH, hormones, and pesticides.[36-41] The new hierarchical catalyst increases the peroxidase activity, reduces substrate inhibition, limits inactivation from products, and allows for reusability. These advantages might pave the way for using HRP in large-scale processes by eliminating most of the limitations that have prevented the use of free or conventionally immobilized enzymes to date.

REFERENCES

1. Michalowicz, J.; Duda, W. Phenols–Sources and Toxicity. *Pol. J. Environ. Stud.* **2007**, *16*, 347–362.

2. Adelman, D. A Cautiously Pessimistic Appraisal of Trends in Toxic Regulation. *Wash. U. J. Law & Pol.* **2010**, *32*, 377–442.

3. Keith, Larry H;Telliard, W. A. Priority Pollutants: I-a Perspective View. *Environ. Sci. Technol.* **1979**, *13*, 416–423.

4. Ahmaruzzaman, M. Adsorption of Phenolic Compounds on low-Cost Adsorbents: a Review. *Adv. Colloid Interface Sci.* **2008**, *143*, 48–67.

5. Aitken, M. D. Waste Treatment Applications of Enzymes: Opportunities and Obstacles. *Chem. Eng. J.* **1993**, *52*, B49–B58.

6. Gianfreda, L.; Iamarino, G.; Scelza, R.; Rao, M. A. Oxidative Catalysts for the Transformation of Phenolic Pollutants: a Brief Review. *Biocatal. Biotransform.* **2006**, *24*, 177–187.

7. Oller, I.; Malato, S.; Sánchez-Pérez, J. A. Combination of Advanced Oxidation Processes and Biological Treatments for Wastewater Decontamination--a Review. *Sci. Total Environ.* **2011**, *409*, 4141–4166.

8. Gao, L.; Zhuang, J.; Nie, L.; Zhang, J.; Zhang, Y.; Gu, N.; Wang, T.; Feng, J.; Yang, D.; Perrett, S. *et al.* Intrinsic peroxidase-Like Activity of Ferromagnetic Nanoparticles. *Nat. Nanotechnol.* **2007**, *2*, 577–583.

9. Wei, H.; Wang, E. Fe_3O_4 Magnetic Nanoparticles as Peroxidase Mimetics and Their Applications in H2O2 and Glucose Detection. *Anal. Chem.* **2008**, *80*, 2250–2254.

10. Andrés, R.; Natálio, F.; Humanes, M.; Leppin, J.; Heinze, K.; Wever, R.; Schröder, H.-C.; Müller, W. E. G.; Tremel, W. V2O5 Nanowires with an Intrinsic Peroxidase-Like Activity. *Adv. Funct. Mater.* **2011**, *21*, 501–509.

11. Mu, J.; Wang, Y.; Zhao, M.; Zhang, L. Intrinsic peroxidase-Like Activity and catalase-Like Activity of Co_3O_4 Nanoparticles. *Chem. Commun.* **2012**, *48*, 2540–2542.

12. Chen, Z.; Yin, J.-J.; Zhou, Y.-T.; Zhang, Y.; Song, L.; Song, M.; Hu, S.; Gu, N. Dual Enzyme-Like Activities of Iron Oxide Nanoparticles and Their Implication for Diminishing Cytotoxicity. *ACS Nano* **2012**, *6*, 4001–4012.

13. Su, R.; Tiruvalam, R.; He, Q.; Dimitratos, N.; Kesavan, L.; Hammond, C.; Lopez-Sanchez, J. A.; Bechstein, R.; Kiely, C. J.; Hutchings, G. J. *et al.* Promotion of Phenol Photodecomposition over TiO2 Using Au, Pd, and Au-Pd Nanoparticles. *ACS Nano* **2012**, *6*, 6284–6292.

14. Klibanov, A. M.;Tu, T.; Scott, K. P. Peroxidase-Catalyzed Removal of Phenols from Coal-Conversion Waste Waters. *Science* **1983**, *221*, 259–261.

15. Wu, J.; Taylor, K. E.; Bewtra, J. K.; Biswas, N. Optimization of the Reaction Conditions for Enzymatic Removal of Phenol from Wastewater in the Presence of Polyethylene Glycol. *Water Res.* **1993**, *27*, 1701–1706.

16. Nicell, J. A.; Bewtra, J. K.; Taylor, K E; Biswas, N.; St.Pierre, C. Enzyme Catalyzed Polymerization and Precipitation of Aromatic Compounds from Wastewater. *Water Sci. Technol.* **1992**, *25*, 157–164.

17. Nakamoto, S; Machida, N. Phenol Removal from Aqueous Solutions by Peroxidase-Catalyzed Reaction Using Additives. *Water Res.* **1992**, *26*, 49–54.

18. Nicell, J. A. Kinetics of Horseradish Peroxidase-Catalysed Polymerization and Precipitation of Aqueous 4-Chlorophenol. *J. Chem. Technol. Biotechnol.* **1994**, *60*, 203–215.

19. Nicell, J. A.; Wright, H. A Model of Peroxidase Activity with Inhibition by Hydrogen Peroxide. *Enzyme Microb. Technol.* **1997**, *21*, 302–310.

20. Veitch, N. C. Horseradish Peroxidase: a Modern View of a Classic Enzyme. *Phytochemistry* **2004**, *65*, 249–259.

21. Tischer, W.; Wedekind, F. Immobilized Enzymes: Methods and Applications. *Top. Curr. Chem.* **1999**, *200*, 95–126.

22. Ikemoto, H.; Chi, Q.; Ulstrup, J. Stability and Catalytic Kinetics of Horseradish Peroxidase Confined in Nanoporous SBA-15. *J. Phys. Chem. C* **2010**, *114*, 16174–16180.

23. Dalal, S.; Gupta, M. N. Treatment of Phenolic Wastewater by Horseradish Peroxidase Immobilized by Bioaffinity Layering. *Chemosphere* **2007**, *67*, 741–747.

24. Bornscheuer, U. T. Immobilizing Enzymes: How to Create More Suitable Biocatalysts. *Angew. Chem. Int. Ed.* **2003**, *42*, 3336–3337.

25. Takahashi, H.; Li, B.; Sasaki, Toshiya; Miyazaki, Chie; Kajino Tsutomu; Inagaki, S. Catalytic Activity in Organic Solvents and Stability of Immobilized Enzymes Depend on the Pore Size and Surface Characteristics of Mesoporous Silica. *Chem. Mater.* **2000**, *12*, 3301–3305.

26. Chalkias, N. G.; Kahawong, P.; Giannelis, E. P. Activity Increase of Horseradish Peroxidase in the Presence of Magnetic Particles. *J. Am. Chem. Soc.* **2008**, *130*, 2910–2911.

27. Corgié, S. C.; Kahawong, P.; Duan, X.; Bowser, D.; Edward, J. B.; Walker, L. P.; Giannelis, E. P. Self-Assembled Complexes of Horseradish Peroxidase with Magnetic Nanoparticles Showing Enhanced Peroxidase Activity. *Adv. Funct. Mater.* **2012**, *22*, 1940–1951.

28. Yu, W. W.; Falkner, J. C.; Yavuz, C. T.; Colvin, V. L. Synthesis of Monodisperse Iron Oxide Nanocrystals by Thermal Decomposition of Iron Carboxylate Salts. *Chem. Commun.* **2004**, 2306–2307.

29. Mahadevan, S.; Gnanaprakash, G.; Philip, J.; Rao, B. P. C.; Jayakumar, T. X-ray Diffraction-based Characterization of Magnetite Nanoparticles in Presence of Goethite and Correlation with Magnetic Properties. *Physica E: Low-dimensional Systems and Nanostructures* **2007**, *39*, 20–25.

30. Pabisch, S.; Feichtenschlager, B.; Kickelbick, G.; Peterlik, H. Effect of Interparticle Interactions on Size Determination of Zirconia and Silica Based Systems – A Comparison of SAXS , DLS , BET , XRD and TEM. *Chemical physics letters* **2012**, *521*, 91–97.

31. Taraban, M. B.; Leshina, T. V Magnetic Field Dependence of Electron Transfer and the Role of Electron Spin in Heme Enzymes: Horseradish Peroxidase. *J. Am. Chem. Soc.* **1997**, *119*, 5768–5769.

32. Chignell, C. F.; Sik, R. H. Effect of Magnetite Particles on Photoinduced and Nonphotoinduced Free Radical Processes in Human Erythrocytes. *Photochem. Photobiol.* **1998**, *68*, 598–601.

33. Cohen, A. E. Nanomagnetic Control of Intersystem Crossing. *J. Phys. Chem. A* **2009**, *113*, 11084–11092.

34. Lee, H.; Yang, N.; Cohen, A. E. Mapping Nanomagnetic Fields Using a Radical Pair Reaction. *Nano Lett.* **2011**, *11*, 5367–5372.

35. Karogodina, T. Y.; Sergeeva, S. V.; Stass, D. V.; Steiner, U. E. Magnetic Field Effect on Recombination of Nitric Oxide and Superoxide Anion in High Magnetic Field. *Dokl. Phys. Chem.* **2011**, *436*, 5–7.

36. Auriol, M.; Filali-Meknassi, Y.; Tyagi, R. D.; Adams, C. D. Oxidation of Natural and Synthetic Hormones by the Horseradish Peroxidase Enzyme in Wastewater. *Chemosphere* **2007**, *68*, 1830–1837.

37. Auriol, M.; Filali-Meknassi, Y.; Tyagi, R. D.; Adams, C. D.; Surampalli, R. Y. Endocrine Disrupting Compounds Removal from Wastewater, a New Challenge. *Process Biochem.* **2006**, *41*, 525–539.

38. Wagner, M.; Nicell, J. A. Peroxidase-Catalyzed Removal of Phenols from a Petroleum Refinery Wastewater. *Water Sci. Technol.* **2001**, *43*, 253–260.

39. Tsutsumi, Y.; Haneda, T.; Nishida, T. Removal of Estrogenic Activities of Bisphenol A and Nonylphenol by Oxidative Enzymes from lignin-Degrading Basidiomycetes. *Chemosphere* **2001**, *42*, 271–276.

40. Tatsumi, K.; Wada, Shinji; Ichikawa, H. Removal of Chlorophenols from Wastewater by Immobilized Horseradish Peroxidase. *Biotechnol. Bioeng.* **1996**, *51*, 126–130.

41. Zhang, G.; Nicell, J. A. Treatment of Aqueous Pentachlorophenol by Horseradish Peroxidase and Hydrogen Peroxide. *Water Res.* **2000**, *34*, 1629–1637.

42. Osborne, R. L.; Raner, G. M.; Hager, L. P.; Dawson, J. H. C. Fumago Chloroperoxidase Is Also a Dehaloperoxidase: Oxidative Dehalogenation of Halophenols. *J. Am. Chem. Soc.* **2006**, *128*, 1036–1037.

43. Rantwijk, F. Van; Sheldon, R. A. Selective Oxygen Transfer Catalysed by Heme Peroxidases: Synthetic and Mechanistic Aspects. *Curr. Opin. Biotechnol.* **2000**, *11*, 554–564.

CHAPTER 3

A HIGHLY EFFICIENT AND SELECTIVE POLYSILSESQUIOXANE SORBENT FOR HEAVY METAL REMOVAL[1]

3.1 Introduction

Considerable efforts are under way worldwide to remove heavy metal ions from contaminated water because of their detrimental effect on the environment and human health.[1] For instance, Cu (II) ions inhibit growth of plants and adversely affect the liver and nervous system of humans.[1-3] As a result of their toxicity, various approaches such as precipitation, ion-exchange, reverse osmosis and adsorption have already been developed to remove heavy metals from various sources. Among these methods, adsorption has drawn particular attention due to its ease of handling, low energy consumption, and high process flexibility.[4-6]

Two of the most widely studied sorbents for heavy metal removal are based on polymers and mesoporous organosilicas. For practical applications, both a high adsorption capacity and a high selectivity are desirable. High adsorption capacity results in an effective removal of contaminants while high selectivity is necessary to recover particularly valuable ions.[2,4] Polymer-based sorbents include both synthetic and semi-natural polymers with carboxylic acid, sulfonic acid, and imidazole

[1] Reprinted in part with permission from Duan, X.; Qi, G.; Wang, P.; Giannelis, E. P. ChemPhysChem 2012, *13*, 2536–2539. Copyright © 2012 WILEY-VCH Verlag GmbH & Co. KGaA, Weinheim.

functional groups.[2-8] Generally, polymer-based sorbents are non-selective toward heavy metals and an increase in their selectivity comes at the expense of capacity.[8]

In contrast to polymer-based sorbents, mesoporous organosilicas are potentially more promising candidates for metal ion adsorption due to a number of advantages including high surface area, tunable pore structure, and ease of functionalization.[9-17] Two major synthetic approaches have been used to synthesize mesoporous organosilicas a) grafting or co-condensation of functional groups on the surface of mesoporous silica and b) one-pot synthesis involving direct incorporation of functional groups inside the silica framework (poly-silsesquioxane sorbents) using appropriate precursors.[10,18]

In the former approach, a number of silanes containing various pendant groups have been grafted onto silica[19-21] and their metal adsorption capacities were investigated. For instance, the adsorption selectivity of MCM-41-based materials toward Ag (I) and Cu (II) ions was successfully fine-tuned by manipulating the chemistry of the post-grafted functional groups.[19] The Cu (II) adsorption capacity of the thiol-functionalized SBA-16 and of the N-propylsalicylaldimino-functionalized SBA-15 were 36 and 59 mg/g.[20-24] Furthermore, a series of nanoporous sorbents with chelating diamines were studied to selectively remove Cu (II) from natural waters, and a maximum capacity of 26 mg/g of sorbent was reported.[25] High adsorption of Cu (II) ion with 139 mg/g (2.2 mmol/g) was obtained by attaching N-[3-(trimethoxysilyl)propyl]diethylenetriamine onto the silica surface. Co-condensation of thiol-silane and a silica precursor gave a mesoporous material with adsorption capacities of 82, 170, 186 mg/g for Cu (II), Cr (III), and Cd (II) respectively.[22-24] Amine ligands can also be immobilized with mesoporous silica non-covalently. High adsorption of Cu (II) (278 mg/g) was achieved by post-expanding the pores of the sorbent with N-N dimethyldodecylamine

(DMDDA), but regeneration was poor due to the progressive loss of amines.[26,27] In this method, an increase in the density of functional groups in the sorbent comes usually at the expense of surface area available for metal ions, ultimately compromising the performance of the sorbent.

In the latter approach, a precursor, with a formula of $(R'O)_3$-Si-R-Si-$(OR')_3$, where R contains a potentially active group, such as an amine, is used to allow integration of active groups inside the framework, and not just as side chains. This direct incorporation of functional groups in the sorbent walls offers many advantages including: 1) uniform distribution of active groups throughout the material in a one-pot process; and 2) high concentration of these groups accessible to metal ions. [28,29]

Several studies have already been reported using such intraframework organosilicas in the hope of attaining high capacity of heavy metal removal. In 2002, Mercier et al. [29] first reported the use of an organosilica-based sorbent for metal ion adsorption, synthesized by adding 2 - 5 mol% of N, N'-bis-[3-(trimethoxysilyl)propyl]-ethylenediamine (TMSEN) into tetraethyl orthosilicate. However, the Cu (II) adsorption capacity reported for that system was relatively low (2.2 mg/g) due to the low concentration of amine groups present. The adsorption capacity did not increase by adding ethylenediamine into the organosilica network.[10,30] A better performance (39 mg/g for Cu (II)) was obtained from mesoporous organosilicas synthesized by co-condensation of N-(2-aminoethyl)-3-aminopropyltrimethoxysilane and bis(triethoxysilyl)ethane. However, in this case, the amine groups were grafted onto the surface and, thus, did not reflect intra-framework metal ion adsorption.[31] The results above show that organosilica, including polysilsesquioxane-based sorbents, can compete effectively in terms of adsorption capacity only if a high concentration of active groups are integrated into the framework, while the porous network, usually

indicated by the accessible surface area, is maintained. To that end, Burleigh et al. and Tang et al. prepared poly-(TMSEN)s in emulsions using either cationic or anionic surfactant templates. Unfortunately, they obtained materials with low surface areas (30 m ²/g), which was attributed to the pore collapse during surfactant extraction.[17,31]

In this chapter, we report a high capacity polysilsequioxane sorbent based on TMSEN. In contrast to previous work, the new sorbent was synthesized using TMSEN as the sole precursor in a one-pot synthesis to obtain a high amine loading and a high surface area, which is the first attempt of such a system for heavy metal ion removal. The sorbent thus synthesized exhibited a high adsorption capacity towards Cu (II) and Pb (II) ions. After adsorption, the system can be readily regenerated to its full capacity. It also shows high selectivity for Cu (II) over Ni (II) and Co (II). As such this new sorbent may pave the way for new applications in the fields of wastewater treatment, drinking water purification, and even soil remediation.

3.2 Experimental sections

3.2.1 Chemicals and Materials

All chemicals were obtained from commercial sources and were used without further purification. N, N'-bis-[3-(trimethoxysilyl)propyl]-ethylenediamine (TMSEN, 62% in methanol) was purchased from Gelest, Inc. Nitrate-heavy metal salts ($Co(NO_3)_2$ $6H_2O$, $Pb(NO_3)_2$, $Cu(NO_3)_2$ $2½$ H_2O and $Cr(NO_3)_3$ $9H_2O$), nickel chloride($NiCl_2$ $6H_2O$) and Poly (ethylene glycol)-block-poly (propylene glycol)-block-poly (ethylene glycol) block polymer (P123, MW=5800) were all obtained from

Sigma-Aldrich. Ethanol (95%) was supplied from VWR. Deionized water was generated with a Milli-Q integral ultrapure water purification system.

3.2.2 Synthesis of amine-bridged organosilica sorbent

The amine-bridged organosilica was synthesized by condensation of TMSEN in the presence of a nonionic surfactant, P123. In a typical procedure, TMSEN (4g) were mixed first with P123 (4g, preheated to 50 ºC) before deionized water (1 g) was added at room temperature under vigorous stirring. The mixture was stirred until it became a gel, typically within five minutes. The gel was then aged for 1 day at room temperature and for 2 more days at 70 º C. The templating surfactant (P123) was removed by washing the sample several times with ethanol before freeze-drying overnight.

3.2.3 Materials Characterization

Bright-field transmission electron micrographs (TEM) images were obtained on a FEI Tecnai T12 Spirit Twin TEM/STEM operated at 120kV. Scanning electron microscope (SEM) images were obtained on a Keck Field Emission SEM, LEO 1550 model.

X-ray Diffraction (XRD) patterns were obtained on a Scintag diffractometor using CuKα (λ=1.54 Å) radiation. Nitrogen adsorption-desorption isotherms were obtained on a Micrometrics ASAP 2020 physi-sorption instrument. The specific surface areas of the samples were calculated by the Brunauer-Emmett-Teller (BET) method. Pore size distributions were calculated from the N_2 adsorption isotherm using the Barrett–Joyner–Halenda (BJH) method.

Thermogravimetric analysis (TGA) was performed from 35℃ to 1000 ℃ on a TA Instruments Q5000 thermal graphic analyzer using compressed air and a heating rate of 10℃/min. Elemental analysis was conducted by Mircro-analysis Inc. (Wilmington, DE). X-ray photoelectron spectroscopy (XPS) analysis of the sorbents before and after ion adsorption was obtained with a Surface Science Instruments (SSI) model SSX-100 utilizing monochromated Aluminum K-alpha x-rays (1486.6 eV). To rule out any potential interference from the nitrate ions on the XPS spectra, the chloride analogs were used for these measurements. The neutral C1s peak at 284.6 was used as a reference in all spectra. For spectra fitting, we used the CasaXPS 2.3.14 software.

Metal ion adsorption capacity was evaluated using an Inductively Coupled Plasma-atomic emission spectrometer (ICP-AES; model ICAP 61E trace analyzer, Thermo Electron, Waltham Ma). The transfer optics had been replaced with a short depth of field transfer optics to reduce matrix effects.

3.2.4 Adsorption studies

For all adsorption tests, the solid to liquid ratio was kept constant at 11.5 mg sorbent in solution (46 ml) and the adsorption was conducted in tubes at room temperature for more than 12 hours, which was proved enough to reach equilibrium. The pH was adjusted to 5.0-5.5 in all non-competitive adsorption experiments and there is not significant pH change before and after adsorption. For the competitive adsorption experiments, the pH was also adjusted to 5.0-5.5 except for the Cu (II)/Cr (III) adsorption, which was left at 4.0 (to avoid precipitation at a higher pH value). All other conditions were the same as in the non-competitive adsorption.

The suspension, after equilibrium, was centrifuged and the supernatant (5ml) was further filtered for ICP-AES analysis. The concentration of the metal ion sorbed, Q (mg/g) was calculated by

$$Q = (C_0 - C_e) \cdot V / m$$

where Co and Ce are the initial and equilibrium ion concentrations, respectively, V is the volume of the solution, and m is the mass of the sorbent. The percent removal was calculated by

$$(C_0 - C_e) \times 100 / C_0$$

3.2.5 Sorbent regeneration

The sorbent was regenerated by stirring with HNO_3 (1M) overnight at room temperature, followed by washing with DI water and ethanol. Before being added to an ion solution, the sorbents were conditioned in concentrated ammonium hydroxide solution to eliminate any residual acid.

3.3 Results and discussions

3.3.1 Materials and Characterization

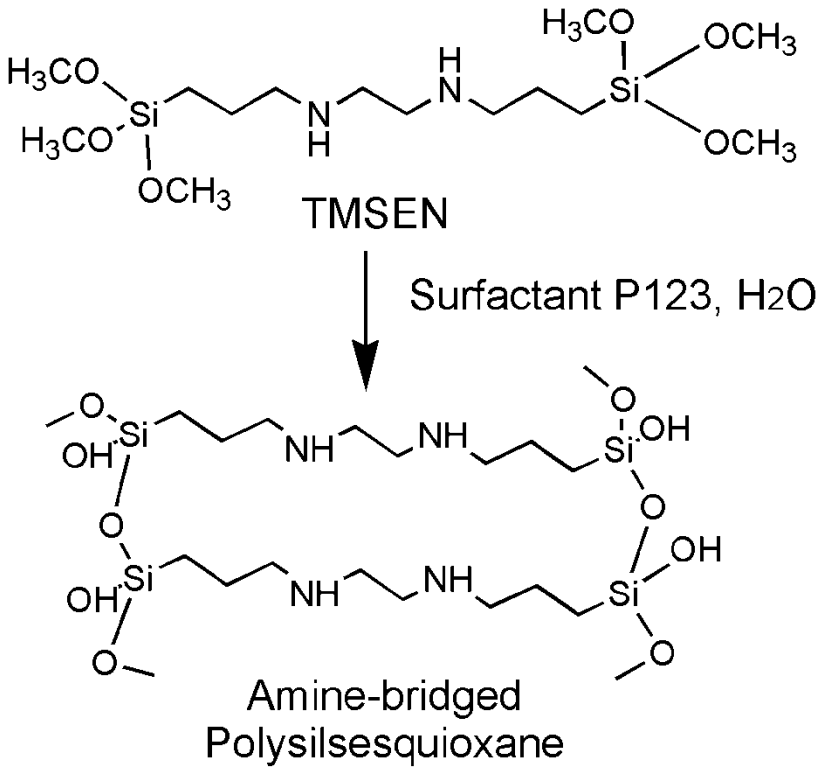

Figure 3.1 Schematic illustration of the synthesis of the mesoporous organosilica.

The bis-amine-bridged polysilsesquioxane was synthesized in a simple, one-step process with TMSEN as the sole precursor, as shown schematically in Figure 3.1. The amount of surfactant P123 and the water content controlled both the cross-linking rate of TMSEN precursors and the morphology of the hybrids.

The synthesis leads to a sponge-like material with a uniform pore structure as shown in the SEM images (Figure 3.2). The mesoporous organosilicas synthesized in this study exhibit a type IV adsorption isotherm (Figure 3.3) with a BET surface area of 310 m ²/g. [32] The average pore size of the sorbent based on the Barrett-Joyner-Halenda (BJH) model is 8.5 nm (Figure 3.3), in agreement with estimates from TEM.

The ^{29}Si MAS NMR spectrum (Figure 3.4a) shows a dominant peak at 57.9 ppm, corresponding to the T^2 structure ($CSi(OH)(OSi)_2$). The small shoulder around 49.0 ppm is attributed to the T^1 ($CSi(OH)_2(OSi)$) silicon sites. The absence of signal in the range of 90 to 110 ppm indicates that there is no cleavage of Si-C bonds during the synthesis.[33] The XRD patterns are basically featureless (Figure 3.4b) implying that the pores are not highly ordered.

From elemental analysis, the content of the diamine ligand (-NH-CH_2-CH_2-NH-) of the sorbent is 3.5 mmol/g. This large amount of functional groups within the sorbent, can act potentially as binding sites to metal ions. Moreover, with our synthesis method, we expected a homogeneous distribution of the amine functional groups embedded within the wall of the materials.

Owing to our interest in developing sorbents for heavy metal removal, we evaluated the capacity and selectivity of the new material for the removal of several ions and ion combinations.

a)

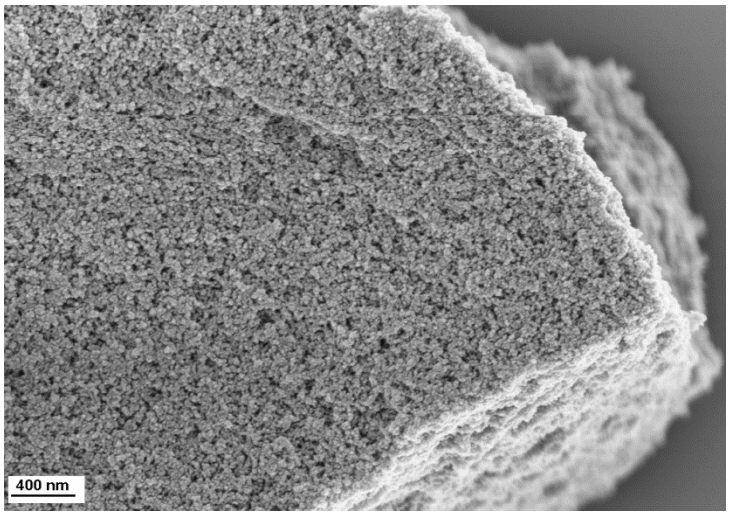

b)

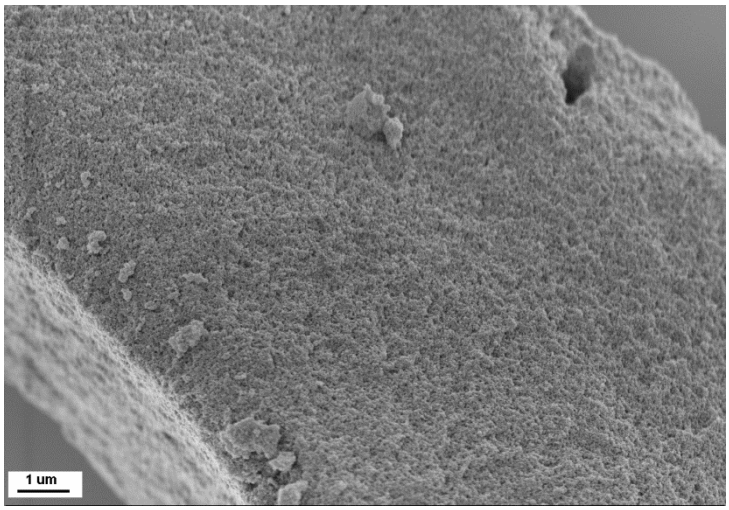

Figure 3.2 SEM images of the synthesized sorbent: 1) scale bar = 200nm; 2) scale bar=1 μm.

a)

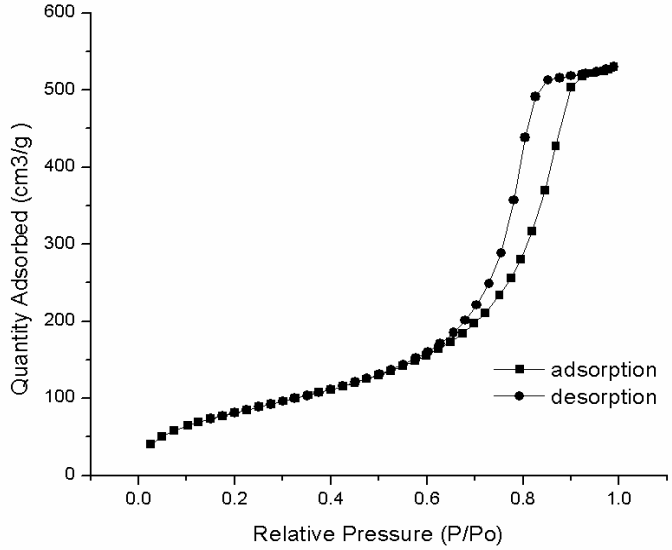

b)

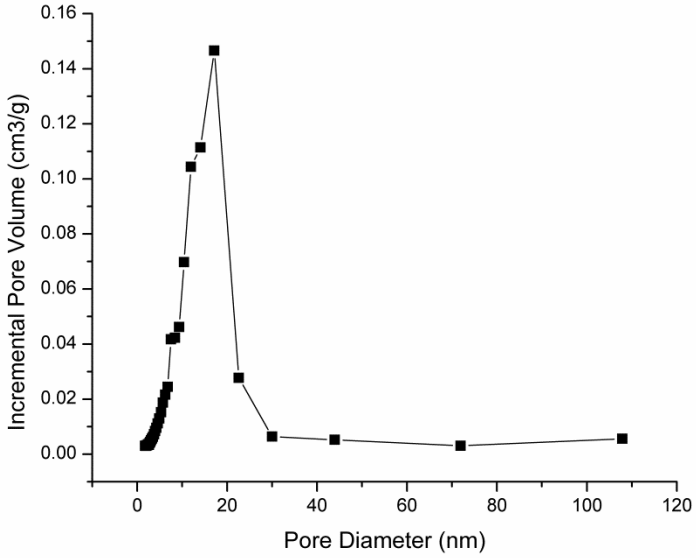

Figure 3.3 a) N_2 adsorption-desorption isotherm of the synthesized sorbent. b) The corresponding pore size distribution.

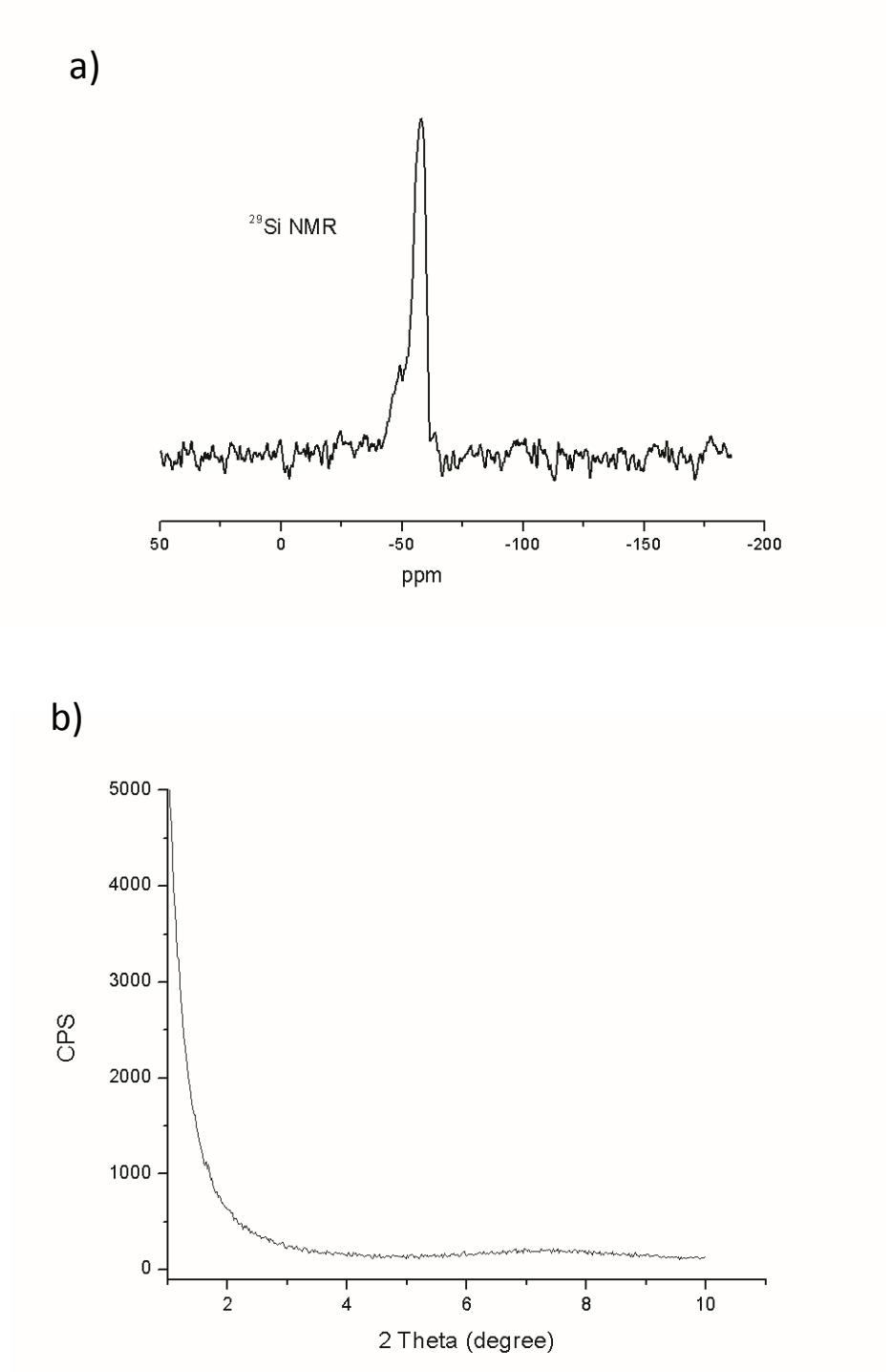

Figure 3.4 a) ^{29}Si MAS NMR spectrum b) XRD pattern of the sorbent.

3.3.2 Metal ion adsorption isotherms

We performed both non-competitive (single ion) and competitive (multiple ions) adsorption experiments of the sorbent. For non-competitive studies, adsorption trials with different ions and initial concentrations are denoted as S-X-m, where X and m represent the adsorbed ion species and the initial concentration of the ion in mg/L, respectively; for the competitive adsorption experiments, the trials are denoted as S-X/Y-m, where X/Y and m represent the ion pair used and the initial concentration of the solution in mg/ L, respectively.

1) **pH effect**

As pH may significantly affect sorption behavior, the adsorption of Cu (II) and Pb (II) onto the sorbent under different pHs was first investigated (Figure 3.5). The metal ion adsorption increased with increasing pH and the highest adsorption was achieved at pH 6 for both Cu(II) and Pb(II) ions. Lower ion sorption at lower pH is due to the competition between protons and metal ions for the active adsorption sites of the sorbent.[5] It should be noted that adsorption was not studied at pH>6 due to the potential formation of metal hydroxide precipitates, which would have complicated the analysis.

2) **Non-competitive adsorption**

Figure 3.6 presents the adsorption isotherms for Cu (II) and Pb (II) ions, which were determined under non-competitive conditions by varying the initial ion concentrations while keeping the solution pH constant at =5.5. The adsorption of both ions increased initially with the equilibrium ion concentration but leveled off at higher concentrations, in agreement with a typical Langmuir adsorption behavior.

a)

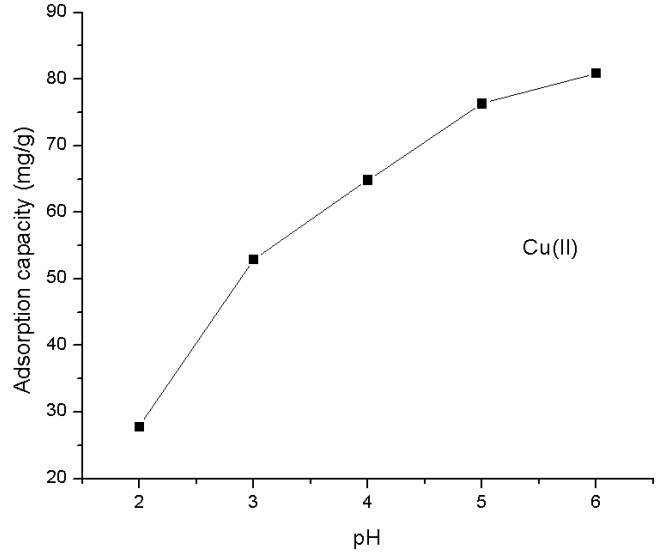

b)

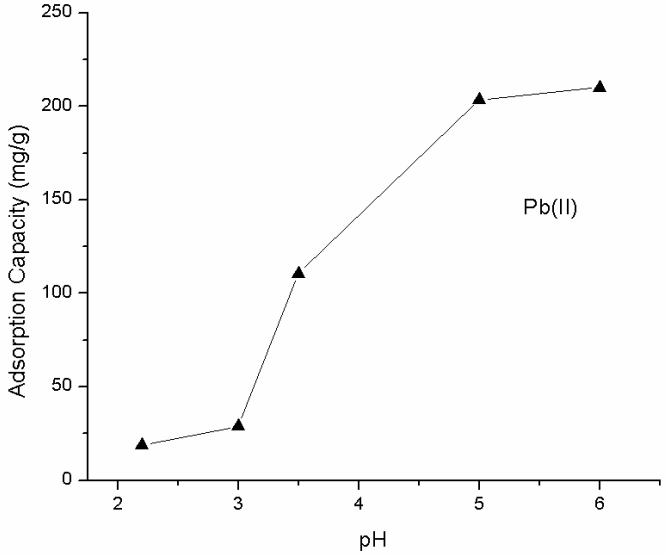

Figure 3.5 pH effect on the adsorption of a) Cu (II) and b) Pb (II) ions. The initial concentration of both solutions was 100 mg/ L.

The adsorption capacities (determined from the plateaus of Figure 3.6) were 76.8 and 275.8 mg/g (1.2 and 1.3 mmol/g) for Cu (II) and Pb (II) ions, respectively. The enhanced capacity, compared with the one previously reported (2.2 mg of Cu(II) per gram of sorbent) can be contributed to the sorbent's robust porous structure and high amine ligand content. These capacities are amongst the highest reported for organosilicas.

The adsorption data were fitted to the Langmuir isotherm:

$$Q_e = \frac{aQ_m C_e}{1 + aC_e}$$

where Ce and Qm represent the equilibrium ion concentration and the maximum adsorption capacity (mg/g) of the sorbent for the specific ion, respectively, and a is a constant, characteristic of the adsorption energy.[2] Clearly the adsorption data can be fitted to the Langmuir model with R^2 being greater than 0.99 in both cases (Table 3.1).

Elemental analysis revealed the ligand content (-NH-NH-) of the sorbent to be 3.5 mmol/g. Given that the Cu (II) and Pb (II) ion adsorption capacities are 1.2 and 1.3 mmol/g respectively, we estimate that 34% and 37% of these binding sites are accessible to Cu (II) and Pb (II) ions for adsorption. This binding efficiency of Cu (II) ions is 7 times higher than previously reported (4.7%).[29]

a)

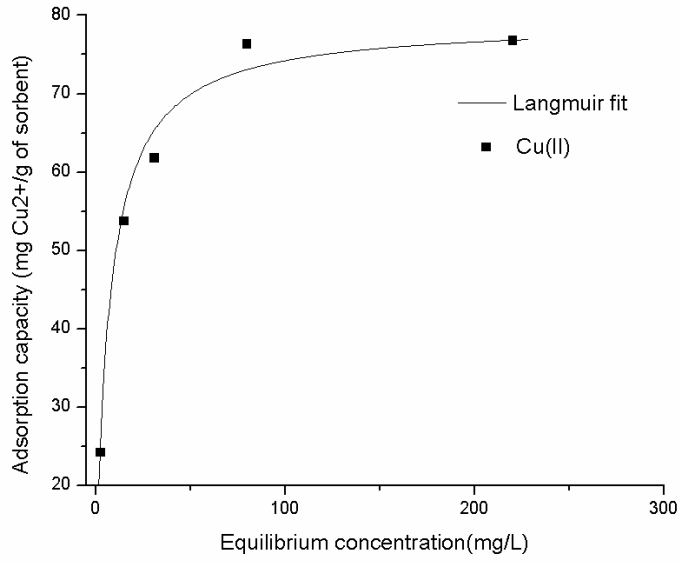

b)

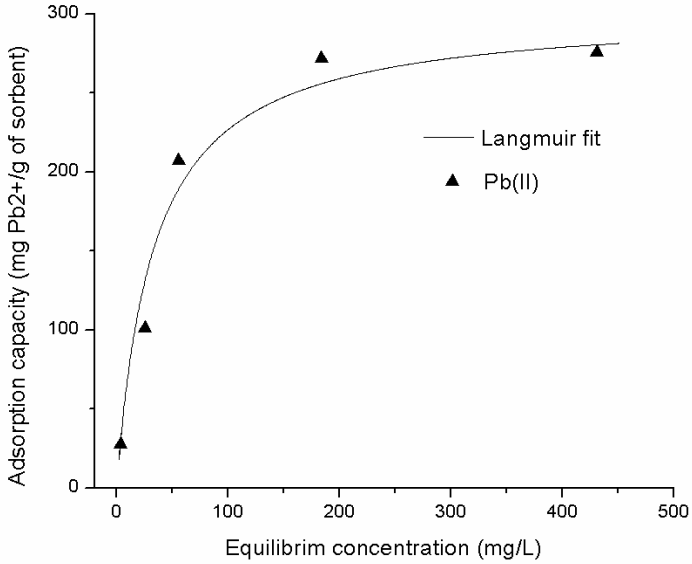

Figure 3.6 Adsorption of a) Cu (II) and b) Pb (II) ions on the sorbent.

Table 3.1 Langmuir isotherm model parameters for adsorption of Cu (II) and Pb (II) ions on the sorbent.

	Langmuir		
metal ion	Qm (mg/g)	a (L/mg)	R^2
Cu(II)	79	0.15	0.999
Pb(II)	301	0.03	0.994

3.3.3 Recyclability of the sorbents

The regeneration and reuse of the sorbent was studied using Cu (II) ions as a model system. The sorbents were regenerated with HNO_3 (1M) followed by washing with DI water and ethanol. Before exposure to the Cu (II) solution, the sorbents were conditioned in a solution of concentrated ammonium hydroxide to eliminate any residual chemisorbed protons.

As shown in Figure 3.7, the adsorption capacity of the sorbent toward Cu (II) remained almost the same after three cycles of regeneration and reuse. Additionally, the BET surface areas of the pristine and once regenerated sorbent were virtually identical (310 and 315 m^2/g). Furthermore, the pore volume and size distribution of the pristine and regenerated sorbent also remained essentially unchanged (Figure 3.7b). These results imply that the sorbent presented is stable during aqueous solution applications and fully maintains its structures and functional groups even under very strong alkali and acidic conditions during the regeneration and conditioning steps.

a)

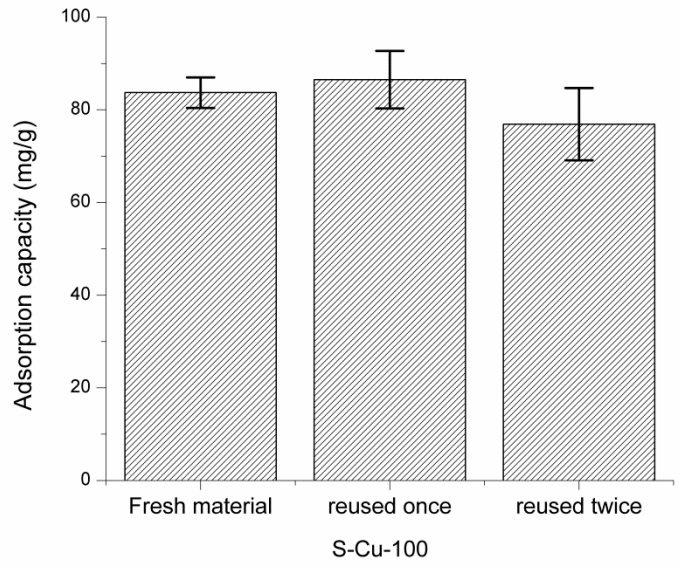

b)

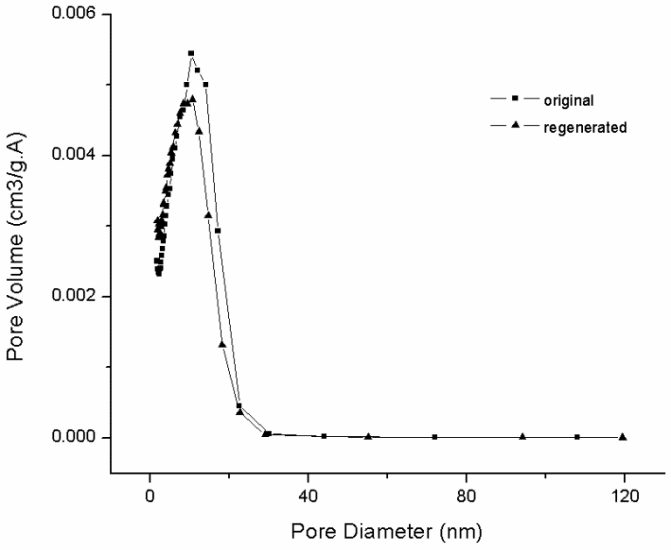

Figure 3.7 a) Cu (II) ion uptake of regenerated sorbent. The initial concentration of solution was 100 mg/L. b) Pore size distribution of the original and once regenerated sorbent.

3.3.4 Selectivity of the sorbents toward heavy metals

In addition to adsorption capacity, selectivity is another critical factor for heavy metal removal and separation applications.

1) Selectivity for Cu (II) over Ni (II) and Co (II) ions

The selectivity for Cu (II) over Ni (II) and Co (II) was studied and the competitive adsorption results are presented in Figure 3.8. The sorbent showed a significantly higher affinity towards Cu (II) compared to Co (II) and Ni (II) ions. The removal efficiency for Cu (II) was around 34% compared to less than 0.4% for Co (II) or Ni (II) ions for the same initial mass concentration (50mg/L) (Figure 3.8). These results indicate that the sorbents form more stable complexes with Cu (II) than with Co (II) or Ni (II) ions. Note that the removal efficiency for Cu (II) under competitive or non-competitive adsorption was virtually identical (34% and 35%, respectively for an initial concentration of 50 mg/L of Cu (II)). Therefore, the presence of Co (II) or Ni (II) ions does not significantly affect the Cu (II) adsorption, which is consistent with earlier reports.[29]

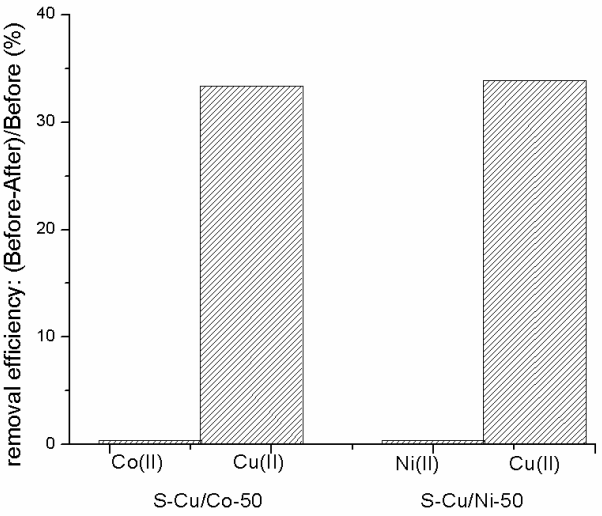

Figure 3.8 Removal efficiency of the sorbents under a competitive adsorption: Cu/Co and Cu/Ni. The initial concentrations were 50 mg/L for each ion.

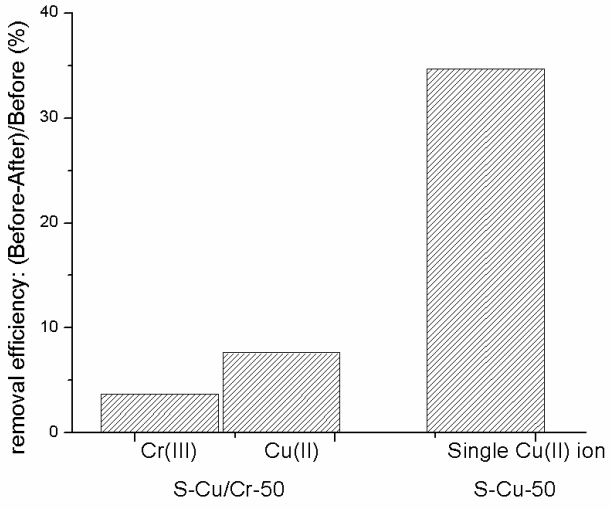

Figure 3.9 Removal efficiency of sorbent under competitive conditions for Cu (II) and Cr (III) ions. The non-competitive removal efficiency for Cu (II) is included for comparison. The concentration of each ion was 50 mg/L.

2) Selectivity between Cu (II) and Cr (III) ions

The adsorption of Cu (II) was also investigated in the presence of Cr (III) under competitive conditions. The initial concentration for each ion was 50 mg/L. In contrast to the behavior observed for Co (II) and Ni (II), the removal efficiency of Cu (II) in the presence of Cr (III) decreased to 7.6 % (Figure 3.9). Recall that the removal efficiency for Cu (II) under either non-competitive or competitive (e.g. in the presence of Co or Ni ions) adsorption conditions was ~35%. These results imply that Cr (III) ions essentially "poison" the sorbent, adversely affecting the adsorption of Cu (II) ions.

To further understand the sorbent poisoning by Cr (III) ions, we carried out a set of additional experiments. The first set involved Cu (II) adsorption with the sorbent previously exposed to a solution of Cr (III) ions (S-Cr-100). After exposure to Cr (III) ions, the sorbent was either simply washed with water to remove weakly adsorbed Cr (III) or fully regenerated to remove strongly adsorbed Cr (III) as described above (i.e treatment with HNO_3 acid followed by ammonium hydroxide). XPS shows the presence of Cr in the water-washed sorbent but not in the fully-regenerated, HNO_3-washed one (Figure 3.10). The fully-regenerated sorbent recovered its full Cu (II) uptake capacity (Table 3.2). In contrast, the water washed sorbents lost most of their Cu (II) adsorption capacity (Table 3.2). A second experiment was conducted to test the influence of Cr (III) ions on the sorbent that had been previously exposed to a solution of Cu (II) (S-Cu-100). After exposure to Cu (II) a concentrated Cr (III) solution was added into the tube containing the sorbent that has been exposed to Cu (II) solution (initial concentration of 100 mg/L). Almost 3/4 of Cu (II) ions initially adsorbed on the sorbent were released into the solution by the addition of Cr (III). These results

suggest that even a slight amount of sorbed Cr (III) 'poisons' or deactivates the sorbent in terms of their Cu (II) adsorption capacity.

a)

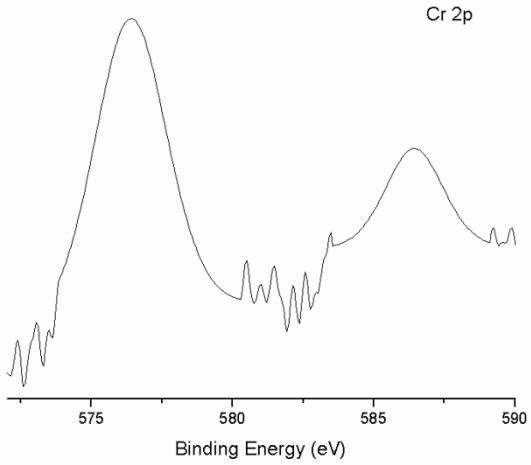

b)

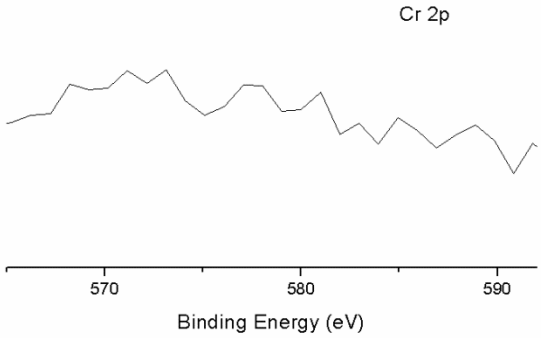

Figure 3.10 XPS of a) water-washed S-Cr-100; b) HNO_3-washed S-Cr-100.

Table 3.2 Cu (II) ion adsorption (initial concentration at 100 mg/L) after treatment with Cr (III) ion solution.

Trial	Regeneration method	Adsorption capacity (mg Cu(II)/ g)
S-Cr-100	Water-washed	9
	Fully-regenerated	75

Table 3.3 N 1s binding energies for the sorbent before and after Cu (II) or Cr (III) ion adsorption.

Trial	Binding Energy of N 1s, eV		
	Before adsorption	After adsorption	Shift (eV)
S-Cu-100	398.5	399.8	1.3
	400.8	402.1	1.3
S-Cr-100	398.5	399.9	1.4
	-	397.9	-

To better understand the adsorption mechanism, especially the "poisoning" effect of Cr (III) ions, we carried out a series of XPS measurements (Figure 3.11). The corresponding binding energies of N1s after exposure to Cu (II) and Cr (III) ions (S-Cu-100 and S-Cr-100, respectively) are summarized in Table 3. The XPS pattern of the pristine sorbent can be resolved into a large peak with a binding energy of 398.5 eV and a small peak at 400.8 eV (Figure 3.11a), characteristic of neutral amine groups and protonated amine groups, respectively.[34-36] The sorbents after exposure to Cu (II) showed a similar spectrum, but the ratio of the large to small peak decreased and both peaks shifted to higher binding energies (from 398.5 to 399.8 eV and 400.8 to 402.1 eV, respectively). The changes in the ratio and the shift of binding energies are consistent with the mechanism that the lone electron pairs of N in the amine-bridging group coordinated with Cu. The complex formation leads to spectral shifts and an increase in the binding energy of nitrogen as described previously.[34-36] When the sorbent was exposed to Cr (III) (see spectrum for S-Cr-100 in Figure 3.11c), a very different spectrum was seen. While there was a similar shift to a higher binding energy for one of the peaks, the other appeared at a lower binding energy (Figure 3.11c, Table 3.3). In addition, the intensity of the two peaks was comparable. The results indicate the sorbents synthesized in this study have a much more complex interaction with Cr (III) ion compared to Cu (II) ion, which translates into the sorption behavior.

We hypothesize that the "poisoning" effect is due to differences in complexation strength and complex geometry of the ethylendiamine (en) ligand with the metal ions. It is well-known that Cu (II) preferentially coordinates to four amine ligands (two en ligands) in a square planar geometry.[37-39] On the other hand, Cr (III) requires six amine ligands in an octahedral coordination, an arrangement probably difficult to achieve in the constrained, solid environment of the sorbent.[40-42]

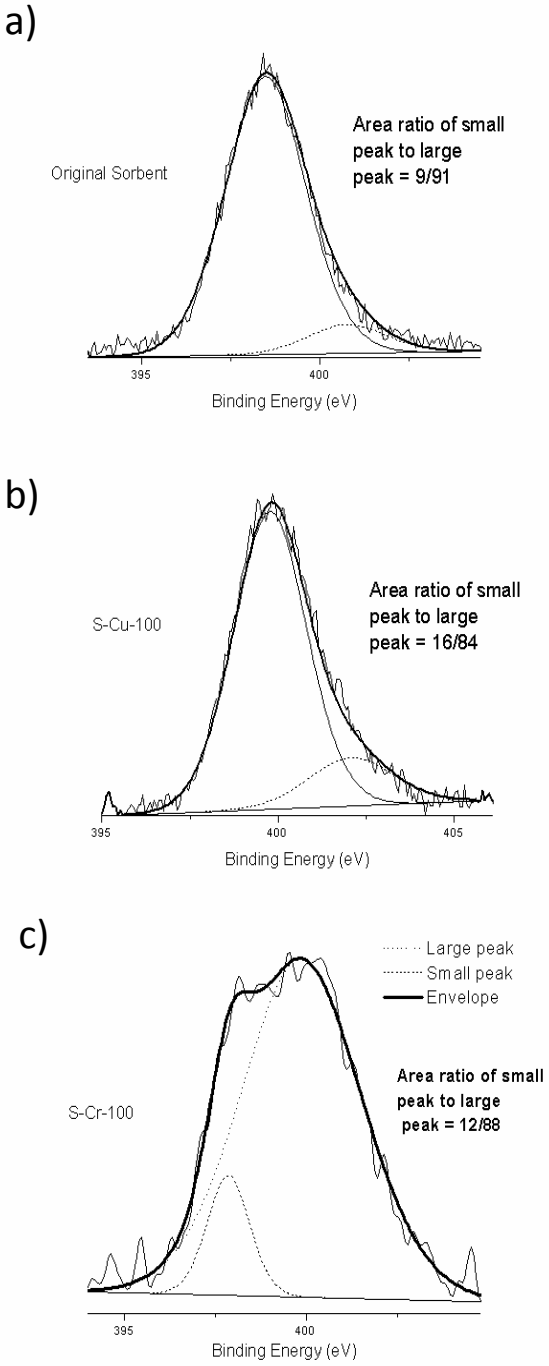

Figure 3.11 XPS spectra of sorbent before and after ion adsorption: (a) N1s for pristine sorbent; (b) N1s for S-Cu-100; (c) N1s for S-Cr-100.

Furthermore, complexation of Cr (III) to en ligands is more favored compared to Cu(II) (the $\log K_1$ for Cr (III) and Cu (II) is 16.5 and 10.72, respectively).[41] Thus, although Cr (III) has a higher affinity to the en ligands, the sorbent shows lower Cr (III) sorption capacity because of the structural inflexibility of the ligands in the sorbent and the challenge of achieving an octahedral coordination. However, Cr (III) can preferentially bind to the sorbent, displace Cu (II) ions and effectively poison the adsorption sites.[43] Nevertheless, removal of Cr (III) by treating with an acid can restore the initial sorption capacity.

3.4 Conclusions

A pure bis-amine bridged polysilsesquixane was synthesized and evaluated as a sorbent for heavy metal removal. The synthesis of the sorbent involved hydrolysis and condensation of TMSEN in the presence of a non-ionic surfactant, P123. The adsorption capacity for Cu (II) and Pb(II) is 77 mg (1.2 mmol) and 276 mg (1.3 mmol) per gram of sorbent, respectively, which are amongst the highest reported to date for organosilicas. The sorbent shows a high selectivity for Cu (II) over Ni (II) and Co (II) ions. The sorbent can be fully regenerated using HNO_3 followed by NH_4OH.

REFERENCES

1. Lagrana, C. C.; Apodaca, D. C.; David, C. P. C. Toxicity of Cu2+ , Cd2+ and Pb2+ Metal Ions in Chironomids and Factors That Affect Metal Accumulation. *International Conference on Environment Science and Engineering* **2011**, *8*, 9–13.

2. Denizli, A.; Sanli, N.; Garipcan, Bora;Patir, S; Alsancak, G. Methacryloylamidoglutamic Acid Incorporated Porous Poly (methyl Methacrylate) Beads for Heavy-metal Removal. *Ind. Eng. Chem. Res.* **2004**, *43*, 6095–6101.

3. Hassan, M. L.; El-Wakil, N. A. Heavy Metal Ion Removal by Amidoximated Bagasse. *J. Appl. Polym. Sci.* **2003**, *87*, 666–670.

4. Dabrowski, A.; Hubicki, Z.; Podkościelny, P.; Robens, E. Selective Removal of the Heavy Metal Ions from Waters and Industrial Wastewaters by Ion-exchange Method. *Chemosphere* **2004**, *56*, 91–106.

5. Demir-Cakan, R.; Baccile, N.; Antonietti, M.; Titirici, M.-M. Carboxylate-Rich Carbonaceous Materials via One-Step Hydrothermal Carbonization of Glucose in the Presence of Acrylic Acid. *Chem. Mater.* **2009**, *21*, 484–490.

6. Kaşgöz, H.; Özgümüş, S.; Orbay, M. Investigation of Metal Ion Removal Selectivity Properties of the Modified Polyacrylamide Hydrogels Prepared by Transamidation and Hofmann Reactions. *J. Macromol. Sci., Part A: Pure Appl.Chem.* **2005**, *42*, 1287–1298.

7. Cavus, S.; Gurdag, G. Noncompetitive Removal of Heavy Metal Ions from Aqueous Solutions by Poly[2-(acrylamido)-2-methyl-1-propanesulfonic Acid-Co -Itaconic Acid] Hydrogel. *Ind. Eng. Chem. Res.* **2009**, *48*, 2652–2658.

8. Takafuji, M.; Ide, S.; Ihara, H.; Xu, Z. Preparation of Poly (1-vinylimidazole)-Grafted Magnetic Nanoparticles and Their Application for Removal of Metal Ions. *Chem. Mater.* **2004**, *16*, 1977–1983.

9. Asefa, T.; MacLachian, M. J.; Coombs, N.; Ozin, G. A. Periodic Mesoporous Organosilicas with Organic Groups Inside the Channel Walls. *Nature* **1999**, *402*, 867–871.

10. Walcarius, A.; Mercier, L. Mesoporous Organosilica Adsorbents: Nanoengineered Materials for Removal of Organic and Inorganic Pollutants. *J. Mater. Chem.* **2010**, *20*, 4478–4511.

11. Yoshitake, H. Design of Functionalization and Structural Analysis of Organically-modified Siliceous Oxides with Periodic Structures for the Development of Sorbents for Hazardous Substances. *J. Mater. Chem.* **2010**, *20*, 4537–4550.

12. Hunks, W. J.; Ozin, G. A. Challenges and Advances in the Chemistry of Periodic Mesoporous Organosilicas (PMOs). *J. Mater. Chem.* **2005**, *15*, 3716–3724.

13. Munoz, B.; Ramila, A.; Perez-Pariente, J.; Diaz, I.; Vallet-Regi, M. MCM-41 Organic Modification as Drug Delivery Rate Regulator. *Chem. Mater.* **2003**, *15*, 500–503.

14. Dai, S.; Burleigh, M. C.; Ju, Y. H.; Gao, H. J.; Lin, J. S.; Pennycook, S. J.; Barnes, C. E.; Xue, Z. L. Hierarchically Imprinted Sorbents for the Separation of Metal Ions. *J. Am. Chem. Soc.* **2000**, *122*, 992–993.

15. Burleigh, M. C.; Dai, S.; Hagaman, E. W.; Lin, J. S. Imprinted Polysilsesquioxanes for the Enhanced Recognition of Metal Ions. *Chem. Mater.* **2001**, *13*, 2537–2546.

16. Descalzo, A. B.; Jimenez, D.; Marcos, M. D.; Mart ́nez-manez, R.; Soto, J.; Haskouri, J. El; Guillem, C.; Beltr μn, D.; Amor ós, P.; Borrachero, M. V. A New Approach to Chemosensors for Anions Using MCM-41 Grafted with Amino Groups. *Adv. Mater.* **2002**, *14*, 966–969.

17. Tang, Y.; Landskron, K. CO2 -Sorption Properties of Organosilicas with Bridging Amine Functionalities Inside the Framework. *J. Phys. Chem. C* **2010**, *114*, 2494–2498.

18. Wahab, M. a.; Kim, I.; Ha, C.-S. Bridged Amine-functionalized Mesoporous Organosilica Materials from 1,2-bis(triethoxysilyl)ethane and Bis[(3-trimethoxysilyl)propyl]amine. *J. Solid State Chem.* **2004**, *177*, 3439–3447.

19. Lam, K. F.; Chen, X.; Fong, C. M.; Yeung, K. L. Selective Mesoporous Adsorbents for Ag+/Cu2+ Separation. *Chem. Commun.* **2008**, 2034–2036.

20. Xue, X.; Li, F. Removal of Cu(II) from Aqueous Solution by Adsorption onto Functionalized SBA-16 Mesoporous Silica. *Microporous Mesoporous Mater.* **2008**, *116*, 116–122.

21. Heidari, A.; Younesi, H.; Mehraban, Z. Removal of Ni(II), Cd(II), and Pb(II) from a Ternary Aqueous Solution by Amino Functionalized Mesoporous and Nano Mesoporous Silica. *Chem. Eng. J.* **2009**, *153*, 70–79.

22. Dey, R. K.; Oliveira, F. J. V. E.; Airoldi, C. Mesoporous Silica Functionalized with Diethylenetriamine Moieties for Metal Removal and Thermodynamics of Cation–basic Center Interactions. *Colloids Surf., A* **2008**, *324*, 41–46.

23. Mureseanu, M.; Reiss, A.; Stefanescu, I.; David, E.; Parvulescu, V.; Renard, G.; Hulea, V. Modified SBA-15 Mesoporous Silica for Heavy Metal Ions Remediation. *Chemosphere* **2008**, *73*, 1499–1504.

24. Yang, Q.; Liu, J.; Yang, J.; Zhang, L.; Feng, Z.; Zhang, J.; Li, C. Acid Catalyzed Synthesis of Ordered Bifunctionalized Mesoporous Organosilicas with Large Pore. *Microporous and Mesoporous Mater.* **2005**, *77*, 257–264.

25. Chouyyok, W.; Shin, Y.; Davidson, J.; Samuels, W. D.; LaFemina, N. H.; Rutledge, R. D.; Fryxell, G. E.; Sangvanich, T.; Yantasee, W. Selective Removal of copper(II) from Natural Waters by Nanoporous Sorbents Functionalized with Chelating Diamines. *Environ. Sci. Technol.* **2010**, *44*, 6390–6395.

26. Benhamou, A.; Baudu, M.; Derriche, Z.; Basly, J. P. Aqueous Heavy Metals Removal on Amine-functionalized Si-MCM-41 and Si-MCM-48. *J. Hazard. Mater.* **2009**, *171*, 1001–1008.

27. Sayari, A.; Hamoudi, S.; Yang, Y. Applications of Pore-Expanded Mesoporous Silica . 1 . Removal of Heavy Metal Cations and Organic Pollutants from Wastewater. *Chem. Mater.* **2005**, 212–216.

28. Park, S. S.; Shin, J. H.; Zhao, D.; Ha, C.-S. Free-standing and Bridged Amine-functionalized Periodic Mesoporous Organosilica Films. *J. Mater. Chem.* **2010**, *20*, 7854–7858.

29. Hossain, K. Z.; Mercier, L. Intraframework Metal Ion Adsorption in Ligand-Functional Mesoporous Silica. *Adv. Mater.* **2002**, *14*, 1053–1056.

30. Jayasundera, S.; Burleigh, M. C.; Zeinali, M.; Spector, M. S.; Miller, J. B.; Yan, W.; Dai, S.; Markowitz, M. a Organosilica Copolymers for the Adsorption and Separation of Multiple Pollutants. *J. Phys. Chem. B* **2005**, *109*, 9198–9201.

31. Burleigh, M. C.; Markowitz, M. A.; Spector, M. S.; Gaber, B. P. Amine-functionalized Periodic Mesoporous Organosilicas. *Chem. Mater.* **2001**, *13*, 4760–4766.

32. Kruk, M.; Jaroniec, M. Gas Adsorption Characterization of Ordered Organic−Inorganic Nanocomposite Materials. *Chem. Mater.* **2001**, *13*, 3169–3183.

33. Zhang, L.; Liu, J.; Yang, J.; Yang, Q.; Li, C. Direct Synthesis of Highly Ordered Amine-functionalized Mesoporous Ethane-silicas. *Microporous and Mesoporous Mater.* **2008**, *109*, 172–183.

34. Liu, C.; Bai, R. Adsorptive Removal of Copper Ions with Highly Porous Chitosan/cellulose Acetate Blend Hollow Fiber Membranes. *J. Membr. Sci.* **2006**, *284*, 313–322.

35. Zhang, X.; Bai, R. Mechanisms and Kinetics of Humic Acid Adsorption onto Chitosan-coated Granules. *J. Colloid Interface Sci.* **2003**, *264*, 30–38.

36. Liu, C.; Bai, R.; Hong, L. Diethylenetriamine-grafted Poly(glycidyl Methacrylate) Adsorbent for Effective Copper Ion Adsorption. *J. Colloid Interface Sci.* **2006**, *303*, 99–108.

37. Dai, S.; Burleigh, M. C.; Shin, Y.; Morrow, C. C.; Barnes, C. E.; Xue, Z. Prägungsbeschichtung: Eine Neue Synthese Selektiv Funktionalisierter, Geordneter Mesoporöser Sorbentien. *Angewandte Chemie* **1999**, *111*, 1314–1318.

38. Yoshitake, H.; Nakajima, H.; Oumi, Y.; Sano, T. Control of Spacing Between Aminoalkyl Functions by Mesostructural Transition in a Polysilsesquioxane Lamellar Assembly. *J. Mater. Chem.* **2010**, *20*, 2024–2032.

39. Goubert-Renaudin, S.; Etienne, M.; Brandès, S.; Meyer, M.; Denat, F.; Lebeau, B.; Walcarius, A. Factors Affecting copper(II) Binding to Multiarmed Cyclam-grafted Mesoporous Silica in Aqueous Solution. *Langmuir* **2009**, *25*, 9804–9813.

40. Fee, B. W. W.; Harrowfield, J. N. M. B.; Jackson, W. G. Octahedral Bis(ethylenediamine)chromium(III) Complexes. Part I. Preparation and Characterization. *J. Chem. Soc. A* **1970**, 2612–2620.

41. Paoletti, P. Formation of Metal Complexes with Ethylenediamine: A Critical Survey of Equilibrium Constants, Enthalpy And Entropy Values. *Pure Appl. Chem.* **1984**, *56*, 491–522.

42. Raymond, K. N.; Ibers, J. A. Structure of Tris (ethylenediamine) chromium(III) Hexacyanocobaltate(III) Hexahydrate, [Cr(C2H8N2)3] [CO(CN)6] 6H2O. *Inorganic Chemistry* **1968**, *7*, 2333–2338.

43. Jiang, Y.; Gao, Q.; Yu, H.; Chen, Y.; Deng, F. Intensively Competitive Adsorption for Heavy Metal Ions by PAMAM-SBA-15 and EDTA-PAMAM-SBA-15 Inorganic–organic Hybrid Materials. *Microporous and Mesoporous Mater.* **2007**, *103*, 316–324.

CHAPTER 4

A MESOPOROUS POLYSILSESQUIOXANE SORBENT FOR CO_2 CAPTURE APPLICATION

4.1 Introduction

Climate changes due to global warming have received widespread public concern. It is called greenhouse effect, which represents the phenomenon in which gases in the upper atmosphere absorb heat radiated by the earth and raise the temperature. The IPCC (Intergovernmental Panel on Climate Change) has identified six anthropogenic gases with climate change potential: CO_2, CH_4, N_2O, SF_6, CFCs (chlorofluorocarbons), and HFCs (hydrofluorocarbons).[1] Among these, CO_2 has the largest climate change impact, due to its overwhelming emissions in recent decades. The amount of CO_2 in the atmosphere kept relatively balanced until the beginning of industrialized civilization.[2] It is estimated that annual global emissions of CO_2 have escalated by approximately 80% between 1970 and 2004.[3]

Governments and international organizations have recently started to takeactions and estabilished regulations with the aim of reducing CO_2 emission control to the atmosphere. A large amount of programs have been established such as IPCC, the United Nations Framework Commission on Climate Change, and the Global Climate Change Initiative.[3] Therefore, CO_2 capture and conversion is regarded as one of the grand challenges for the 21st century.[4]

CO_2 emission arises mostly from power plants. Taking the U.S. as an example, 40 % of the total CO_2 emission is produced by fossil-fuel power plants, with coal-fired

plants being the main contributor.[5] From this perspective, control of CO_2 emission from power plants plays a vital role in the goal of reducing CO_2 emissions.

The most common CO_2 capture process in industry employs Amine-CO_2 chemistry in the form of gas-liquid absorption. Monoethanolamine (MEA), diethanolamine (DEA), and methyldiethanolamine (MDEA) are commonly used as aqueous adsorbents. Their chemical structures are shown in Figure 4.1. Taking MEA as an example, MEA has a high CO_2 carrying capacity and can quickly react with CO_2 at low temperature.[6] It is, relatively inexpensive, making it a good choice in commercial processes.[6-8] The fundamental process is the reversible reaction between a weak acid (e.g., CO_2) and a weak base (e.g., MEA) to form a soluble salt at low temperature with desorption at elevated temperatures. However, there are numerous associated drawbacks.[9] It is corrosive and viscous, which requires the use of dilute aqueous solutions. The corrosive nature triggers problems during MEA flowing in pipes and, therefore, it increases construction and maintenance cost.[10] Moreover, water has a high specific heat capacity, thus the whole process becomes very energy consuming. The energy penalty for a coal-fired power station using traditional aqueous MEA for capture has been estimated as 25% to 40%.[3] In addition, MEA has relatively high vapor pressure, which causes inevitable loss during regeneration. Thus a fresh injection of solution is periodically needed.

To that end, diverse new solid adsorbents have been developed and are considered as promising alternatives for CO_2 capture in recent studies. Among these, solid-supported amines have been an active research area.[11,12] Various amines, supports and immobilizing techniques have been studied, and the results have been quite satisfactory.[10,13-15] In contrast to MEA adsorption, amine-based porous solid sorbents

offer several advantages for CO_2 capture, including significant reduction of corrosion issues and lower energy cost during regeneration and transport.

In this chapter, mesoporous amine-bridged polysilsesquioxane, which is synthesized solely by a single silica precursor, N, N'-bis-[3-(trimethoxysilyl)propyl]-ethylenediamine (TMSEN), is applied to absorb CO_2. The CO_2 capture performance using this inorganic/organic hybrid material is discussed. This sorbent is the same material used in the Chapter 3 for heavy metal ion removal. Amine groups have versatile functions, and in this chapter the specific CO_2-amine chemistry is used.[16]

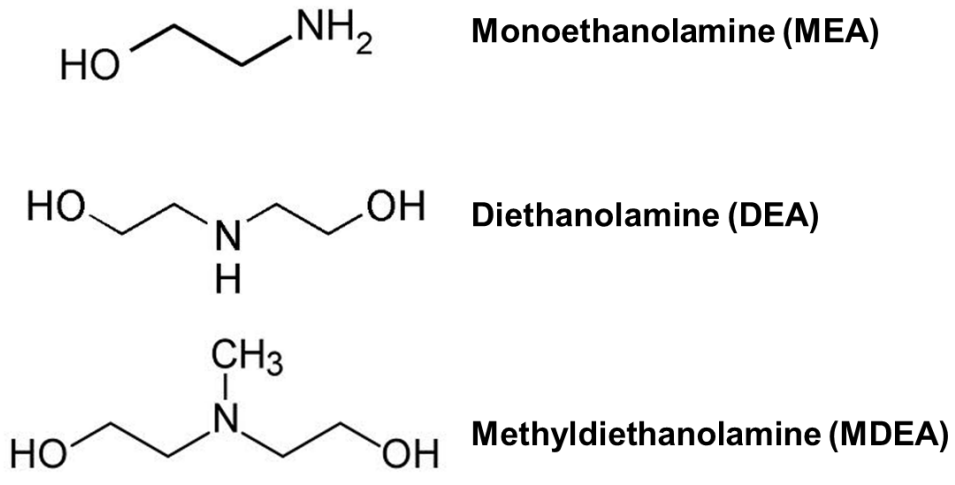

Figure 4.1 Chemical structures of conventional amines in CO_2 capture.

4.2 Experimental sections

4.2.1 Chemicals and Materials

All chemicals were obtained from commercial sources and were used without further purification. N, N'-bis-[3-(trimethoxysilyl)propyl]-ethylenediamine (TMSEN, 62% in methanol) was purchased from Gelest, Inc. Poly (ethylene glycol)-block-poly (propylene glycol)-block-poly (ethylene glycol) block polymer (P123, MW=5800) and branched Poly(ethyleneimine) (PEI) solution (average Mn ~1800, 50 wt. % in H_2O) were all obtained from Sigma-Aldrich. Ethanol (95%) was supplied from VWR. Deionized water was generated with a Milli-Q integral ultrapure water purification system.

4.2.2 Synthesis of amine-supported sorbents

The synthesis method of poly-TMSEN was described in the previous chapter. PEI/ poly-TMSEN is also followed the same sol-gel procedure as the one in pure poly-TMSEN synthesis, except it uses the mixture of TMSEN precursor and PEI instead. The total real weight of the mixtures is controlled to be 2.5 g.

4.2.3 Characterization

Bright-field transmission electron micrographs (TEM) images were obtained on a FEI Tecnai T12 Spirit Twin TEM/STEM operated at 120kV. Nitrogen adsorption-desorption isotherms were obtained on a Micrometrics ASAP 2020 physi-sorption instrument. The specific surface areas of the samples were calculated by the Brunauer-Emmett-Teller (BET) method. Pore size distributions were calculated from the N_2 adsorption isotherm using the Barrett–Joyner–Halenda (BJH) method.

Thermogravimetric analysis (TGA) was performed from 35 ℃ to 1000 ℃ on a TA Instruments Q5000 thermal graphic analyzer using compressed air and a heating rate of 10 ℃/min.

4.2.4 CO_2 capture measurements

The adsorption and desorption measurements were performed on a TA Instruments Q5000 thermogravimetric analysis (TGA) at ambient pressure. Pure dry CO_2 (99.99%) and ultra high purity N_2 (99.995%) were used as the adsorption and purging gas respectively. In a typical adsorption run, sorbents were placed in a platinum sample pan. After the sorbent was purged with a N_2 stream (40 ml/min) at 110 ℃ for 30 min, the temperature was cooled to 25 ℃ at a rate of 15 ℃/min. The CO_2 gas (40 ml/min) was then switched into the system and the sorbent was kept at 25 ℃ for 60 min for adsorption. The CO_2 capacity of the sorbent in mmol/g (based on the dry weight of the sorbent) was calculated from the weight gain of the sample in the adsorption process.

$$\text{CO}_2 \text{ capture capacity} = \frac{\text{Moles of CO}_2 \text{ absorbed}}{\text{Mass of dried absorbent}}$$

For cyclic performance, the desorption is achieved by firstly purging N_2 at 110 ℃ for 30 min, and then adsorption is under CO_2 gas at 25 ℃ for 30 min. Each cycle is followed the same procedure described above.

4.3 Results and discussion

4.3.1 Materials and Characterization

This polysilsesquioxane was developed in a one-pot sol-gel process. The TEM images of the poly-TMSEN are shown in Figure 4.2. The sorbent consists of nanoparticle aggregates in a porous structure, where the voids are created by the removed surfactants.

TGA of the sorbent is conducted from room temperature to 1000 ℃ (Figure 4.3). It shows a weight loss of 6% at temperatures below 100 ℃, which could be attributed to solvent residue evaporation. A significant weight loss (up to 50 %) in the temperature range 300-800 ℃ is mainly due to the decomposition of the bridging organic groups (Figure 4.3). Matrix decomposition gives a broad peak in the derivative plot in this range. Above 800 ℃, a slight weight gain was noticed, which has been attributed to the formation of oxides or nitrides from reactions with the purge gas at high temperature.[17] The large weight change of the material supports the existence of a large amount of amine groups within the sorbent, which can act potentially as active sites for CO_2 capture. Moreover, the high porosity (310 m^2/g) enables the amine groups integrated within the structure to be available and effectively react with CO_2. Other characterization including NMR and XRD were discussed in the Chapter 3.

4.3.2 Amine-CO_2 chemistry

In this work, the structure of alkanolamine in poly-TMSEN is secondary amine. This tailored functional group reacts reversibly with CO_2. At low temperature, amines react

a)

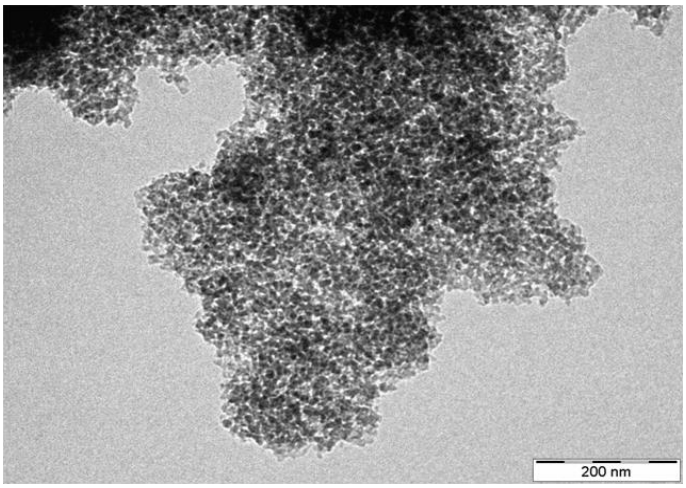

b)

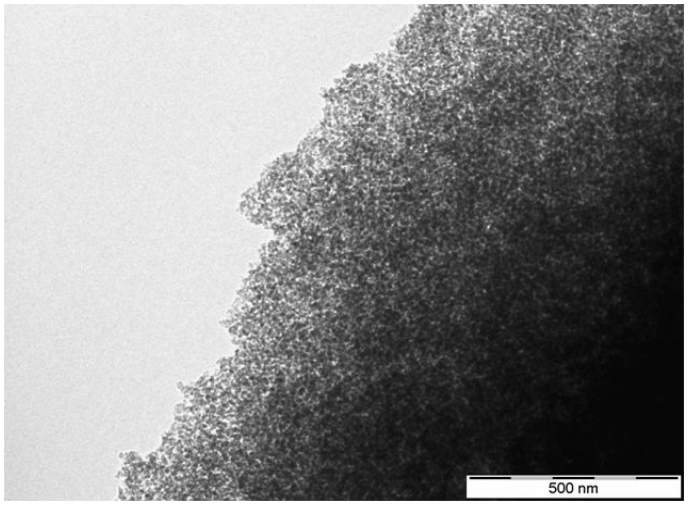

Figure 4.2 TEM images of sorbent Poly-TMSEN.

with CO_2 through a zwitterion mechanism to form a carbamate.[18] The CO_2 loading capacity for secondary amine is 0.5 mole of CO_2 per mole of amine in dry conditions, as can be seen from Figure 4.4. Regeneration of the sorbent occurs upon heating to liberate CO_2. Figure 4.5 demonstrates the cycle scheme and the corresponding weight change during capture-release process. The CO_2 capacity is measured by the weight change in mmol/g (based on the dry weight of the sorbent) by TGA.

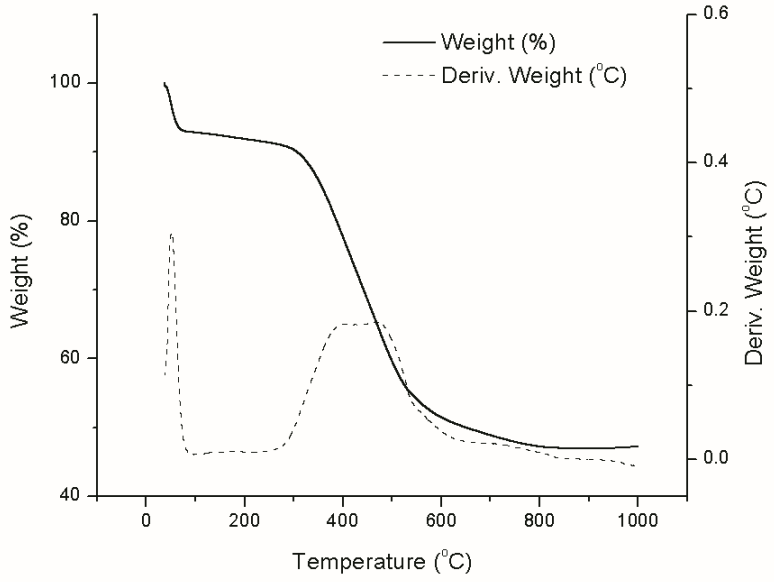

Figure 4.3 Thermogravimetric weight-loss and derivative plot of the sorbent, a heating rate of 10 ℃/min in air.

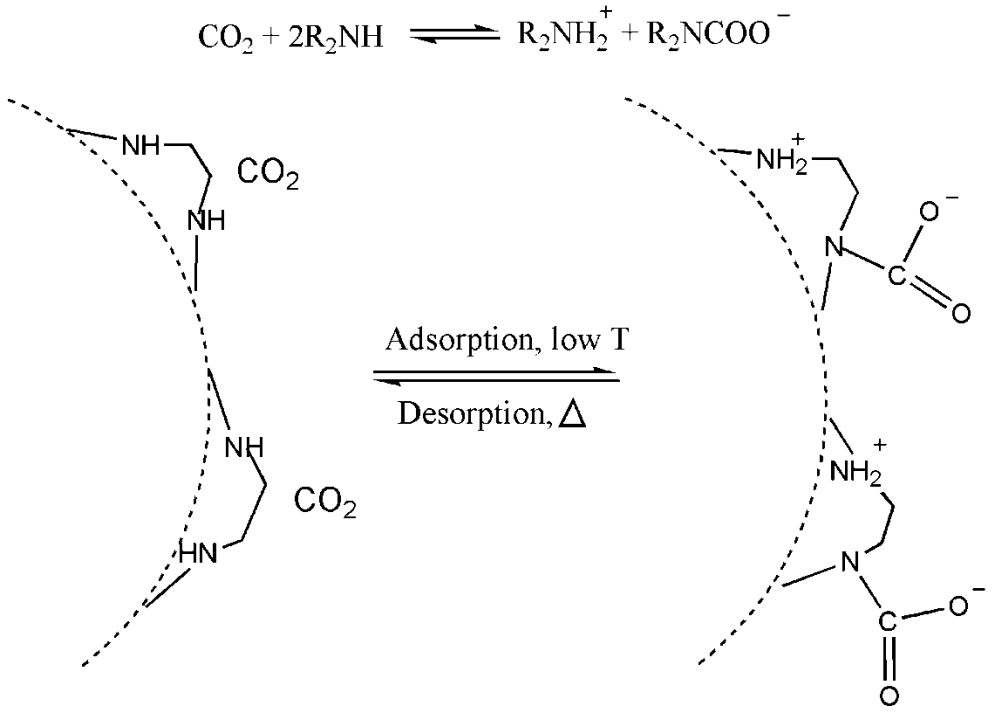

Figure 4.4 Reaction scheme of Amine-CO_2 chemical adsorption and desorption.

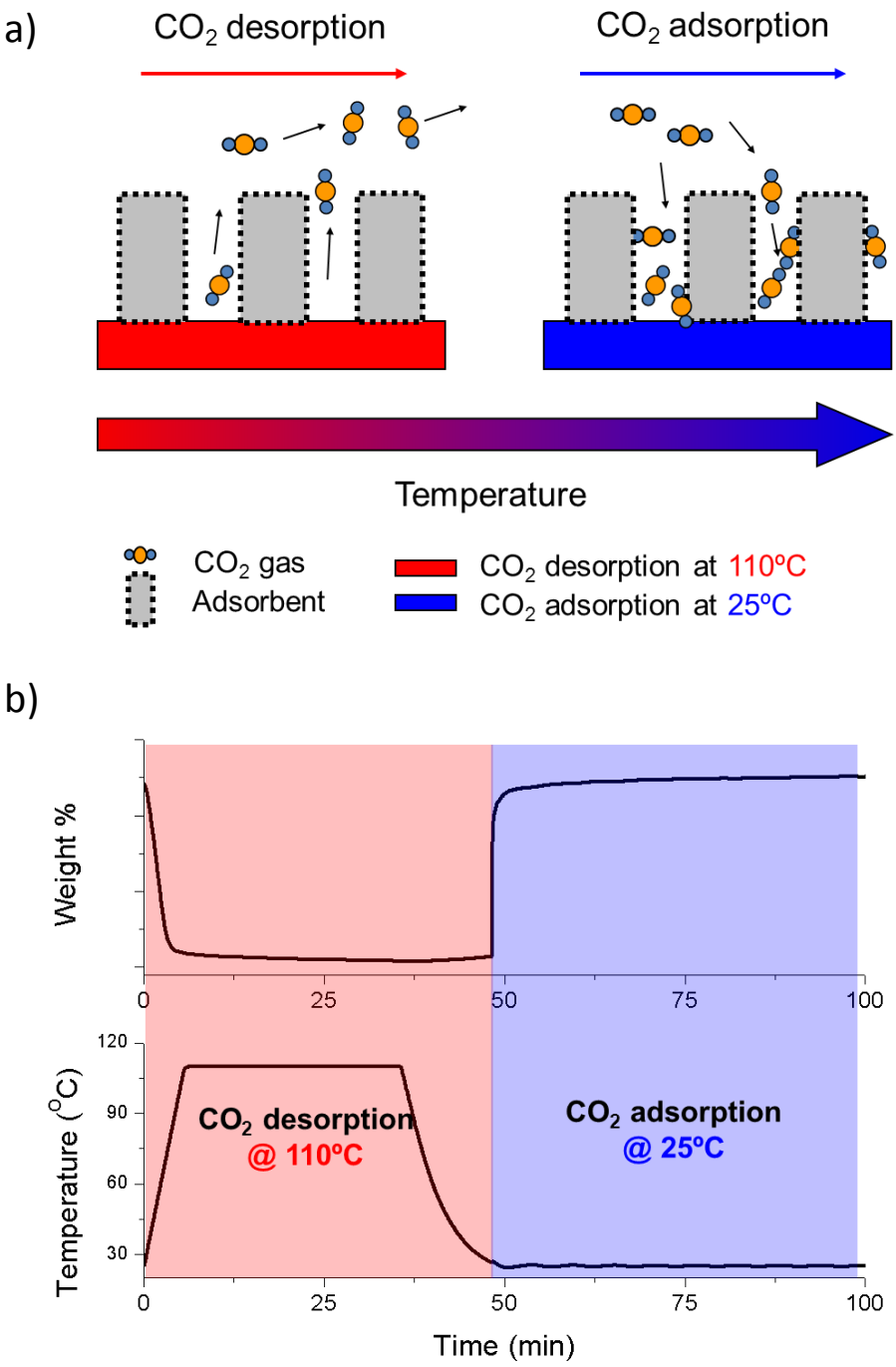

Figure 4.5 Adsorption-desorption cycle a) schematic illustration of the process b) the TGA weight % results according to the temperature and time change.

4.3.3 Kinetics of CO_2 capture

The adsorption kinetics is investigated in dry CO_2 at 25 ℃. As shown in Figure 4.6, the sorbent has a rapid linear weight gain within 5 min, with the capacity to 2.3 mmol/g. This sharp adsorption rate is attributed to the large amount of easily accessible amine groups on the large surface of particles. A slower capture process then follows due to the diffusion resistance,[10] and reaches a plateau at capacity of 2.4 mmol/g after 60 min. The poly-TMSEN exhibits favorable adsorption kinetics, since 95% of the equilibrium capacity was reached within 5 min, which is beneficial in shortening capture cycle time industrially.

The CO_2 capacity is 2.4 mmol/g. From elemental analysis, the content of the secondary amine (-NHRR´) of the sorbent is 7 mmol/g. Therefore, the effective molar ratio of CO_2/amine is 35%. Recalling the theoretical stoichiometric ratio is 0.5 mole of CO_2/mole of amine (50%), it is revealed that 70% of amine groups are effectively reacted with CO_2.

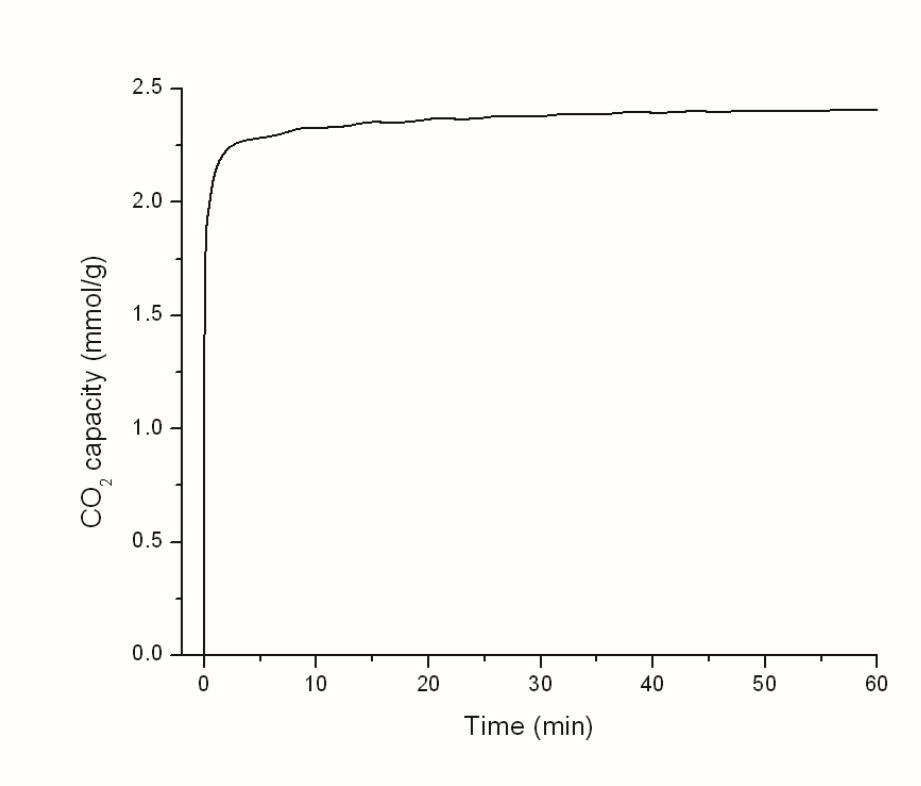

Figure 4.6 Kinetics of CO_2 adsorption using poly-TMSEN sorbent. Capture is under pure dry CO_2 (40 ml/min) at 25 ℃.

4.3.4 Regeneration and cyclic performance of the sorbent

In order to be employed industrially, long-term stability and reusability is highly desired for sorbents. Figure 4.7 reveals the multiple CO_2 capture cycles using poly-TMSEN. As shown, the cyclic performance is very stable. The amine-impregnated sorbent quickly releases all the CO_2 in each desorption cycle upon heating at 110 °C. And no capacity loss is observed after 10 adsorption-desorption cycles.

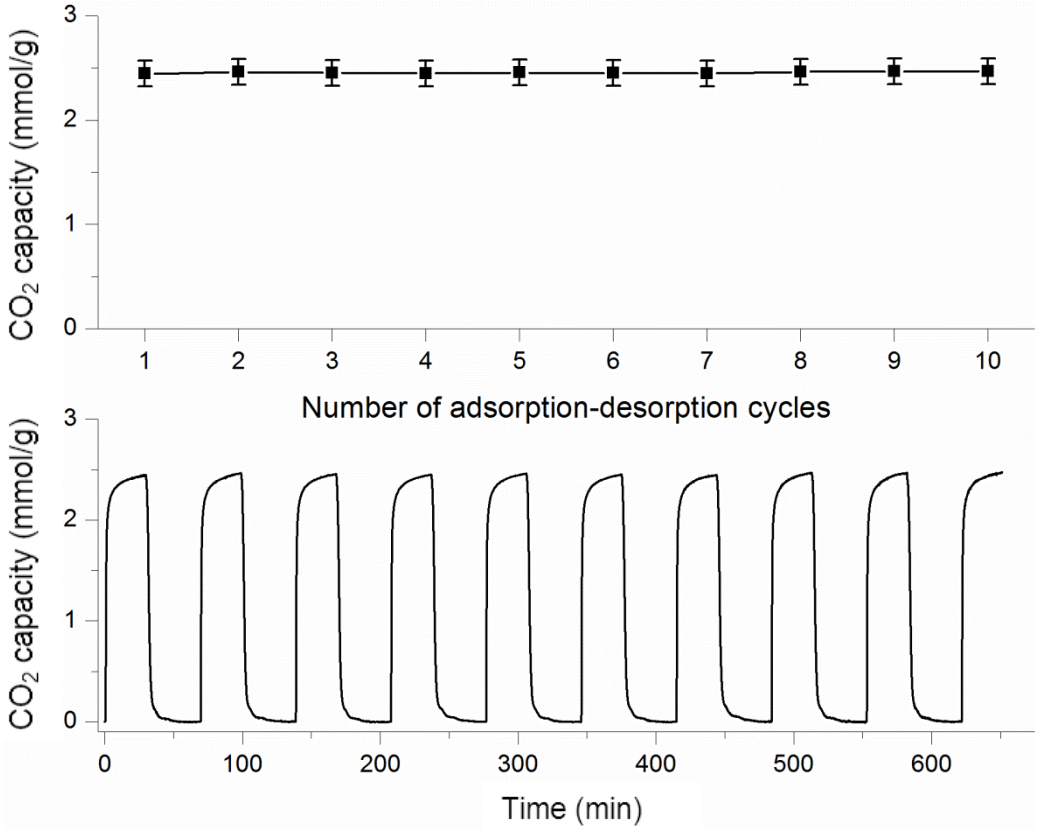

Figure 4.7 Cyclic tests of CO_2 capture using poly-TMSEN over 10 cycles. Reproduced from ref. 15, Copyright © 2011 Society of Chemical Industry and John Wiley & Sons, Ltd.

4.3.5 Adding PEI to poly-TMSEN

PEI was added to the TMSEN precursors during the synthesis in order to achieve higher amine content. The PEI structure is shown in Figure 4.8. The motivation is the CO_2 uptake might be enhanced as the increase of amine loading in the sorbent. Four samples with different molar ratios of poly-TMSEN/PEI (19.5, 11, 7 and 5) were prepared and tested for CO_2 capture. As shown in Figure 4.9, the CO_2 uptake does not increase when the hybrid contains more PEI. The CO_2 capacity is only 0.8 ± 0.01 mmol/g when the hybrid sorbent has the highest portion of PEI. A further investigation of BET surface area of each sorbent is shown in Figure 4.9b. Efforts to increase the amine loading of the sorbent have come at the expense of surface area, because the PEI block and cover some of the pores. In this system, it is indicated that the surface area of the sorbent plays a more vital role in terms of CO_2 capacity than the ultra-amine addition, as the amine content of poly-TMSEN is already high.

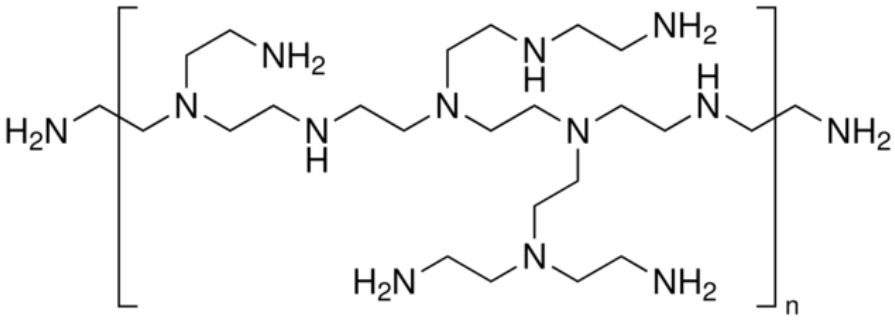

Figure 4.8 Structure of PEI (average Mn ~1800).

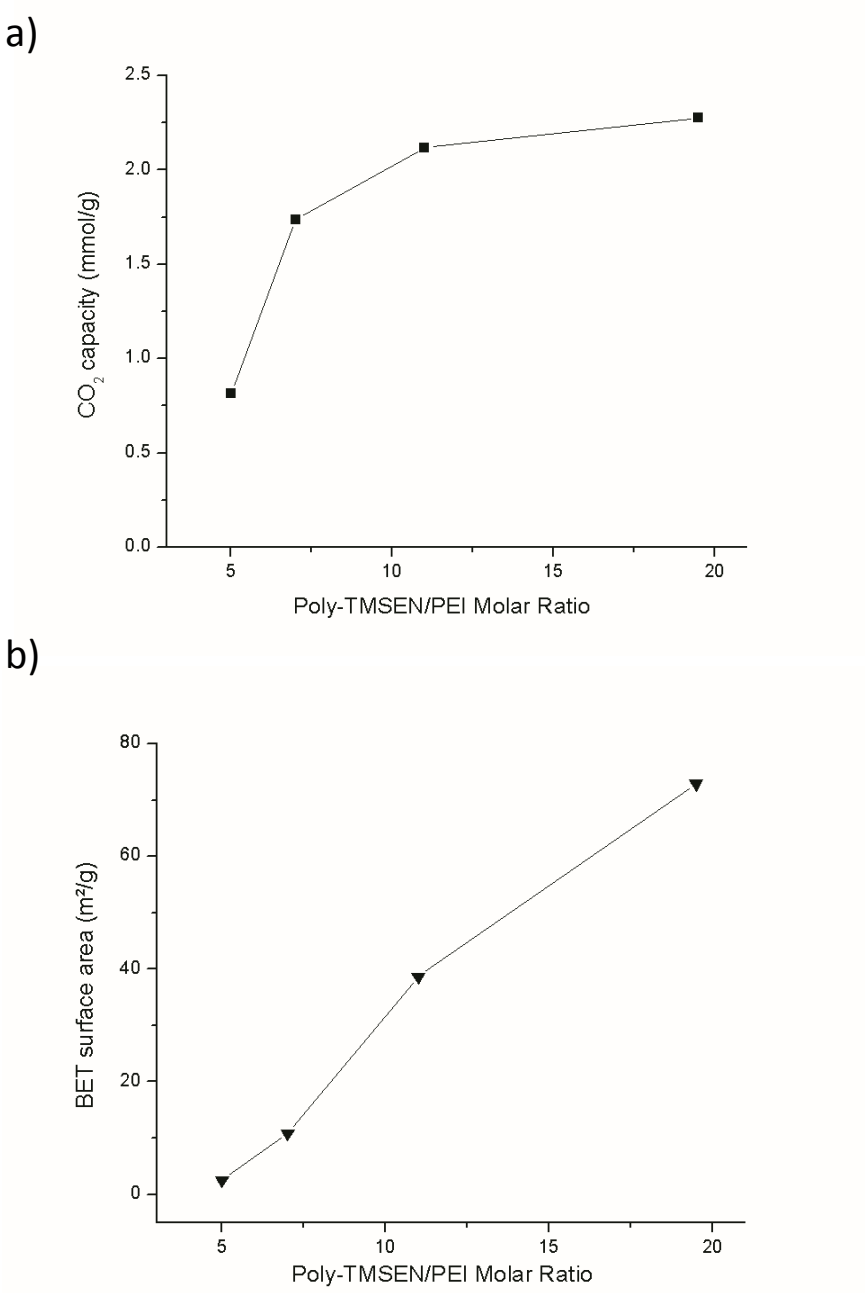

Figure 4.9 a) CO_2 capture by poly-TMSEN/PEI in different molar ratios b) the BET surface area changes accordingly.

The surface area of the mesoporous network comes from the nonionic surfactant P123's assembly during synthesis. Therefore the interaction between the surfactant and organosilica during the sol-gel process is important. Due to the amine's hydrophilic nature, the hydrolysis rate of TMSEN precursor is much faster than the one of conventional silane precursor, such as tetraethyl orthosilicate (TEOS). Although the sorbent structure is porous and robust, the pores are not periodically uniform. In order to increase the sorbent's surface area, a future direction could be how to control the aggregation mechanism for a slow gelation rate so as to create long-range order mesoporous poly-TMSEN.

4.4 Conclusions

In this chapter, mesoporous amine-bridged polysilsesquioxane is prepared in a one-pot sol-gel process. This poly-TMSEN is applied to the CO_2 capture. The solid sorbent brings advantages of ease-of-handling and low energy requirement for regeneration. The sorbent shows rapid adsorption kinetics within 5 min and reaches a CO_2 capacity of 2.43 ± 0.05 mmol/g under dry CO_2 at 25 ℃. In addition to the high capacity, it also shows fast complete desorption, excellent long-term stability and maintains its full capacity after 10 adsorption-desorption cycles.

REFERENCES

1. Alie, C. F. CO_2 Capture With MEA: Integrating the Absorption Process and Steam Cycle of an Existing Coal-Fired Power Plant. *Master Thesis in University of Waterloo* **2004**, 1–2.

2. Yang, H.; Xu, Z.; Fan, M.; Gupta, R.; Slimane, R. B.; Bland, A. E.; Wright, I. Progress in Carbon Dioxide Separation and Capture: a Review. *J. Environ. Sci.* **2008**, *20*, 14–27.

3. D'Alessandro, D. M.; Smit, B.; Long, J. R. Carbon Dioxide Capture: Prospects for New Materials. *Angew. Chem. Int. Ed.* **2010**, *49*, 6058–6082.

4. Jacobson, M. Z. Review of Solutions to Global Warming, Air Pollution, and Energy Security. *Energy Environ. Sci.* **2009**, *2*, 148–173.

5. Adminstration, E. I. Emissions of Greenhouse Gases in the United States 2007. *U.S. DOE* **2008**, 4–5.

6. Liu, Y.; Zhang, L.; Watanasiri, S. Representing Vapor-Liquid Equilibrium for an Aqueous MEA-CO_2 System Using the Electrolyte Nonramdom-Two-Liquid Model. *Ind. Eng. Chem. Res.* **1999**, *38*, 2080–2090.

7. Bates, E. D.; Mayton, R. D.; Ntai, I.; Davis, J. H. CO_2 Capture by a Task-specific Ionic Liquid. *J. Am. Chem. Soc.* **2002**, *124*, 926–927.

8. Alie, C.; Backham, L.; Croiset, E.; Douglas, P. L. Simulation of CO_2 Capture Using MEA Scrubbing: a Flowsheet Decomposition Method. *Energy Convers. Manage.* **2005**, *46*, 475–487.

9. Anthony, J. L.; Aki, S. N. V. K.; Maginn, E. J.; Brennecke, J. F. Feasibility of Using Ionic Liquids for Carbon Dioxide Capture. *Int. J. Environ. Technol. Manage.* **2004**, *4*, 105–115.

10. Qi, G.; Wang, Y.; Estevez, L.; Duan, X.; Anako, N.; Park, A.-H. A.; Li, W.; Jones, C. W.; Giannelis, E. P. High Efficiency Nanocomposite Sorbents for CO_2 Capture Based on Amine-functionalized Mesoporous Capsules. *Energy Environ. Sci.* **2011**, *4*, 444–452.

11. Hicks, J. C.; Drese, J. H.; Fauth, D. J.; Gray, M. L.; Qi, G.; Jones, C. W. Designing Adsorbents for CO_2 Capture from Flue Gas-hyperbranched Aminosilicas Capable of Capturing CO_2 Reversibly. *J. Am. Chem. Soc.* **2008**, *130*, 2902–2903.

12. Knowles, G. P.; Graham, J. V.; Delaney, S. W.; Chaffee, A. L. Aminopropyl-functionalized Mesoporous Silicas as CO_2 Adsorbents. *Fuel Process. Technol.* **2005**, *86*, 1435–1448.

13. Xu, X.; Song, C.; Andresen, J. M.; Miller, B. G.; Scaroni, A. W. Novel Polyethylenimine-Modified Mesoporous Molecular Sieve of MCM-41 Type as High-Capacity Adsorbent for CO_2 Capture. *Energy Fuels* **2002**, 1463–1469.

14. Franchi, R. S.; Harlick, P. J. E.; Sayari, A. Applications of Pore-Expanded Mesoporous Silica . 2 . Development of a High-Capacity , Water-Tolerant Adsorbent for CO_2. *Ind. Eng. Chem. Res.* **2005**, *44*, 8007–8013.

15. Qi, G.; Fu, L.; Duan, X.; Choi, B. H.; Abraham, M.; Giannelis, E. P. Mesoporous Amine-Bridged Polysilsesquioxane for CO_2 Capture. *Greenhouse Gases: Sci. Technol.* **2011**, *284*, 278–284.

16. Hicks, J.; Dabestani, R.; Buchanan III, A. C.; Jones, C. W. Spacing and Site Isolation of Amine Groups in 3-aminopropyl-grafted Silica Materials: The Role of Protecting Groups. *Chem. Mater.* **2006**, *18*, 5022–5032.

17. Burleigh, M. C.; Markowitz, M. A.; Spector, M. S.; Gaber, B. P. Amine-functionalized Periodic Mesoporous Organosilicas. *Chem. Mater.* **2001**, *13*, 4760–4766.

18. Vaidya, P. D.; Kenig, E. Y. CO_2-Alkanolamine Reaction Kinetics: A Review of Recent Studies. *Chem. Eng. Technol.* **2007**, *30*, 1467–1474.

CONCLUSIONS AND FUTURE DIRECTIONS

Conclusions

The dissertation has been a study of hybrid materials for environmental remediation. It has included three developments as original work. The first of these developments, presented in Chapter 2, involved a new study on the hierarchical hybrid biocatalysts comprised of HRP, magnetic nanoparticles and microparticles for phenol remediation application. The hybrid peroxidase catalysts exhibit activity three times higher than free HRP and are able to remove three times more phenol compared to free HRP under similar conditions. In addition, the hybrid catalysts reduce substrate inhibition, which is common with free or conventionally immobilized enzymes. We improve the reusability of the system when the HRP/magnetic nanoparticle hybrids are supported on micron scale magnetic particles.

The second part of the dissertation, presented in Chapter 3, focuses on a mesoporous bis-amine bridged polysilsesquioxane sorbent for heavy metal ion removal. We synthesize a mesoporous sorbent by hydrolysis and condensation of amine-bridged precursor in the presence of a nonionic surfactant. The sorbent exhibits a high adsorption capacity of 77 mg/g (1.2 mmol/g) and 276 mg/g (1.3 mmol/g) for Cu (II) and Pb(II), respectively. After metal adsorption we can easily regenerate the system to full capacity. The sorbent shows high selectivity for Cu (II) over Ni (II) and Co (II) ions. In the third part of the dissertation, we also apply the amine-bridged sorbent to adsorb CO_2. It exhibits fast CO_2 capture kinetics and has a CO_2 capacity of 2.4 mmol/g. We can fully regenerate the sorbent and it shows good stability over repetitive adsorption-desorption process over 10 cycles.

Future directions

a) Hierarchical biocatalyst for phenol removal

Future work can further explore fundamental characterization of BNCs. Questions remain on the detailed interaction mechanism between HRP and MNP. Some advanced characterization investigation including high-resolution TEM for the enzyme distribution in catalysts could be beneficial.

Second, by using magnetic microparticles, the reusability for phenol removal is improved. However, there is still a drop of the phenol removal extent after three cycles, which is mainly due to the accumulation of end-product polyphenols onto the used biocatalysts. Much research remains to be done on how to remove polyphenols from the catalysts. One future direction could be to apply some process treatments on the biocatalyst after each use. Since the MH-BNC is magnetic, it allows certain flexibility to operate and control its movement. Using external magnetic fields, the magnetic catalysts can be kept in a restricted area to gain reaction efficiency. Because of the magnetic confinement, catalysts can be manipulated and decoupled from other treatment steps. Through a collaboration, a magnetic bioreactor was designed. The electromagnets in the reactor can provide the necessary magnetic field, where the field intensity, direction and frequency are controlled by computer program. Further studies can provide additional information on how this bioreactor can help to minimize the build-up of polyphenols in the catalysts for better reuse.

b) Amine-bridged polysilsesquioxane

Although the structure of the amine-bridged polysilsesquioxane is porous and robust, the pores are not periodically uniform. The adsorption capacity both for heavy metal

removal and for CO_2 capture would be enhanced if there is an increase of the sorbent's surface area. It remains to be seen how to further control the gelation rate during synthesis and thus the microstructure. Because the amine is hydrophilic, one possibility is to add non-polar solvents during sol-gel synthesis in the hope of getting a slower reaction rate for long-range ordering of the pores.